T.C.
ERCIYES UNIVERSITY
GRADUATE SCHOOL OF NATURAL AND APPLIED SCIENCES
DEPARTMENT OF ELECTRICAL AND ELECTRONIC ENGINEERING

EFFECT OF SEGMENTATION ERRORS ON OFF-ANGLE IRIS RECOGNITION

Prepared by
Sema KELEŞ ÇETİN

Supervisor
Assist. Prof. Dr. Hasan ZORLU

MSc Thesis

January 2017
KAYSERİ

T.C.
ERCIYES UNIVERSITY
GRADUATE SCHOOL OF NATURAL AND APPLIED SCIENCES
DEPARTMENT OF ELECTRICAL AND ELECTRONIC ENGINEERING

EFFECT OF SEGMENTATION ERRORS ON OFF-ANGLE IRIS RECOGNITION

(MSc Thesis)

Prepared by
Sema KELEŞ ÇETİN

Supervisor
Assist. Prof. Dr. Hasan ZORLU

January 2017
KAYSERİ

SCIENTIFIC ETHICS DECLARATION

I hereby declare that all information in this document has been obtained and presented in accordance with academic rules and ethical conduct. I also declare that, as required by these rules and conduct, I have fully cited and referenced all material and results that are not original to this work.

Sema KELEŞ ÇETİN

SUITABILITY FOR GUIDE

The MSc thesis entitled **Effect of Segmentation Errors on Off-Angle Iris Recognition** has been prepared in accordance with Erciyes University Graduate Education and Teaching Institute Thesis Preparation and Writing Guide.

Prepared by

Sema KELEŞ ÇETİN

Supervisor

Assist. Prof. Dr. Hasan ZORLU

Chairman of the Department of Electrical And Electronic Engineering

Prof. Dr. Necmi TAŞPINAR

ACCEPTANCE AND APPROVAL PAGE

This study entitled "**Effect Of Segmentation Errors On Off-Angle Iris Recognition**" prepared by Sema KELEŞ ÇETİN under the supervision of Assist. Prof. Dr. Hasan ZORLU was accepted by the jury as MSc. Thesis in Electrical And Electronic Engineering Department.

12/06/2017

JURY:

Supervisor : Assist. Prof. Dr. Hasan ZORLU

Juror : Assoc. Prof. Dr. Alper BAŞTÜRK

Juror : Assist. Prof. Dr. Bekir Hakan AKSEBZECİ

APPROVAL:

That the acceptance of this thesis has been approved by the decision of the Institute's Board of Directors with the 20/06/2017 date and ..2017/27-25 numbered decision.

..29.V.06/....2017

Prof. Dr. Mehmet AKKURT

Director of the Institute

ACKNOWLEDGEMENT

I would like to express sincere appreciation to my supervisor Asst. Prof. Dr. Hasan ZORLU for his support.

I express my special thanks and appreciation to my husband Ahmet ÇETİN for his understanding motivation and endless patience during the course of my thesis.

I have to thank my friends Merve BALKİ for her encouragement, support, understanding and patience.

I want to thank all colleagues and friends who made my thesis phase a memorable and valuable experience.

EFFECT OF SEGMENTATION ERRORS ON OFF-ANGLE IRIS RECOGNITION

Sema KELEŞ ÇETİN

Erciyes University, Graduate School of Natural and Applied Sciences
M. Sc. Thesis, Jan, 2017
Supervisor: Asst. Prof. Dr. Hasan ZORLU

ABSTRACT

Biometric systems are used for determine identification by using properties of the subjects such as fingerprint, face, voice, signature, hand and vessel geometry and iris recognition. Because iris texture is unique and most stable biometric in the human body. Previous work show that iris recognition system's accuracy depends on quality of captured image and similarity of the data capture conditions. In this thesis, our main objective examines effect of segmentation errors on off-angle iris recognition. Initially we used automatic segmentation algorithm for doing off-angle segmentation and then we fixed iris segmentation error with using Ground Truth Tool. After that we add error on off-angle segmentation parameters to observe how Hamming distance change for different off-angle iris image. Then, we investigate different normalization techniques where reference points are pupil center or limbus center and bit shift methods to decrease the segmentation errors. Finally, we test these techniques with the same errors in the off-angle iris parameters at the Melikşah University off-angle dataset (-50 to +50 degree with increment 10 degree). We present our experimental results for without errors for using pupil center and iris center. Based on our experimental results, pupil center Hamming distance result well than iris center Hamming distance result. So we choose pupil center for doing better normalization on off-angle iris images. We observed that orientation along with errors effect of segmentation and orientation much more decrease accuracy from other parameters. We used bit shift method to fix and decrease error on orientation. We observe that bit shift method give effective result for our experiments.

Keywords: Iris recognition systems, off-angle iris segmentation, parameters of off-angle iris segmentation, off-angle iris recognition systems, stand-off iris recognition systems.

SEGMANTASYON HATALARININ YAN CEPHE İRİS TANIMAYA ETKİSİ

Sema KELEŞ ÇETİN

Erciyes Üniversitesi, Fen Bilimleri Enstitüsü
Yüsek Lisans Tezi, Ocak 2017
Danışman: Yrd. Doç. Dr.Hasan ZORLU

ÖZET

Biyometrik sistemler, bireylerin özelliklerini kullanarak kimlik tespiti yapabilmektedir, örnek olarak parmak izi, yüz, ses, imza, el ve damar geometrisi ve iris tanıma gösterilmektedir. Yapılan çalışmalar iris tanıma sisteminin doğru ve güvenilir olabilmesi için çekilen göz görüntüsünün aynı şartlar altında ve iyi kalitede olması gerektiğini göstermektedir. Bu tezde bizim temel amacımız yan cephe iris görüntülerinde segmantasyon parametrelerinin etkilerini incelemek. İlk olarak yan cephe görüntülerde segmantasyon yapabilmek için otomotik segmantasyon algoritmasından yararlandık ve otomotik segmantasyon algoritmasında oluşan iris segmantasyon hatalarını Ground Truth Tool kullanarak manuel ve otomotik bir şekilde hataları düzelttik. Farklı yan cephe iris görüntüleri için Hamming uzaklığın nasıl değiştiğini sunduk. Gözbebeği ve iris merkezlerini kullanarak farklı normalizasyon tekniklerini araştırdık ve bit kaydırma yöntemini açıklayarak hatalı segmantasyon parametreleri üzerindeki etkisi incelendi. Farklı normalizasyon tekniklerinde iris ve gözbebeği merkezleri kullanarak orjinal yan cephe görüntüler için hatasız Hamming sonuçlarını sunduk. Bu sonuçlara dayanarak normalizasyon ve segmantasyon yaparken gözbebeği merkezi kullandık. Son olarak yan cephe iris segmantasyon parametrelerinden hangisinin iris tanıma doğruluğunu daha çok etkilediğini gözlemlemek için düzelttiğimiz iris segmantasyon parametrelerine hata ekledik. Segmantasyon parametrelerinden hata eklenen açı parametresinin diğer parametrelere göre doğruluğu daha çok azalttığını gözlemledik. Bit kaydırma metodu kullanarak hatalı açı parametresinin hata oranını ve hatayı azaltmayı hedefledik. Bit kaydırma metodu deneylerimiz için etkili sonuçlar elde ettik.

Anahtar kelimeler: İris tanıma sistemleri, yan cephe iris segmantasyon, yan cephe iris segmantasyon parametreleri, yancephe iris tanıma sistemleri, uzaktan iris tanıma.

TABLE OF CONTENTS

EFFECT OF SEGMENTATION ERRORS ON OFF-ANGLE IRIS RECOGNITION

CHAPTER 3

EFFECT OF SEGMENTATION ERRORS IN OFF-ANGLE IRIS RECOGNITION

CHAPTER 4

TOLERATION OF SEGMENTATION ERRORS IN OFF-ANGLE IRIS IMAGES

CHAPTER 5

EXPERIMENTAL SETUP AND RESULTS

CHAPTER 6

LIST OF FIGURES

CHAPTER 1

INTRODUCTION

Advancement in technology along with the ever growing human population led to the need of better security systems. Biometric systems provide the recognized electronically by using the properties of the people. Examples of biometric systems fingerprint, face, voice, hand geometry, vein and iris recognition can be given.

Previous works in biometric systems shows that iris recognition system is the most reliable, accurate and distinctive system in comparison any other systems [1-3]. Because iris recognition system is unique and most stable biometrics in the human body. Iris recognition system provides strong security, higher usability and faster approach.

Initially the idea of iris recognition has designed by Flom and Safir in 1987. Their works result showed that iris anatomy unique and constant during a human's life [3,5-7]. John Daugman is developed first iris recognition system in 1993 [1]. John Daugman can be counted as the inventor of this area. His similar versions of his inspiring approach are still using by the current systems. Daugman's approach is to use iris image for iris recognition system. He designed traditional iris recognition system. His design is the most important work for iris recognition. For this reason in 1994, with his design publications, he took patented that shows how traditional iris recognition systems formed. Iris biometrics improved by means of Daugman's iris recognition design. Recent studies in the literature have generally focused on deriving new algorithms to remove the effects of eyelid occlusions, specular refraction, illumination and depth of field for the frontal iris images.

Iris recognition systems have started using much more in 2001 [5].These systems provide identity management to strengthen global security. The need of high efficiency

access control millions of people passing sensitive locations. Examples of these locations are passport control, restricted military zones, identification of employees, and staff payroll system to airports for security control, criminal/terrorist seek, missing person and shopping centers.

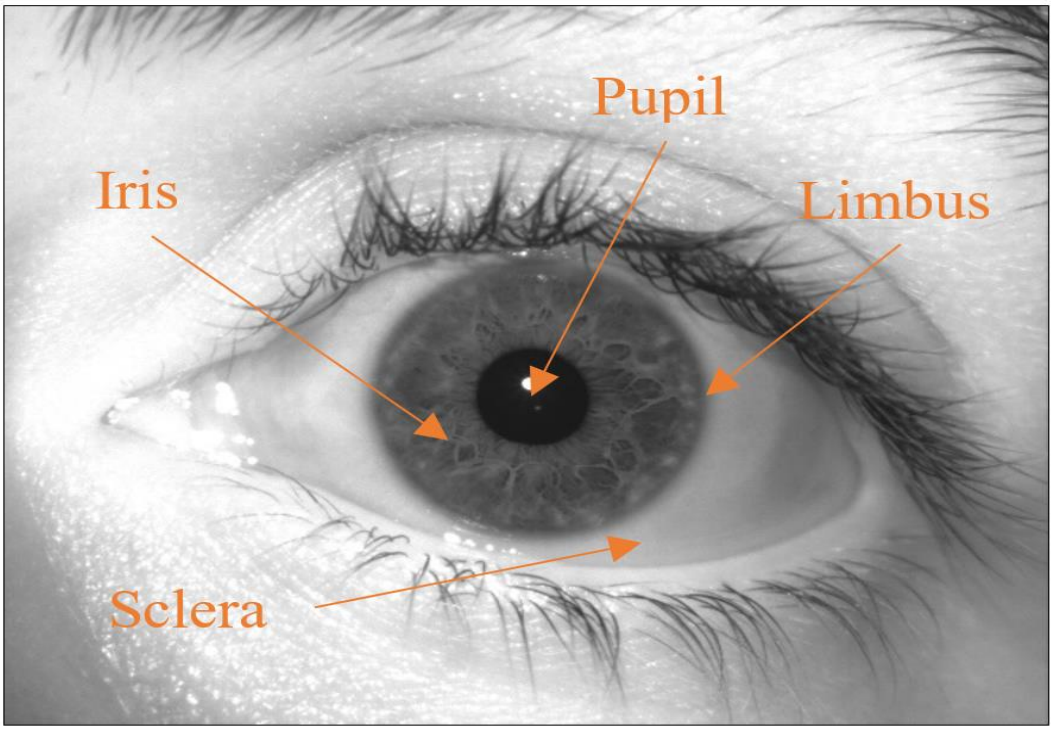

Figure 0.1. Illustration of captured eye image.

Iris recognition system is known these properties accuracy, distinctiveness and reliability. However the iris recognition system's accuracy depends on the quality of iris images capture, this means, several factors such as image acquisition angle, occlusion, pupil dilation, image clarity, and focus, and same conditions of iris images must be frontal image for the traditional iris recognition system.

The most difficult problems of iris recognition systems are stand-off iris recognition and off-angle iris recognition. Stand-off iris recognition systems challenges are gaze angle, corneal refraction, limbus occlusion, depth of field blur and dilation. The aim of this thesis, investigate the effect of iris parameters errors as well as proposing new techniques, to improve the performance of iris parameters on off-angle iris recognition.

1.1. IRIS RECOGNITION

First iris recognition system developed by John Daugman in 1993 [1]. His method includes five main steps. These names are iris capture, iris segmentation, iris normalization, iris encoding and iris matching. Other methods in iris recognition systems include same steps. This system shows that which eye belongs to same or different people. Figure 1.2 illustrates flowchart of iris recognition systems.

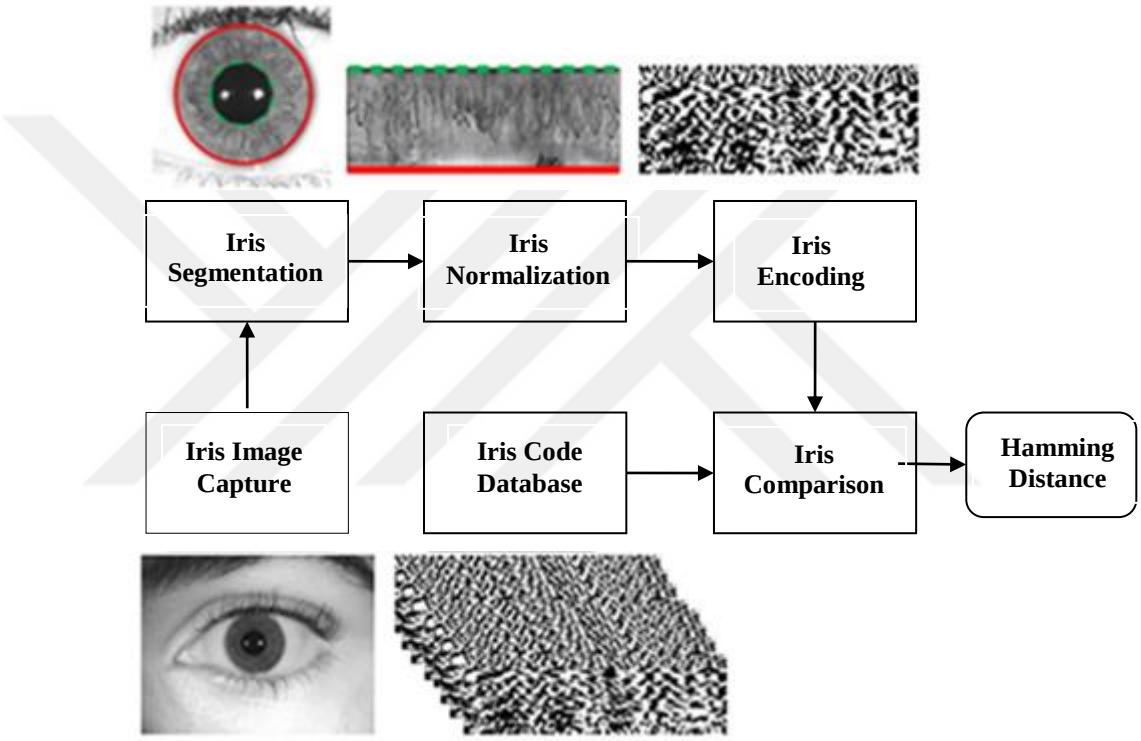

Figure 0.2. Illustrates flowcharts of iris recognition systems.

Iris image capturing is the first step in traditional iris recognition systems. For this system, person stands in front of near infrared sensitive imaging device and iris image capturing must be given frontal image by person. If the iris recognition systems don't capture ideal iris image, it repeats image capturing until ideal image captured. Received images must be same quality and conditions. If iris image capture from frontal, probability of non-ideal iris image is very low.

Segmentation refers to process of automatically detecting pupil and iris boundaries on eye image. Segmentation determines the area of iris, between pupil and sclera boundaries. This process helps to find iris texture. Incorrect segmentation reduces performance of the recognition system. The most segmentation techniques are integro-

differential operator [1] and the Hough transform [12], respectively. It is used circle algorithm. The performance of iris segmentation techniques based on iris image quality. Effects of segmentation challenges are occlusion, specular reflections, illumination variation, and blur. If eye image under challenging conditions, segmentation performance decrease.

Iris normalization is the third step in iris recognition system. After segmented iris image, it is transformed from Cartesian coordinates to polar coordinates. The homogenous rubber sheet model devised by Daugman remaps each point within the iris region to a pair of polar coordinates theta and rho (r, θ). Theta sample 512 different angle value between 0 and 2π. It consists of 512 matrixes and each matrix size is 1x64. Rho sample 64 different sample points between 0 and 1. This parameter is distance from iris center. It consists of 64 matrixes and each matrix size is 1x512.Using polar coordinate system by iris normalization; circular iris texture converts to dimensionless rectangular configurations. **Hata! Başvuru kaynağı bulunamadı.** shows Daugman's iris normalization rubber sheet model and summarizes the normalization process.

Normalized iris image produced code similar to DNA sequence. This code consists of 0 and 1 by using Gabor wavelet demodulation. If we directly compare iris images without coding, it is possible to more errors between compared pixels, due to the lighting and brightness.

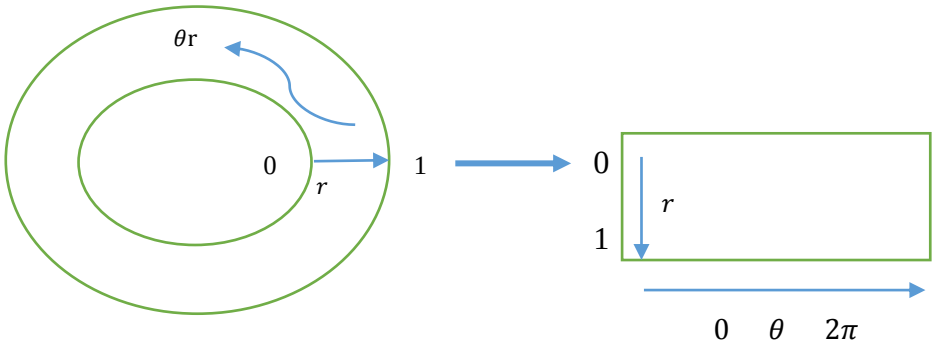

Figure 0.3.Daugman'siris normalization rubber sheet model (adapted from [11])

Iris comparison is the last step in iris recognation system. For this step generally used Hamming distance tecnique. After iris code comparison the other iris code in database, calculated Hamming distance. If hamming distance under the threshold , it is intra class which means iris images belongs to same people. If hamming distance above the

threshold, it is inter class which means these images belongs to different people.Hamming distance can be mathematically expressed as:

$$\mathrm{HD} = \frac{\|(codeA \otimes codeB) \cap maskA \cap maskB\|}{\|maskA \cap maskB\|} \quad (1.1)$$

1.2. ACCURACY DEGRADATION FACTORS FOR IRIS RECOGNITION

In this part we give brief about negative effects of accuracy factors in iris recognition system. Accuracy and reliability of iris recognition system depends on these factors which pupil dilation, occlusion, image quality, focus, blur, specular reflections, illumination variations and off-angle iris images. We want to explain these effects;

Pupil dilation is the negative effect for iris recognition system. Effects of illumination conditions change pupil size. If illumination conditions are different for same people's iris images, hamming distance result change and give false result. Because hamming distance is different and over the threshold it means it is not same people. Pupil dilation directly affected hamming distance score.

Eyelids and eyelashes cover and protect the human eye from dust and foreign bodies. Occlusion reduces the iris pattern so changes segmentation of iris because of eyelids and eyelashes have blink reflex. For this reason, occlusion change visibility and negatively affected segmentation of iris and accuracy in iris recognition system [21].

Iris image quality is the most important for iris recognition. If capturing iris image is bad quality, result of iris recognition accuracy low why each pixel on iris pattern very important for iris recognition. Because of this for taking accuracy result from iris recognition system, iris image quality must be good [2, 17, 22-24].

Specular reflection caused by segmentation errors and degrades iris recognition accuracy. It is captured by imaging device and affected on white color and ambient texture like cornea and aqueous humor [2].

Illumination variations negatively effects of pupil size, reflections of light on cornea and angle. These effects decrease in accuracy in iris recognition system.

1.3. STAND-OFF IRIS RECOGNITON SYSTEMS

Stand-off system's purpose is automatically identification of persons. This system doesn't need any relations between subject and imaging device. Frontal image is using in traditional iris recognition system while off-angle iris image is using stand-off iris recognition system. The eye and camera must be perpendicular to each other, for frontal iris images. Off-angle means different angle between camera and eye. Figure 1.4 shows examples of frontal and off-angle iris images. While in traditional iris recognition system the person stands in front of an infrared sensitive imaging device and iris images must be captured from front, in stand-off iris recognition system automatically identify induvial, using captured iris image at a distance and different angle [7]. For these specialties of stand-off system, it is used a lot of place where passport control, airports, shopping center and much more.

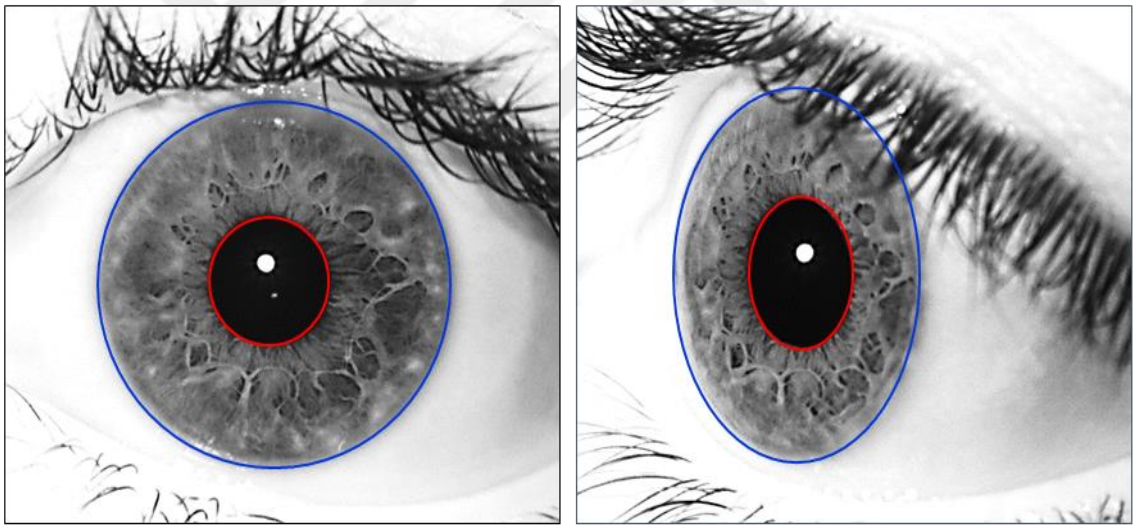

Figure 0.4.Examples of frontal and off-angle images.

An off-angle iris image between frontal iris images different is angle. To captured off-angle iris image, imaging device isn't perpendicular to iris plane. Frontal image's shape is circle but off-angle image's shape is ellipse which means changed iris texture. Therefore off-angle iris image decreases accuracy in iris recognition. Stand-off iris recognition system challenges are corneal refraction, change in form of three-dimensional complex iris texture [16], depth-of-field out of focus blurring, image acquisition angle, and limbus impact. It shows poor performance beyond thirty degree

because of this off-angle iris images cause accuracy degradation both in stand-off iris recognition systems and in frontal iris recognition systems.

1.4. EYE STRUCTURES

In this part we are talking about eye structures which effect on iris recognition. These eye structures are eyelid, limbus, eyelash, cornea, pupil, iris, sclera and lens. To investigate of eye structures' effect on iris segmentation, we must focus on anatomy of human eye. You can find in more details [1, 11-15].Iris structures shown in Figure 1.5.

Eyelid covers and protects the human eye. It protects eye from dust and foreign bodies. Eyelids keep the human eye from drying out when asleep. Furthermore the blink reflexes to protect the human eye from foreign bodies. Eyelashes are human hairs on the upper and lower eyelids. There are small muscles located in the eyelids which, with a muscular contraction, reflexive and automatic response, they blink and close the eyes before an external threat, like particles of dust, or any foreign agent which could cause damages to the eyes. Eye's outermost layer is cornea. It covers front of eye. Moreover, it is the clear, dome-shaped surface that covers the front of the eye. Limbus is a semitransparent tissue which overlaps the side portion of the iris at the intersection of the cornea and sclera.

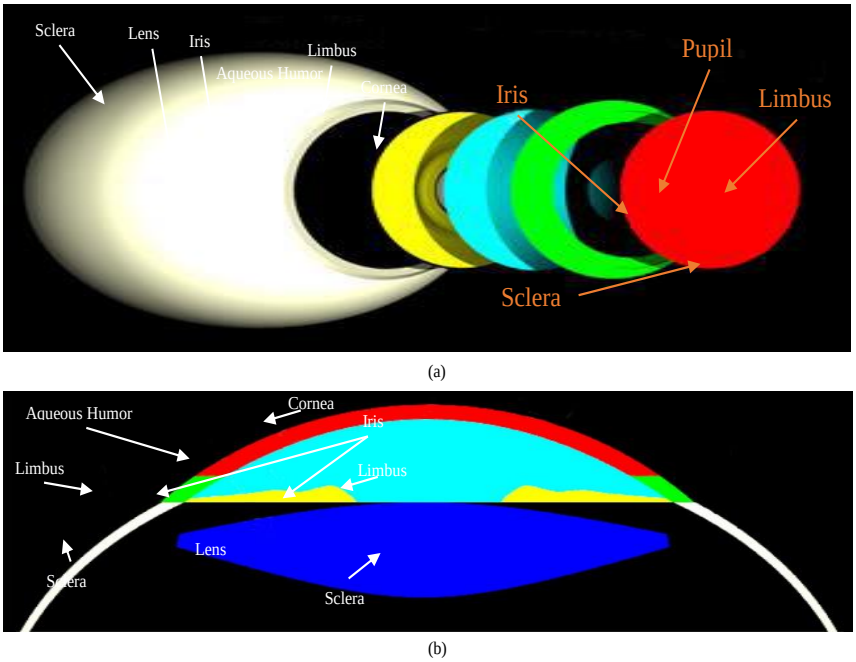

Figure 0.5. Illustration of eye components using (a-b) biometric eye model (adapted from [16])

The aqueous humor is the watery fluid is a semitransparent tissue which overlaps the side portion of the iris at the intersection of the cornea and sclera. The aqueous humor is the watery fluid. Watery fluid is between the cornea and the crystalline lens. Aqueous humor protects the pressure needed to inflate the eye. The colored part of the eye called the iris. Iris is the circular structure in the eye. It is responsible for protects controlling the diameter and size of the pupil and so it protects the amount of light reaching the retina. The pupil is a whole center of the eye. It's color black. That's why light rays entering the pupil are either absorbed by the tissues inside the eye directly. Lens is transparent, biconvex structure in the eye. It helps to refract light to be focused on retina. The sclera is white part of the eye. It gives the eye, shape containing collagen structure [18].

1.5. THESIS OBJECTIVES

The purpose of this thesis is to show the effect of the segmentation errors in off-angle iris images and to improve the segmentation accuracy for off-angle iris images. Off-angle iris is segmented as ellipses due to the appearance of the iris become an ellipse. Therefore, the segmentation parameters of an off-angle iris image is generated as ellipse parameters that are $x, y, r1, r2$ and θ where x, y denote the center coordinates, $r1, r2$ denote the radius of major and minor axis and denotes the angle of the ellipse.

In this thesis, we first study the effect of segmentation errors on off-angle iris recognition. Segmentation errors are occurred by effects of segmentation parameters. For this reason, firstly we work on effects of segmentation errors in off-angle iris images. All parameters examined how effects on iris recognition system. Initially, we observe how Hamming distance changes for different off-angle iris images. Exact segmentation results were obtained from using Ground Truth program. We added errors on these results, after those effects of parameters observed. For off-angle iris images, we were used Melikşah University Iris Dataset (MUID). Finally, we suggest that decrease effect of errors on off-angle iris recognition (such as, -10, -20, -30, -40, -50, 0, 10, 20, 30, 40, and 50 degrees).

1.6. THESIS OUTLINE

The rest of this thesis is structured as follows: Chapter 2 presents previous works in iris recognition system, frontal iris segmentation, and off-angle iris segmentation and degradation factors on iris segmentation. In Chapter 3, the effect of parameters errors on off-angle iris recognition is presented. In addition to this we give information about off-angle segmentation algorithm and Ground Truth Tool.

We present normalization techniques which reference points are pupil center and iris center. We explained bit shift method for decrease segmentation errors in Chapter 4. We show that off-angle iris segmentation errors effect. We used Melikşah University off-angle dataset for our experiments. Experiment and result presented in Chapter 5. Finally, we give result of our thesis and we conclude in Chapter 6.

CHAPTER 2

BACKGROUND AND RELATED WORKS

In this chapter, we introduce the background of the iris segmentation and briefly presented the related works in iris segmentation. Therefore, we divided related works in iris segmentation into four parts as follows:

• Related works on iris recognition

• Related works on frontal iris segmentation

• Related works on off-angle iris segmentation

• Related works on degradation factors in iris segmentation

2.1. RELATED WORKS ON IRIS RECOGNITION

With development technology, researchers need to design an automatic identification system benefit from frontal iris recognition. Limiting factors of frontal iris recognition systems, such as just frontal image captured and person had to stand in front of camera for identification of person. For these limiting factors on frontal iris recognition, researchers build stand-off iris recognition using iris biometrics. Stand-off iris recognition system using where subjects' and operators' collaboration aren't acceptable and without any angle limiting for captured iris images. In this part we give brief related works about regarding stand-off iris recognition systems. In stand-off iris recognition systems, person hasn't to stand in front of the camera. This system allows person identification while person is on the move and capturing off-angle image from person of interest. Changing of acquisition iris image's angle, captured of iris shape transforms circular to elliptical. This situation's challenges are corneal distortions, limbus occlusion, lens distortions, three-dimensional iris texture distortions and depth of field

out of focus blurring. Despite the new research area in off-angle iris recognition, a few works are available.

Bowyer et al. firstly gathered information about iris recognition systems in 2007. They worked on iris recognition's historical development and state of the art. They presented new approaches about traditional iris recognition called Daugman's iris recognition system's part which are iris segmentation, iris normalization, iris encoding and iris matching. After all, they come up with an idea for medical conditions may decrease accuracy of iris recognition [5].Figure 2.1 shows the frontal iris recognition system.

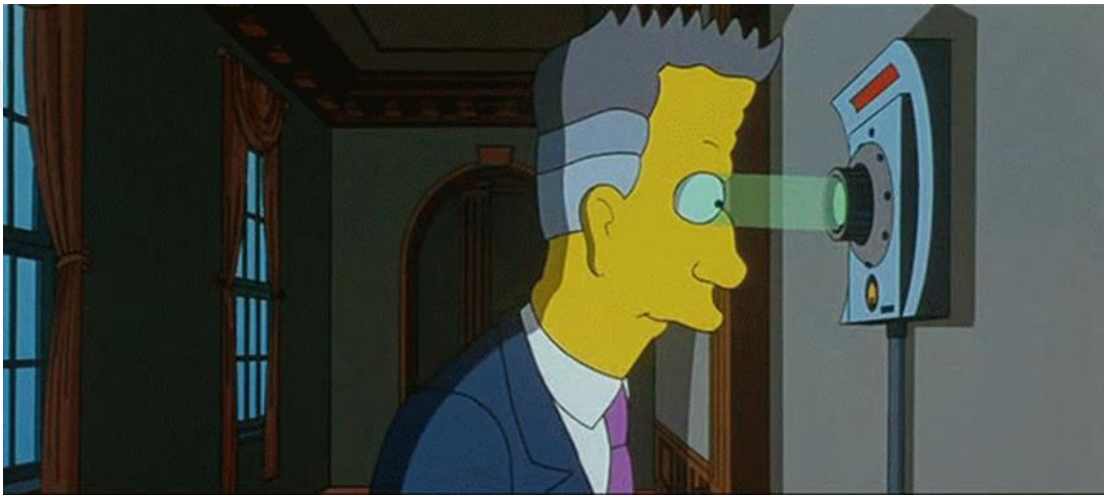

Figure 0.1.Examples of frontal iris recognition system.

Frigero et al. presented rectification method for off-angle iris images [10]. In their method, they worked on effect of distortion eye morphology and reflectance properties. They used Ekional equation. Their method improved in the off-angle iris recognition but this improvement not enough for full accuracy off-angle iris recognition. Because they only focused on corneal refraction effects.

Santos-Villalobos et al. [27] used ray-tracing method on biometric eye model to improve capturing off-angle iris images. This method gave excellent improvement result for synthetic off-angle images but it isn't enough for real iris images. Because they disregarded limbus impact other challenging issues in off-angle iris recognition.

Cerme and Karakaya in [16] created different eye model for investigated three-dimensional iris texture effects of off-angle iris recognition. They showed that if the

image acquisition angle change, iris plane change. Their experiment result is showed that three- dimensional iris texture degrades accuracy in off-angle iris images.

Craig Fancourt et al. in 2005 [4] showed that the distance can up to 10m between person and camera. With helping of infrared camera and telescope, they captured 250 person's iris images are in different distance and different conditions such as illumination variation and image acquisition angle. They presented that this distance has no performance degradation

J.R. Matey et al. showed that iris image can capture while person is walking [6]. They developed "Iris on the Move" system based upon high resolution cameras and video systems. They showed that iris image can captured while subject is walking on place. In their system, person is walking through 3m an access control point in the system area and person is constrained to look at camera.

In the stand-off iris image capturing systems have several related works. S. Yoon et al work on iris image capturing system by using light stripe projection and pon-tilt-zoom (PTZ) camera in [8]. They presented this system based on locating person's position. The other work on stand-off iris image capturing system designed by C. Boehnen et al. in [34]. They presented the stand-off multimodal biometric system at Oak Ridge National Laboratory (ORNL). Their system can manage up to 7 meters in range based on PTZ system. Their developed system show that iris image of person can automatically identification on the move or staying stable. Figure 2.2 shows the stand-off iris recognition system.

Figure 0.2.Examples of the stand-off iris recognition system.

With development technology, researchers need to design an automatic identification system benefit from frontal iris recognition. Limiting factors of frontal iris recognition systems, such as just frontal image captured and person had to stand in front of camera for identification of person. For these limiting factors on frontal iris recognition, researchers build stand-off iris recognition using iris biometrics. Stand-off iris recognition system using where subjects' and operators' collaboration aren't acceptable and without any angle limiting for captured iris images.

2.2. RELATED WORKS ON FRONTAL IRIS SEGMENTATION

In this part we give brief related works about frontal iris segmentation. Firstly we want to start from Daugman's work about iris recognition systems. Daugman presented the first iris recognition system in 1993 [1]. His system includes five parts which are image capturing, iris segmentation, iris normalization, iris encoding and iris matching. We mentioned these parts in Chapter 1. He used integro-differential operator for determine the segmentation boundary. His method based on circular shape for doing segmentation. His integro-differential operator mathematically expressed as:

$$\max(r, x_0, y_0) \left| G_\sigma(r) * \frac{\partial}{\partial r} \oint_{r,x_0,y_0} \frac{I(x,y)}{2\pi r} ds \right| \qquad (2.1)$$

where

$$G_\sigma(r) = \frac{1}{\sqrt{2\pi}\sigma} exp^{-\left(\frac{(r-r_0)^2}{2\sigma^2}\right)} \quad (2.2)$$

This mathematically expression showed that $r0$ is refers to a radial Gaussian with a center, σ is the standard deviation and * symbol denotes the convolution operation. Daugman's integro-differential operator performs circular shape for iris segmentation. Circular shape consist three parameters which are $x0\ and\ y0$ center coordinates and $r$radius of the circle. Iris database including from 152 nations to 316250 subjects consist of 632500 different iris patterns. He compared of iris codes 200 billion times to cross for each iris pairs.

Wildes R.P. [13] presented iris segmentation algorithm. His algorithm fit circle with using circular Hough transform for detects iris and pupil edge points. Hough transform mathematically expressed as:

$$H(x_c, y_c, r) = \sum_{i=1}^{n} h(x_i, y_i, x_c, y_c, r) \quad (2.3)$$

where

$$h(x_i, y_i, x_c, y_c, r) = \begin{cases} 1, & if\ g(x_i, y_i, x_c, y_c, r) = 0 \\ 0, & otherwise. \end{cases} \quad (2.4)$$

and

$$g(x_i, y_i, x_c, y_c, r) = (x_i - x_c)^2 + (y_i - y_c^2) - r^2 \quad (2.5)$$

In mathematical expression, (xi, yi) refers to each edge point in the set, If the parameter refers to $(xc, yc, r), g(xi, yi, xc, yc, r)$ considered to be 0. $H(xc, yc, r)$ is an accumulator array and this array finds most suitable parameters for circle. Equation 2.5.is showed that this equation modified to different contours such as circle, ellipse or parabola but increase computational complexity for parabola and ellipse.

Huang et al. [26] worked on noises in segmented iris regions which are eyelashes, eyelids, reflections and pupil. Their purpose of their work improving the performance of recognition system with using new noise-removing approach. Their approach based on the fusion of edge and region information. These processes have three steps which are

rough localization and normalization, edge information extraction based on phase congruency, and the infusion of edge and region information. Their experimental results showed that proposed method for improving performance iris recognition is hopeful.

Joseph W. Thompson and Patrick J. Flynn [20] presented a new approach for iris recognition system. Their approach based on improving recognition performance perturbations of iris segmentation. Firstly iris segmentation is found by existing segmentation techniques. Normalized iris pattern are provided owing to perturbation of the segmentation parameters, which are x, y and r employed in matching. This match score distributions is used to improve the iris recognition accuracy of the original algorithm. Their experimental results showed that the performance of accuracy iris recognition system improving ranging from %24 to %35.

2.3. RELATED WORKS ONOFF-ANGLE IRISSEGMENTATION

Daugman proposed to find off-angle iris boundary as elliptical shapes by using active contour [26]. This approach uses elliptical unwrapping. His approach ignores challenges of angle such as limbus impact, corneal refraction, three- dimensional iris texture and image acquisition. For this reason, his method showed poor performance beyond 30° images. Figure 2.3 shows the off-angle iris recognition system.

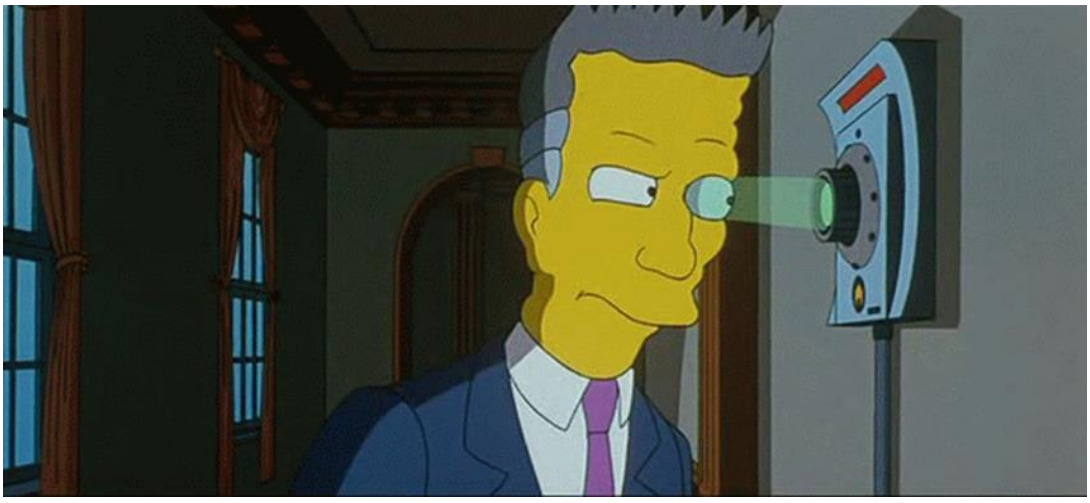

Figure 0.3.Examples of the off-angle iris recognition system.

Purpose of Shuckers et al. [9] transform off-angle iris image to frontal iris image. They used simple techniques such as elliptical unwrapping and affine transforms. However their approach showed poor performance beyond 30° images. Because they only

focused on perspective projection and they neglected other challenging in off-angle iris recognition.

H. Proença and L.A. Alexandre proposed a new algorithm for off-angle iris segmentation [3]. Traditional segmentation method's performance decreases on non-ideal iris images. Their iris segmentation method firstly start with feature extraction from captured iris image and then they used fuzzy clustering algorithm for classify each pixel and produced normalize image. After that canny edge detector detects edge to set edge map on normalized iris image. Finally they apply circular Hough transform on edge map for determine segmented iris. Their proposed algorithm showed that segmentation for off-angle iris image performs well under degradation factors.

Shah and Ross [50] described a new segmentation model with using geodesic active contours (GACs). Traditional segmentation models developed by using active contours which can assume any shape and segment multiple objects. Their proposed scheme shows the iris texture from eye image. Their proposed segmentation algorithm observed to improve matching accuracy on iris recognition.

Karakaya et al. [2] presented segmentation algorithm for off-angle iris recognition. Their algorithm consists of four main steps which are edge detection, edge elimination, edge classification and ellipse fitting. Their approach eliminates the edges which cannot part of iris or pupil boundary with using edge orientation. Result of their experiments showed that their iris segmentation algorithm can segment beyond 30° effectively.

2.4. RELATED WORKS ON DEGRADATION FACTOR IN IRIS SEGMENTATION

In this part, we give information about related works on degradation factors in iris segmentation.

Karakaya et al. [17] studied the impact of limbus on off-angle iris degradation. They measured limbus effect how change the performance of segmentation in iris recognition. They created synthetic iris dataset. They tried to different limbus heights in their simulations. They concluded that limbus effect decreases the performance in iris recognition.

Zuo et al. [25] proposed a segmentation methodology. Their purpose decrease of degradation effects on iris segmentation. These effects are specular reflection, blur, lighting variation and occlusion. They first detected and eliminated specular reflections with using partial differential equation (PDE). Their purpose eliminates occlusions resulting from the pupil area. Pupil and iris segmented by ellipse parameters fitting. They applied contrast-balancing for provide correct iris segmentation. They used ideal and non-ideal data sets which names are the Chinese Academy of Sciences iris data version 3 and the West Virginia University (WVU) data. They compared performance between their implementation to implementation of Camus and Wilde's algorithm. They concluded that their segmentation methodology improved the segmentation performance.

Zhofan H. et al. [23] presented a new algorithm for iris segmentation. They ignored the reflection removal from eye image and then they built on Adaboost-cascade iris detector for extract position iris center. They detected edge points of iris boundaries. Their model localized eyelids via edge detection followed by circular or noncircular shape fitting. Their work based on elimination noise with using rank filter and for ignored the shape irregularity of eyelids with using a histogram filter. They detected eyelashes and shadows on eye image from different iris region. Their experimental results showed that the algorithm performance better for both accuracy and speed.

Mohammad Javad Aligholizadeh et al. [14] proposed a method for eyelid and eyelashes segmentation. Their approach based on wavelet transforms. They used wavelet transforms to detect the eyelashes. Their method have two step, the first step is using wavelet transform for remove eyelashes and the second step eyelashes are segmented by using neural network. Their experimental results for eyelids are eyelashes showed excellent performance. The accuracy of their method for upper eyelid and eyelashes segmentation is 97.88% and for lower eyelid segmentation is 99.2%.

CHAPTER 3

EFFECT OF SEGMENTATION ERRORS IN OFF-ANGLE IRIS RECOGNITION

In this chapter, we give brief about segmentation in off-angle iris recognition. Segmentation is the process of locating pupil and sclera boundary from eye image. Daugman developed traditional iris recognition system in 1993 [1]. His systems have 5 parts which one of them is segmentation. His segmentation shape is circular for frontal eye image. He used circle algorithms such as Hough transform for frontal iris recognition system. In off-angle iris recognition system uses ellipse parameters for off-angle eye image. If segmentation isn't done correctly, iris recognition system's accuracy decreases. Because of that iris recognition system shows poor performance when segmentation isn't true. Eye images are captured from different angles causing the challenging problems in off-angle iris images. As image acquisition angle increases, effects of these problems increases where view of iris plane changes. Challenges in off-angle iris recognition are occlusion, specular reflections, illumination variation, and blur.

3.1. PARAMETERS OF SCLERA AND PUPIL SEGMENTATION

Segmentation is the process of locating pupil and sclera boundaries. Generally iris segmentation methods focused on frontal iris image. These methods used to fit circle for doing segmentation of pupil and iris boundaries. Daugman used integro-differential operator for his iris recognition system [1]. This operator based on three parameters of circle which are x, y and r. Center coordinates of the circle are x and y, radius of the circle is r. These parameters use for frontal iris segmentation. Off-angle iris segmentation used to finding pupil and sclera boundaries in off-angle iris images, both of them are represented with elliptical parameters. As general information about ellipse

have five parameters which are $x, y, r1, r2$ and θ. x and y are the center coordinates, $r1$ and $r2$ are the radius of minor and major axis and θ donates the angle. Figure 3.1shows that pupil and sclera parameters on off-angle iris images.

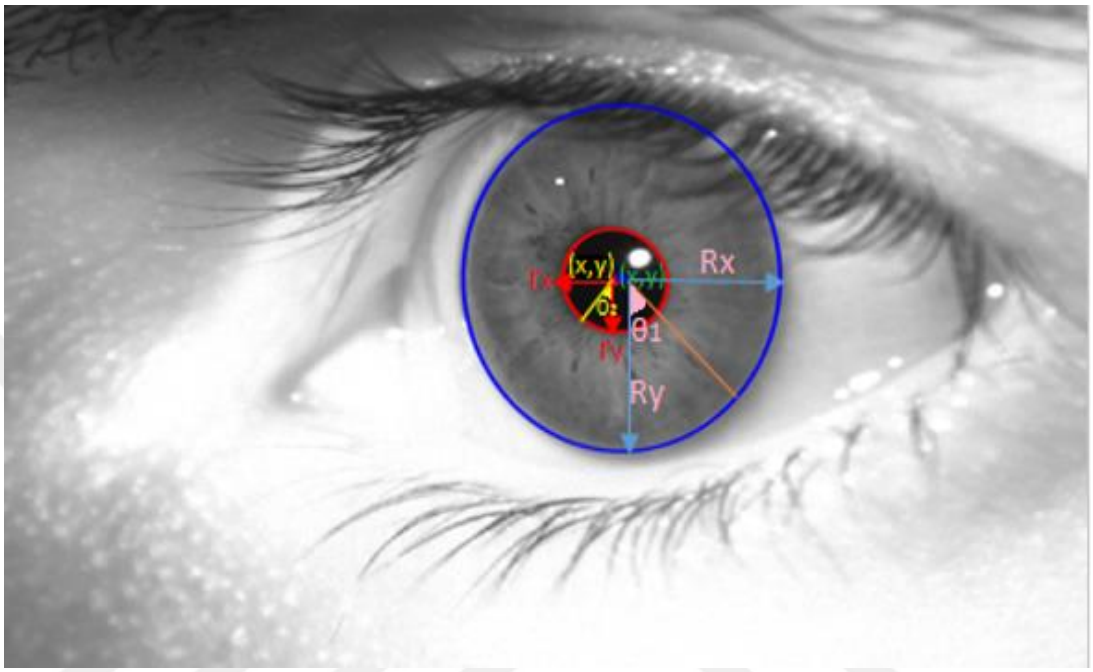

Figure 0.4.Pupil and sclera parameters on off-angle iris images.

3.2. AUTOMATIC SEGMENTATION ALGORITHM

An automatic segmentation algorithm developed by Karakaya et al. [2]. An automatic segmentation algorithm consists of four main steps for doing segmentation in off-angle iris recognition. These steps are edge detection, edge elimination, edge classification and ellipse fitting. Figure 3.2 show that this system firstly detects all candidate edges from eye. These edges not only part of iris and pupil boundary such as eyelid, eyelash and iris texture. Because of this reason, edge orientation is used to eliminate edges which not part of iris and pupil boundary. After that remaining edges are classified as pupil and iris edges. Finally for each subset of pupil and iris fit ellipse and to finding resultant ellipse calculated the average similar parameters. Figure illustration Karakaya et al. [2] work for off-angle iris and pupil segmentation algorithm.

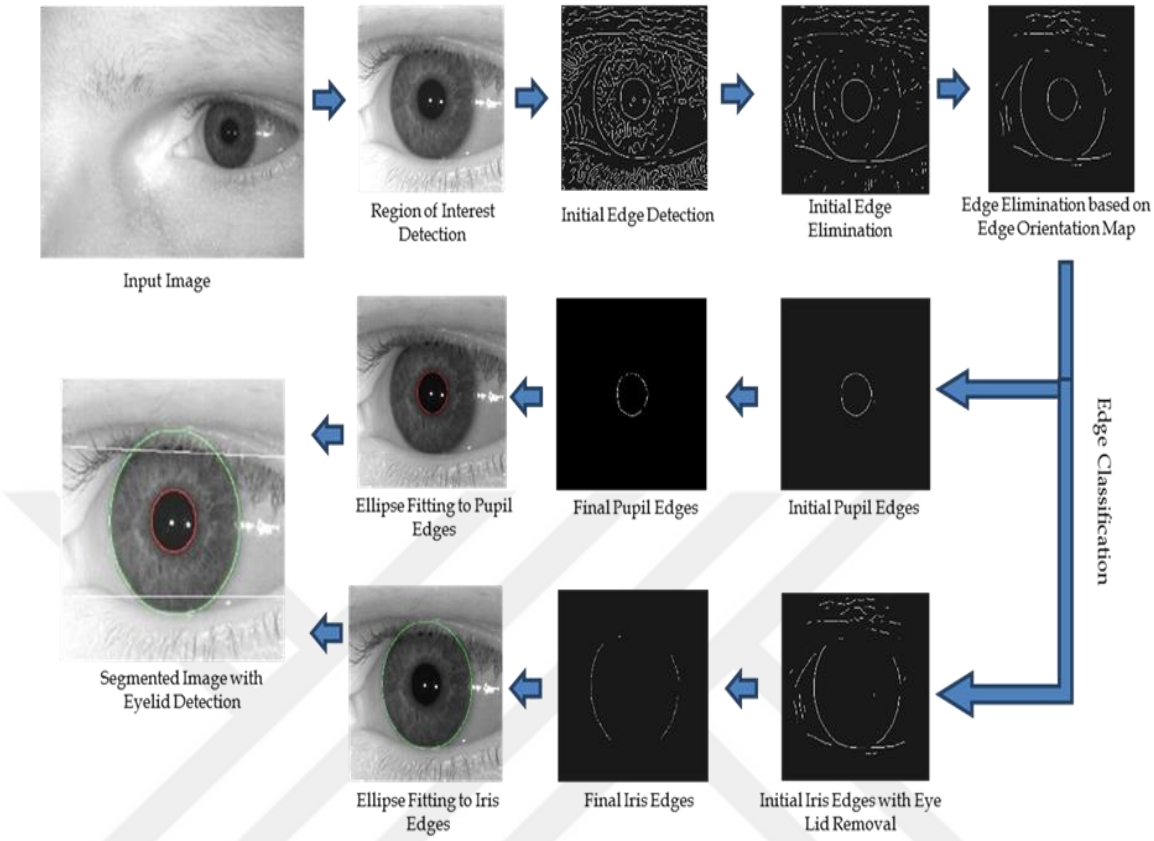

Figure 0.5. Illustration of the proposed off-angle iris and pupil segmentation algorithm [2].

This algorithm tries to find best ellipse for pupil and iris boundary. Overall, the accuracy of pupil center localization is the same for frontal and off-angle iris images. Iris image is changed from frontal to off-angle, the accuracy of iris center localization decreases. When the captured eye image's angle increases, the iris segmentation performance decreases due to the several factors are eyelid occlusion, depth of field blur, and low illumination. This algorithm may give incorrect iris segmentation when processing irises beyond 40°. Figure 3.3 shows examples of true and wrong segmentation on off-angle eye image with using automatic segmentation algorithm [2].

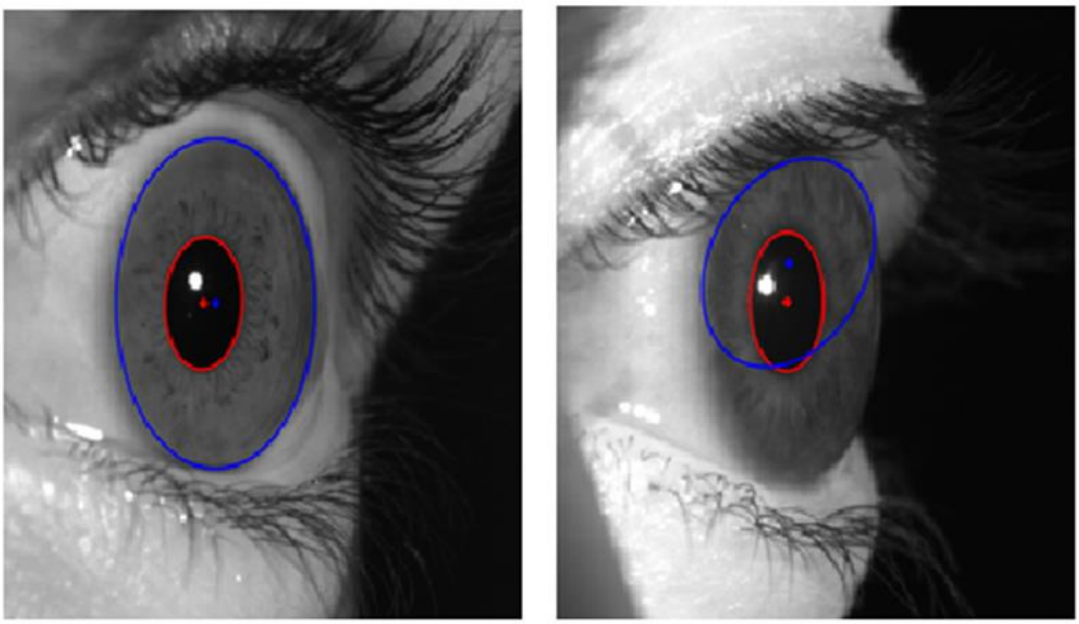

Figure 0.6.Examples of true and wrong segmentation on off-angle eye image.

Generally an automatic segmentation algorithm finds correct pupil segmentation. When captured eye image's angle increases, off-angle iris segmentation performance decreases. For this reason iris segmentation result may give incorrect results. To fixed off-angle iris segmentation is used Ground Truth tool.

3.3. GROUND TRUTH TOOL

Ground Truth Tool (GTT) designed for the Meliksah University IRIS Database by Melih Kurtuncu. The purpose of the GTT is to fix the errors in automated iris segmentation and to find the best ellipse parameters for iris and pupil segmentation and to save these parameters into a text file for the iris recognition. This project provides user to easily control segmentation parameters and fix the segmentation errors. Users can both manually and automatically segment the iris and pupil from the eye image. It is also possible to check the result of the automated segmentation by drawing its results on the screen and changing the prior results. Figure 3.4 shows the graphical user interface (GUI) of the Ground Truth Tool.

Ground Truth Tool (GTT) has several steps for doing segmentation. These steps are depending on the user. General information about the application, firstly user can choose which images want to segmented with a browser. "ReadTxtFile" button check

iris, pupil and eyelid parameters. “MatlabSeg” button is doing automatic segmentation for all chosen and current image. “EyeLid Detect” button detect eyelids. This implementation provides us control segment parameters manually and automatically. As we see in Figure 3.4 parameters of iris and pupil can be controlled with “+”, “-” buttons and the edit box that holds the value.

Figure 0.7.Shows the user interface of the application.

The result of automatic segmentation is not always satisfiable such as the parameters cannot be found or wrong iris segmentation can be occurred. In this situation, the manual segmentation can be used with Ground Truth tool. Blue boundary of iris segmentation is done by automatic segmentation algorithm and green boundary of iris segmentation is done by Ground Truth tool as shown in Figure 3.5.

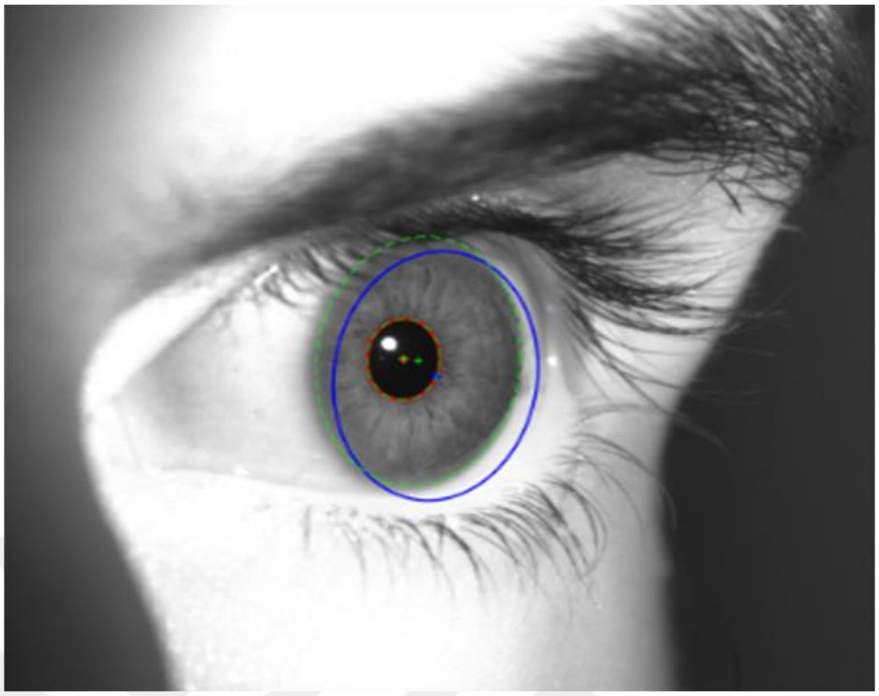

Figure 0.8.Shows the user interface of the application.

3.4. ERRORS IN IRIS SEGMENTATION

An off-angle iris image is segmented as an elliptical region between its inner and outer boundaries. Outer boundary is the region in separating the iris and sclera so it is also called as sclera boundary. In addition, inner boundary is the region in separating the iris and pupil and is also called as pupil boundary. Both sclera and pupil boundaries are segmented by using ellipse parameters for off-angle iris images. Automatic segmentation algorithm [2] finds pupil boundary well but sometimes especially when angle of eye image increase, performance of sclera segmentation decrease for off-angle eye images. Because of this reason we fixed sclera segmentation manually with using Ground Truth tool. In order to present the effect of segmentation parameters, we added errors on the parameters of sclera segmentation. Our purposes how changed iris recognition system with add errors on parameters of iris boundary. We observed parameters of iris segmentation which are $x, y, r1, r2$ andθwegrouped this section into three parts as follows:

• Error in Ellipse Center

• Error in Minor and Major Axis

• Error in Orientation

3.4.1. Error in Ellipse Center

Firstly we used automatic segmentation algorithm [2] for doing iris segmentation. Then we fixed automatic segmentation errors with using Ground Truth Tool. After that we added error on off-angle sclera segmentation with manually and automatically. Initially we observed error in ellipse center on sclera boundary. Ellipse center parameters are $x\ and\ y$ for sclera boundary. When we add errors on ellipse center of iris segmentation, other value of parameters from iris segmentation is stable. Because we observed which parameters affect much more the others. Figure 3.6 shows example of original off-angle iris image and attached error on ellipse parameters of off-angle iris image.

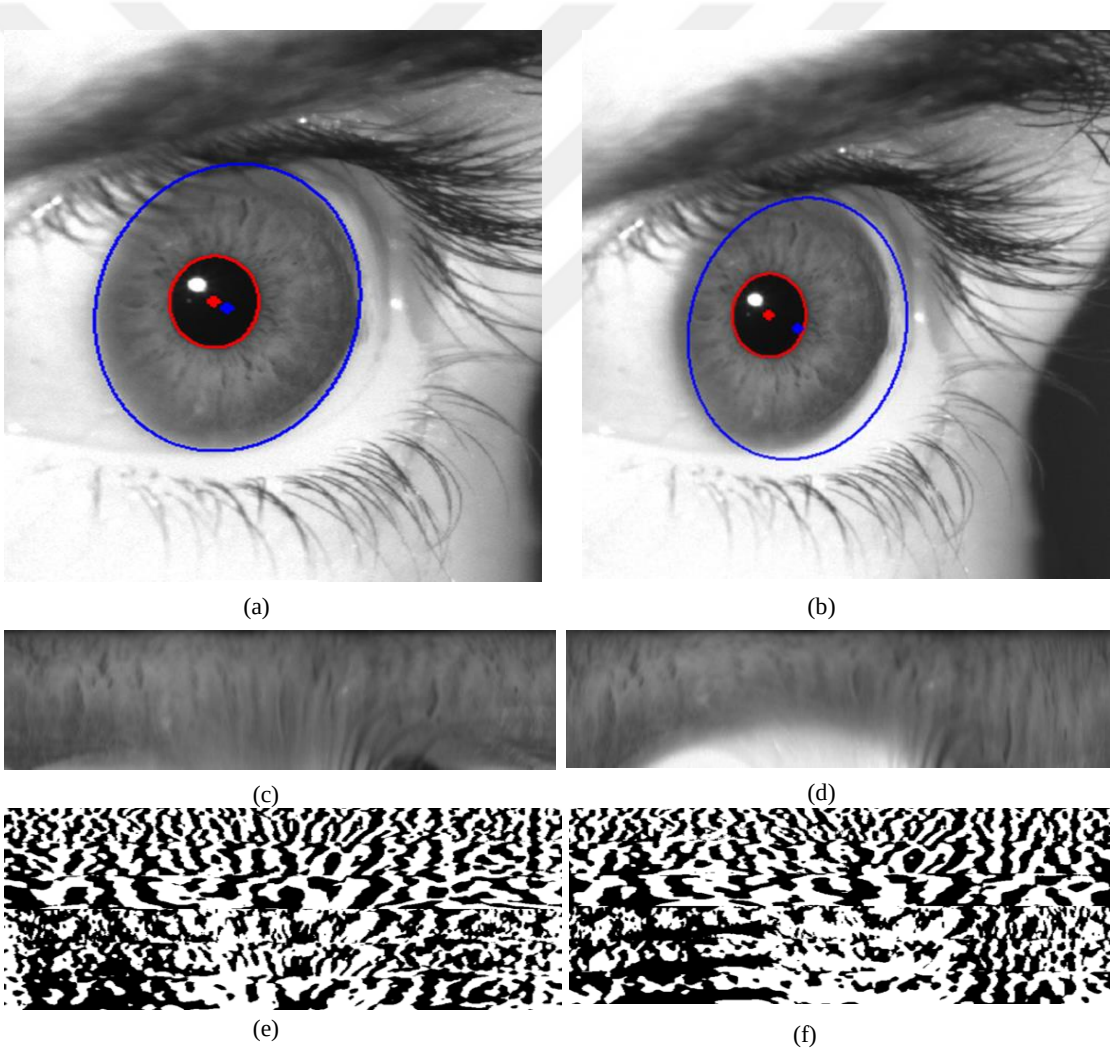

Figure 0.9. Examples of iris images from Melikşah University off-angle iris dataset (a) off-angle segmented iris image (b) off-angle segmented iris image along with error (c) normalized off-angle iris image (d) normalized off-angle iris image along with error (e) off-angle iris image's iris code and (f) off-angle iris image's iris code along with error.

3.4.2. Error in Minor and Major Axis

We can fix automatic segmentation errors and we can control parameters of iris segmentation with using Ground Truth Tool. Initially we fixed segmentation parameters then we added error on off-angle sclera segmentation with manually and automatically. We observed error in minor and major axis on sclera boundary. Minor and major axis parameters are $r1\ and\ r2$ for sclera boundary. When we add errors on minor and major axis of iris segmentation, other value of parameters from iris segmentation is stable. Because we observed which parameters affect much more the others. Figure 3.7 shows example of original off-angle iris image and attached error on minor and major of off-angle iris image.

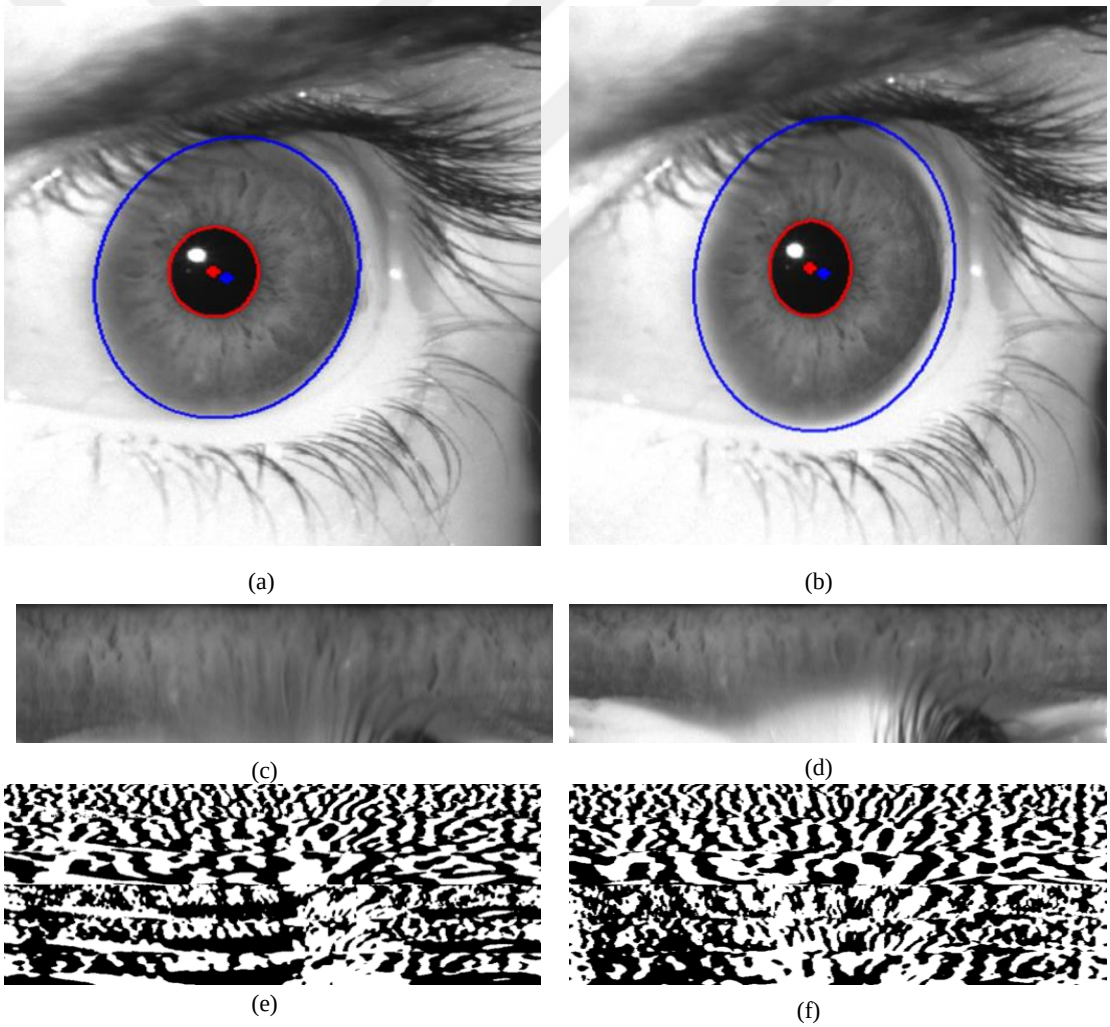

Figure 0.10. Examples of iris images from Meliksah University off-angle iris dataset (a) off-angle segmented iris image (b) off-angle segmented iris image along with error (c) normalized off-angle iris image (d) normalized off-angle iris image along with error (e) off-angle iris image's iris code and (e) off-angle iris image's iris code along with error.

3.4.3. Error in Orientation

We observed error in orientation from iris boundary. We added error on segmentation parameters which is θ. When we add errors on this parameter of iris segmentation, other value of parameters from iris segmentation is stable. Because we observed which parameters affect much more the others. Figure 3.8 shows example of original off-angle iris image and attached error on θ of off-angle iris image.

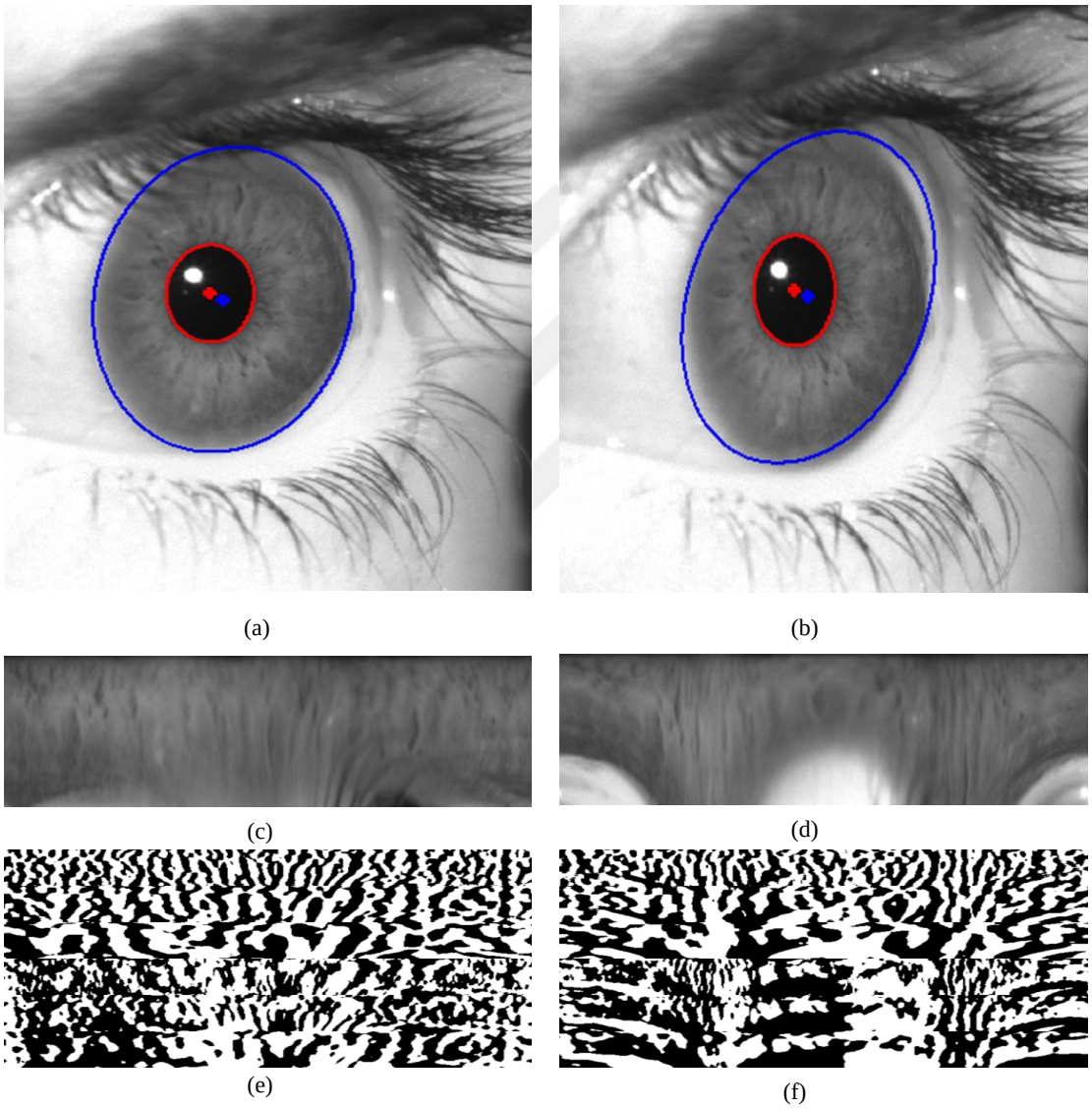

Figure 0.11. Examples of iris images from Meliksah University off-angle iris dataset (a) off-angle segmented iris image (b) off-angle segmented iris image along with error (c) normalized off-angle iris image (d) normalized off-angle iris image along with error (e) off-angle iris image's iris code and (e) off-angle iris image's iris code along with error.

CHAPTER 4

TOLERATION OF SEGMENTATION ERRORS IN OFF-ANGLE IRIS IMAGES

In this chapter, we investigate how to tolerate the segmentation errors in off-angle iris images. For this purpose, we examined the steps in iris recognition system, such as iris normalization and iris matching. Since normalization and matching follows the segmentation step, we might tolerate the errors in segmentations or might generate more robust approaches in these following steps. For example, in the normalization step, we can unwrap the iris images based on more robust iris segmentation parameters. Since there are two possibilities to unwrap the input iris image by using the limbus and pupil center as center point, we search the more robust way to decide which center best for iris segmentation. In order to figure out the more robust approach for normalization, we add errors on the parameters of pupil and limbus segmentation (i.e. $x, y, r1, r2$ and θ) and normalize the iris images with respect to limbus and pupil centers, respectively and compare the results. In addition, we investigate a solution for error in orientation of the segmentation (θ), and figure out the bit shift method is a potential solution to reduce the effect of error in orientation. The remaining of the chapter is grouped into two parts as follows:

• Robust Normalization Approaches for Error in Segmentation

• Toleration of Errors in Orientation using Bit Shift Method

4.1. ROBUST NORMALIZATION APPROACHES FOR ERROR IN SEGMENTATION

In a traditional iris recognition system, first iris image is captured, second iris image is segmented and the third step is the normalization. In normalization step, polar

coordinate system is used to convert the circular iris texture into dimensionless rectangular configurations. Since iris images are seen as ellipse from off-angle, they are segmented by using the elliptical shapes. This elliptical iris texture is converted into dimensionless rectangular configurations in the normalization. In order to unwrap the elliptical iris image, we have two possible centers which are pupil and iris center because pupil center and iris center are generally non-concentric in off-angle iris images. In this section, we investigate to choose which center is the best for iris normalization.

First possible way is to normalize the elliptical iris image with respect to pupil center as shown in Figure 4.1. In this approach, unwrapping is performed by using the pupil center as the reference point where a straight line is drawn from the pupil center in the direction of three-o-clock until the boundary of the limbus segmentation and iris image is sampled from the intersection of the line with the pupil boundary (i.e. point B in the figure) to the intersection of the line with the limbus boundary (i.e. point A in the figure). This process is repeated for every possible angles of the normalization in the clock-wise direction. For each sampling, same amount of points are sampled between the intersection of the line with the pupil and iris boundaries. Therefore, a rectangular iris pattern is formed.

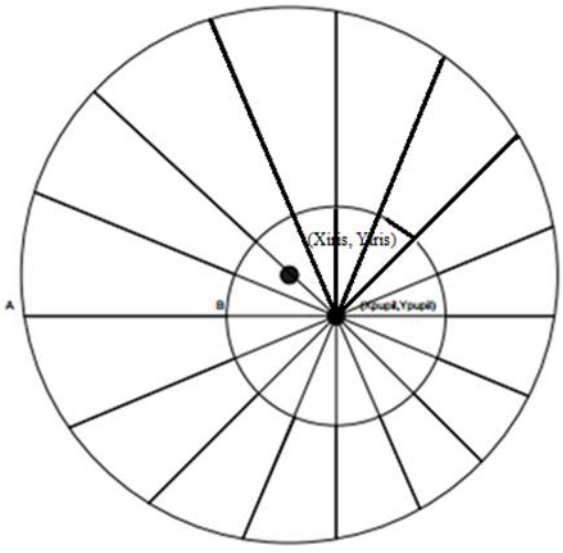

Figure 0.1.Unwrapping using the pupil center as the reference point [28].

First possible way is to normalize the elliptical iris image with respect to limbus center as shown in Figure 4.2. In this approach, unwrapping is performed by using the limbus center as the reference point where a straight line is drawn from the limbus center in the direction of three-o-clock until the boundary of the limbus segmentation and iris image is sampled from the intersection of the line with the pupil boundary (i.e. point B in the figure) to the intersection of the line with the limbus boundary (i.e. point A in the figure). This process is repeated for every possible angles of the normalization in the clock-wise direction. For each sampling, same amount of points are sampled between the intersection of the line with the pupil and limbus boundaries. Therefore, a rectangular iris pattern is formed.

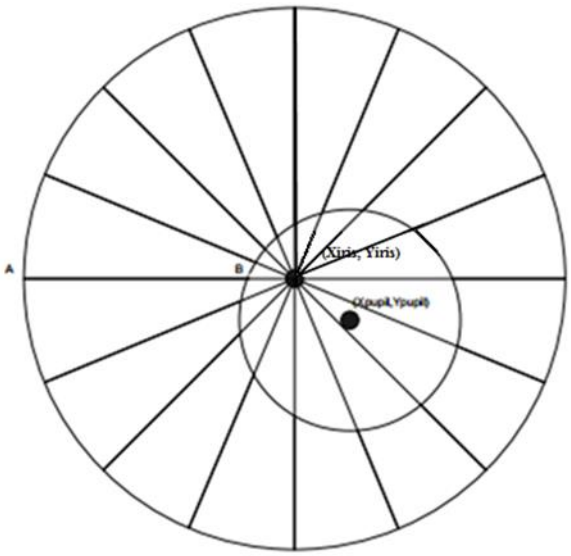

Figure 0.2.Unwrapping using the iris center as the reference point [28].

In order to figure out the more robust normalization approach, we add errors on the parameters of pupil and limbus segmentation (i.e. $x, y, r1, r2$,and θ) and normalize the iris images with respect to limbus and pupil centers, respectively and compare the results in Chapter 5.

4.2. TOLERATION OF ERRORS IN ORIENTATION USING BIT SHIFT METHOD

We used elliptical shape for doing off-angle iris segmentation. Ellipse parameters are $x, y, r1, r2$ and θ. Our purpose decrease error on iris segmentation parameters. We used bit shift method for decrease error on orientation. Because we observed effect of

segmentation parameters with errors on iris recognition system is the most decrease accuracy parameter is the orientation. Bit shift method is to increase similarity of the iris code between two iris patterns. For the lowest Hamming distance score between two template iris codes it must the best match between the two templates.

Figure 4.3 examples of bit shift method. It shows the bit shifting method from two templates between iris codes. Shift two bits means two shift right and two shifts left. We give example for only two bits are moved. We observed lowest Hamming distance for this example is zero, it shows us the best match for two templates.

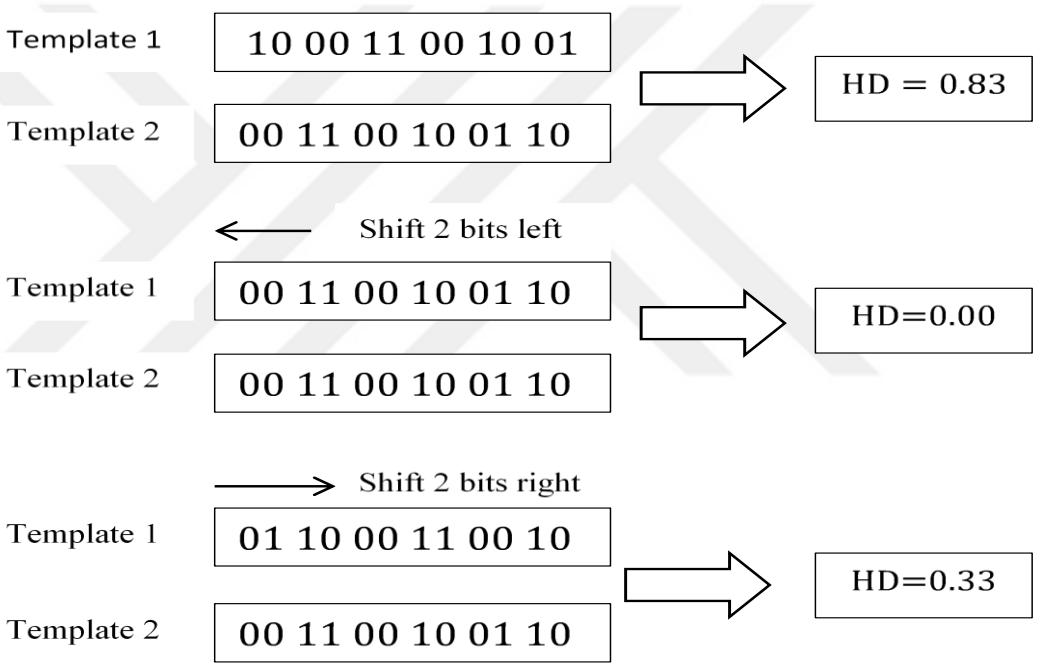

Figure 0.3.Examples of two templates bit shifting and matching.

CHAPTER 5

EXPERIMENTAL SETUP AND RESULTS

We present off-angle iris dataset which we use and show results of our experiments we have performed. We divided this chapter three parts as follows:

- Experimental setup of off-angle dataset (MUID)
- Results of effect of off-angle segmentation parameters
- Results of effect of segmentation errors on off-angle iris images

We introduce Melikşah University off-angle Iris Dataset (MUID) in "*Experimental setups of off-angle dataset (MUID)"* section. The measurement of how segmentation parameters affect the accuracy of iris recognition is shown in "*Results of effect of off-angle segmentation parameters"* subsection. Finally, the experimental results of our proposed off-angle segmentation errors "*Results of segmentation errors on off-angle iris images"* subsection.

5.1. EXPERIMENTAL SETUP OF OFF-ANGLE DATASET (MUID)

We performed our experiments on Melikşah University IRIS off-angle dataset. In this part we give brief about Melikşah University IRIS Dataset. We performed our experiments on MUID set. MUID set contains 24360 iris images from 116 different subjects. Melikşah University IRIS Data capturing platform is composed two near-infrared sensitive IDS-UI-3240ML-NIR cameras. One is frontal camera which captures eye image from in front of the subject this means it captures eye image angle from 0°. Other camera is called off-angle camera captures off-angle eye images horizontally

from -50° to +50° with an increment 10°. The frontal camera is attached on fixed arm and off-angle camera is attached on moving arm to capture iris images.

Figure 0.1. Experimental setup of Melikşah University off-angle iris dataset.

Frontal camera captures eye images from 0° and off-angle camera captures eye images from -50° to +50°. These cameras capture 10 eye images for per each angle. Frontal camera captures 10*10=100 eye images and off-angle camera captures 10*11=110 eye images. This situation showed that frontal and off angle cameras captured 210 iris images for each subject. Melikşah University IRIS Dataset has 64 subjects are males and 57 subjects are females. Race of subjects contain 2 African, 5 Asian and 106 white subjects. Average age of these subjects is 26.Figure 5.2. Illustration of image capturing setup of Melikşah University off-angle iris dataset. Image capturing starts from right eye side (50°), then moving arm rotates to left eye side (-50°) with increment step size of 10° angle.

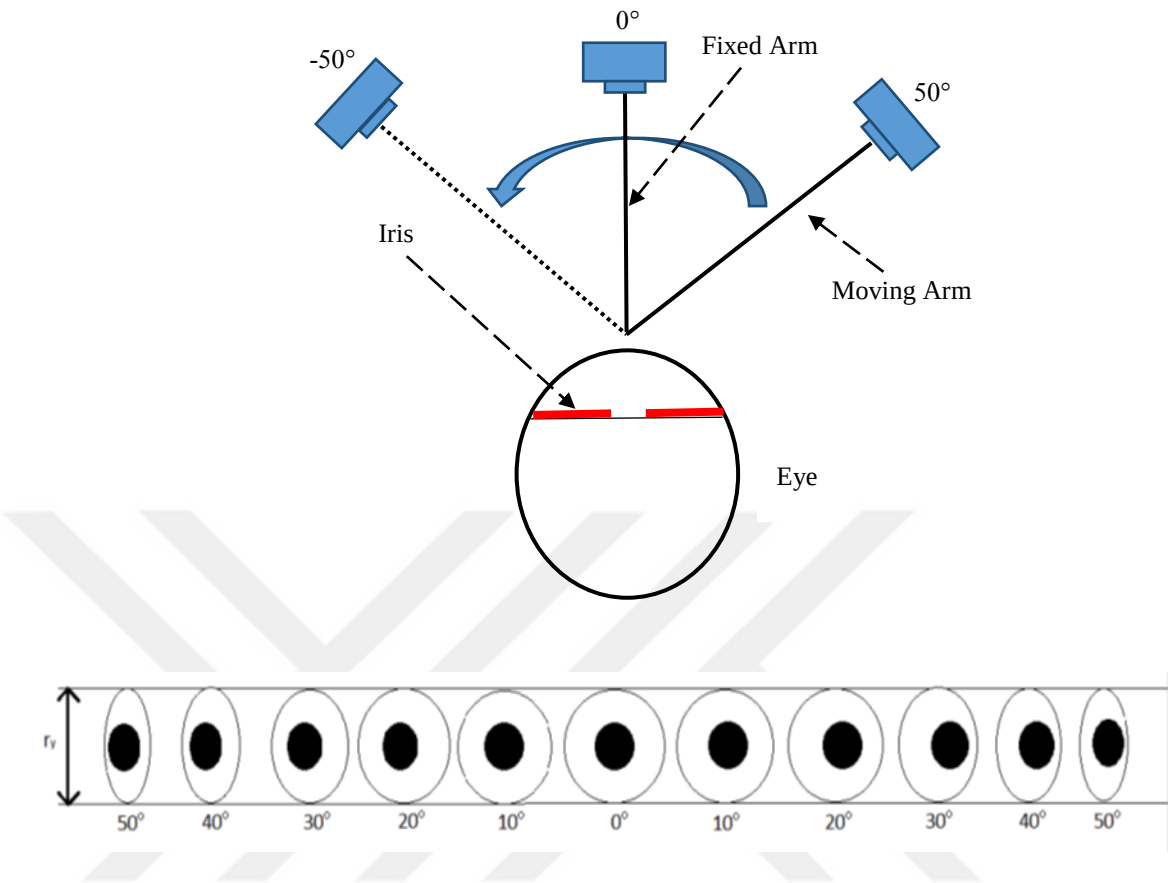

Figure 0.2. Illustration of image capturing setup of Melikşah University off-angle iris dataset. Image capturing starts from right eye side (50°), then moving arm rotates to left eye side (-50°) with increment step size of 10° angle.

We used MUID off-angle dataset for our experiments. We used totally 2200 off-angle iris images captured from left eye of 20 different subjects. These off-angle images collected from -50° to +50°with an increment 10°. Each subject has 110 off-angle images. For doing segmentation from the off-angle iris images, we employed the automatic segmentation algorithm [2]. To decrease of segmentation errors and reduce the accuracy degradation, we used Ground Truth tool for doing more accurate segmentation results for the MUID dataset.

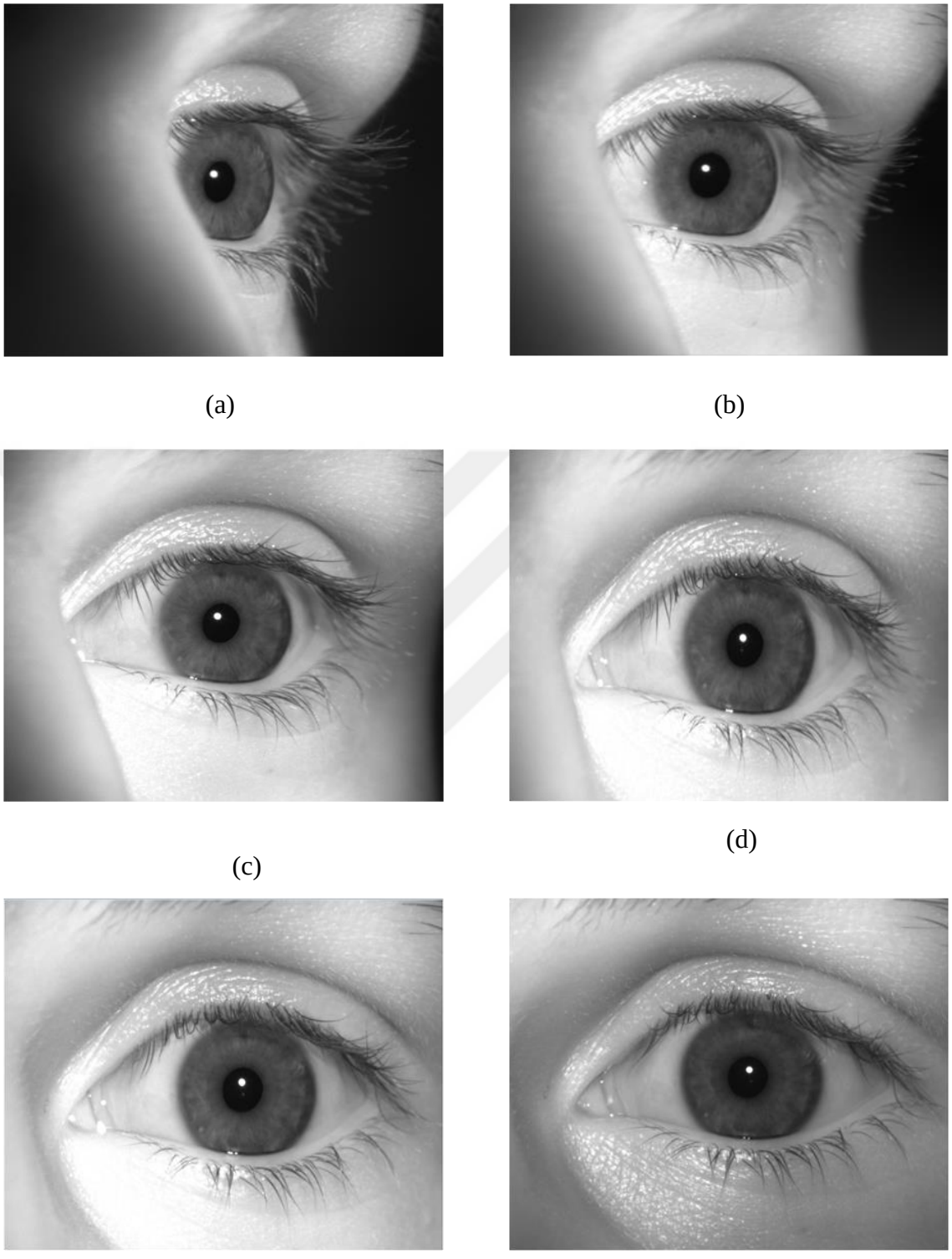

(a) (b)

(c) (d)

(e) (f)

Figure 0.3. Examples of iris images from Melikşah University off-angle iris dataset, where image acquisition angle is between 50° and -50°, (a) 50° angle, (b) 40° angle, (c) 30° angle, (d) 20° angle, (e) 10° angle, (f) frontal (0°) iris image, where axis of lens of camera is perpendicular to iris plane.

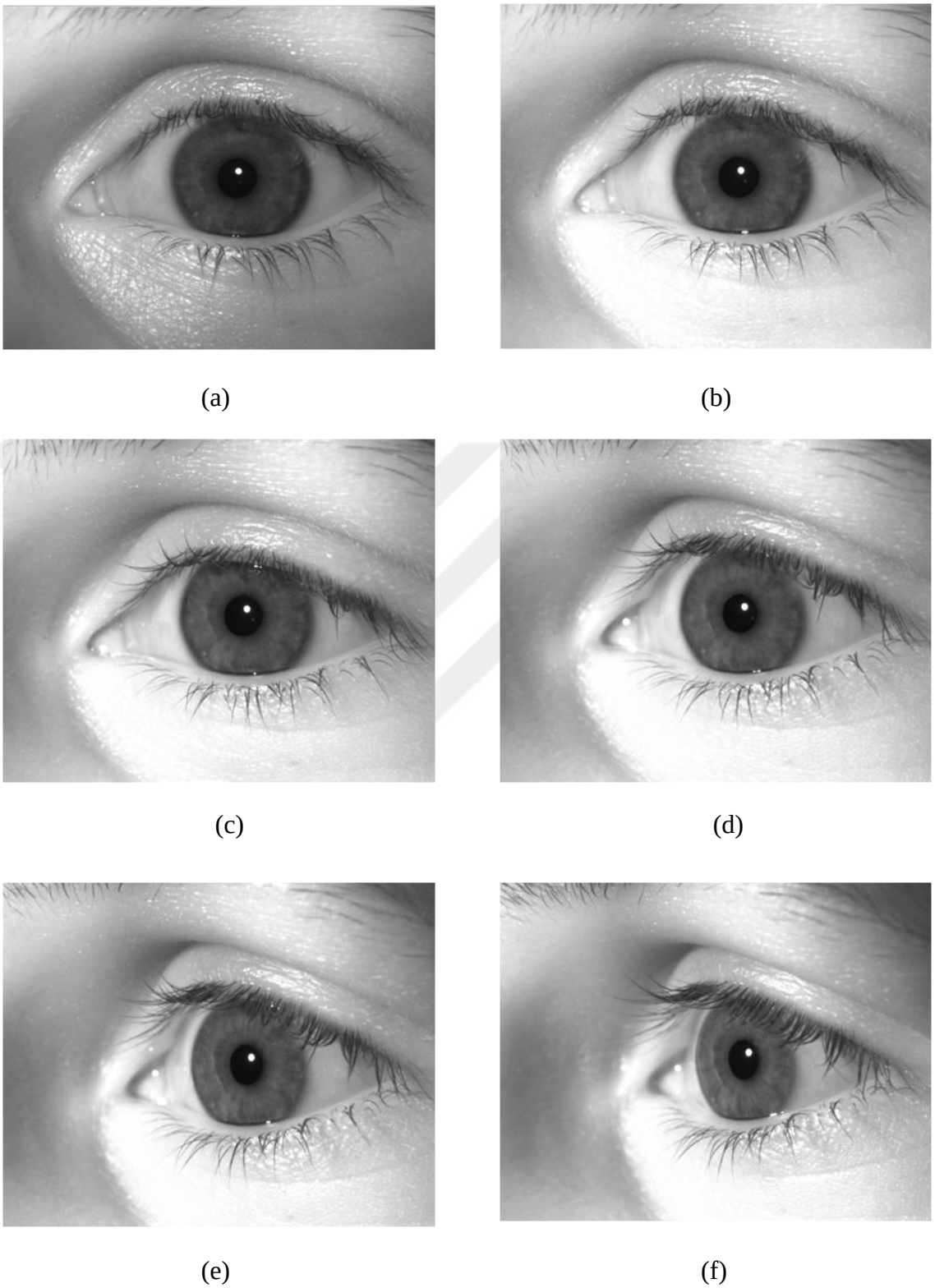

(a) (b)

(c) (d)

(e) (f)

Figure 0.4. Examples of iris images from Melikşah University off-angle iris dataset, where image acquisition angle is between -50° and 0°, (a) frontal (0°) iris image, where axis of lens of camera is perpendicular to iris plane, (b) -10° angle, (c) -20° angle, (d) -30° angle, (e) -40° angle, (f) -50° angle.

We worked on between - 50° to +50° with an increment 10° off-angle iris image. Our dataset have 110 off-angle iris images for each subject and so we worked on 20 subjects (20*110=2200 off-angle iris images) for our experimental result from Melikşah University Dataset. We fixed off-angle iris segmentation parameters by using Ground Truth Tool. Firstly we present fixed iris segmentation parameters result. We present our experimental results with using pupil center for original image. Figure 5.5 shows the Hamming distances distributions for all inter-class and intra-class. Then we observed the error bar of the Hamming distance distribution in Figure 5.6 and we showed that the intra-class Hamming distance distribution of irises with different gaze angle differences in Figure 5.7.

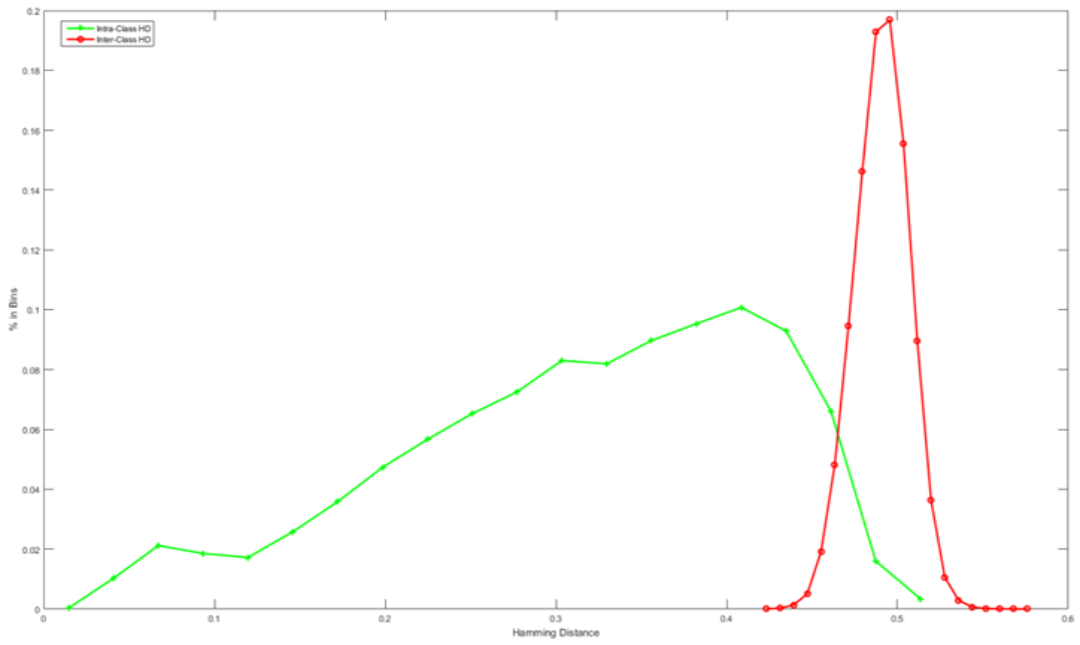

Figure 0.5.Hamming distances distributions for all inter-class and intra-class.

Figure 5.5 shows the Hamming distances distributions for all inter-class and intra-class iris comparisons in the MUID Off-angle dataset. We used off-angle image between -50° to +50° with increment 10° for our experiment. The histogram on the left with solid green line shows the intra-class Hamming distance that represents comparisons between two images of the same subjects. The left histogram with solid green shows Hamming Distance distribution for intra class that represents comparisons between two different subjects. We observe that intra-class Hamming distance varies changed from changes between 0.02-0.52with a mean value of 0.27. The histogram on the left with solid green

line shows the intra-class Hamming distance that represents comparisons between two images of the different subjects. The right histogram with solid red shows Hamming Distance distribution for inter class. Inter class varies changed from 0.42-0.56 with a mean value of 0.49. MUID Off-angle dataset change from -50° to +50° with increment 10° for our experiment, the main reason for the performance degradation in iris recognition system is the comparison of the frontal and off-angle iris images captured from different off-angles.

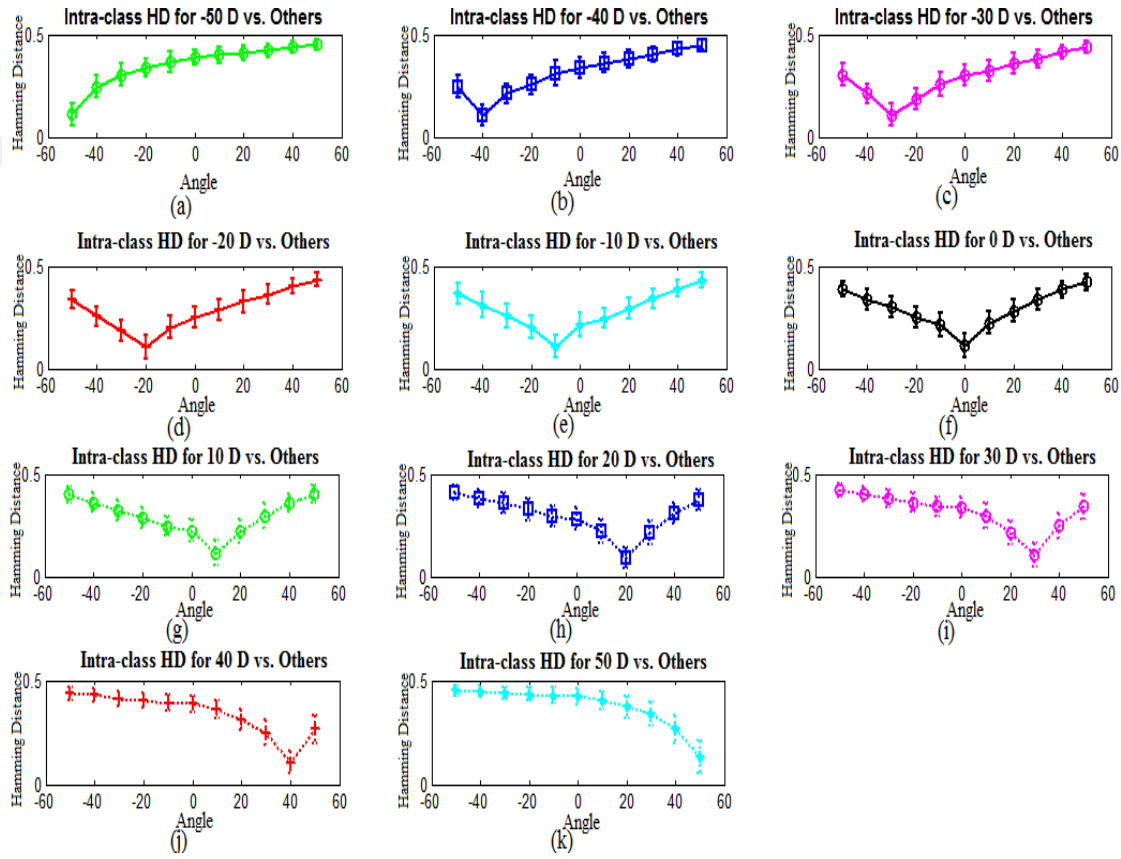

Figure 0.6.The error bar of the Hamming distance distribution.

Figure 5.6 shows the error bar of the Hamming distance distribution of iris comparisons in inter-class comparisons of the iris images captured from -50° to +50° in angle with other iris images captured from all off-angle degrees. The center of the lines represents the mean values and the bars show the standard deviation. Therefore, this figure contains all possible comparisons in intra-class distribution. For example, Figure 5.6(a) represents the comparison of iris images captured at -50° with other iris images captured from -50° to +50°. We observe that mean of Hamming Distance distribution increases from 0.10-0.45 as the gaze angle increase increases from -50° to +50°. The lowest

Hamming distance is observed at iris images captured at -50° in angle because they are captured at the same angle. The highest Hamming distance is seen at iris images captured at 50° in angle because the difference between image acquisition angles of the compared iris images is 100° in angle that is the highest difference in the off-angle iris dataset. Figure 5.6(b) represents the comparison of iris images captured at -40° with other iris images captured from -50° to +50°. We observe that mean of Hamming Distance distribution increases from 0.25-0.47 as the gaze angle increase decreases from -50° to -40°and then increase from -40° to +50°. The lowest Hamming distance is observed at iris images captured at -40° in angle because they are captured at the same angle. The highest Hamming distance is seen at iris images captured at 50° in angle because the difference between image acquisition angles of the compared iris images is 90° in angle that is the highest difference in the off-angle iris dataset. Figure 5.6(c) represents the comparison of iris images captured at -30° with other iris images captured from -50° to +50°. We observe that mean of Hamming Distance distribution increases from 0.30-0.45 as the gaze angle increase decreases from -50° to -30°and then increase from -30° to +50°. The lowest Hamming distance is observed at iris images captured at -30° in angle because they are captured at the same angle. The highest Hamming distance is seen at iris images captured at 50° in angle because the difference between image acquisition angles of the compared iris images is 80° in angle that is the highest difference in the off-angle iris dataset. Figure 5.6(d) represents the comparison of iris images captured at -20° with other iris images captured from -50° to +50°. We observe that mean of Hamming Distance distribution increases from 0.32-0.45 as the gaze angle increase decreases from -50° to -20°and then increase from -20° to +50°. The lowest Hamming distance is observed at iris images captured at -20° in angle because they are captured at the same angle. The highest Hamming distance is seen at iris images captured at 50° in angle because the difference between image acquisition angles of the compared iris images is 70° in angle that is the highest difference in the off-angle iris dataset. Figure 5.6(e) represents the comparison of iris images captured at -10° with other iris images captured from -50° to +50°. We observe that mean of Hamming Distance distribution increases from 0.35-0.42 as the gaze angle increase decreases from -50° to -10°and then increase from -10° to +50°. The lowest Hamming distance is observed at iris images captured at -10° in angle because they are captured at the same angle. The highest Hamming distance is seen at iris images captured at 50° in angle

because the difference between image acquisition angles of the compared iris images is 60° in angle that is the highest difference in the off-angle iris dataset. Figure 5.6(f) represents the comparison of iris images captured at 0° with other iris images captured from -50° to +50°. We observe that mean of Hamming Distance distribution increases from 0.39-0.44 as the gaze angle increase decreases from -50° to 0°and then increase from 0° to +50°. The lowest Hamming distance is observed at iris images captured at 0° in angle because they are captured at the same angle. The highest Hamming distance is seen at iris images captured at 50° in angle and nearly values of -50° same because the difference between image acquisition angles of the compared iris images is 50° in angle that is the highest difference in the both off-angle iris dataset. Figure 5.6(g) represents the comparison of iris images captured at 10° with other iris images captured from -50° to +50°. We observe that mean of Hamming Distance distribution increases from 0.40-0.38 as the gaze angle increase decreases from -50° to 10°and then increase from 10° to +50°. The lowest Hamming distance is observed at iris images captured at 10° in angle because they are captured at the same angle. The highest Hamming distance is seen at iris images captured at -50° in angle because the difference between image acquisition angles of the compared iris images is 60° in angle that is the highest difference in the off-angle iris dataset. Figure 5.6(h) represents the comparison of iris images captured at 20° with other iris images captured from -50° to +50°. We observe that mean of Hamming Distance distribution decreases from 0.41-0.37 as the gaze angle increase decreases from -50° to 20°and then increase from 20° to +50°. The lowest Hamming distance is observed at iris images captured at 20° in angle because they are captured at the same angle. The highest Hamming distance is seen at iris images captured at -50° in angle because the difference between image acquisition angles of the compared iris images is 70° in angle that is the highest difference in the off-angle iris dataset. Figure 5.6(i) represents the comparison of iris images captured at 30° with other iris images captured from -50° to +50°. We observe that mean of Hamming Distance distribution decreases from 0.42-0.30 as the gaze angle increase decreases from -50° to 30°and then increase from 30° to +50°. The lowest Hamming distance is observed at iris images captured at 30° in angle because they are captured at the same angle. The highest Hamming distance is seen at iris images captured at -50° in angle because the difference between image acquisition angles of the compared iris images is 80° in angle that is the highest difference in the off-angle iris dataset. Figure 5.6(j) represents the comparison

of iris images captured at 40° with other iris images captured from -50° to +50°. We observe that mean of Hamming Distance distribution decreases from 0.44-0.25 as the gaze angle increase decreases from -50° to 40°and then increase from 40° to +50°. The lowest Hamming distance is observed at iris images captured at 40° in angle because they are captured at the same angle. The highest Hamming distance is seen at iris images captured at -50° in angle because the difference between image acquisition angles of the compared iris images is 90° in angle that is the highest difference in the off-angle iris dataset. Figure 5.6(k) represents the comparison of iris images captured at 50° with other iris images captured from -50° to +50°. We observe that mean of Hamming Distance distribution decreases from 0.45-0.10 as the gaze angle decrease from -50° to +50°. The lowest Hamming distance is observed at iris images captured at 50° in angle because they are captured at the same angle. The highest Hamming distance is seen at iris images captured at -50° in angle because the difference between image acquisition angles of the compared iris images is 100° in angle that is the highest difference in the off-angle iris dataset.

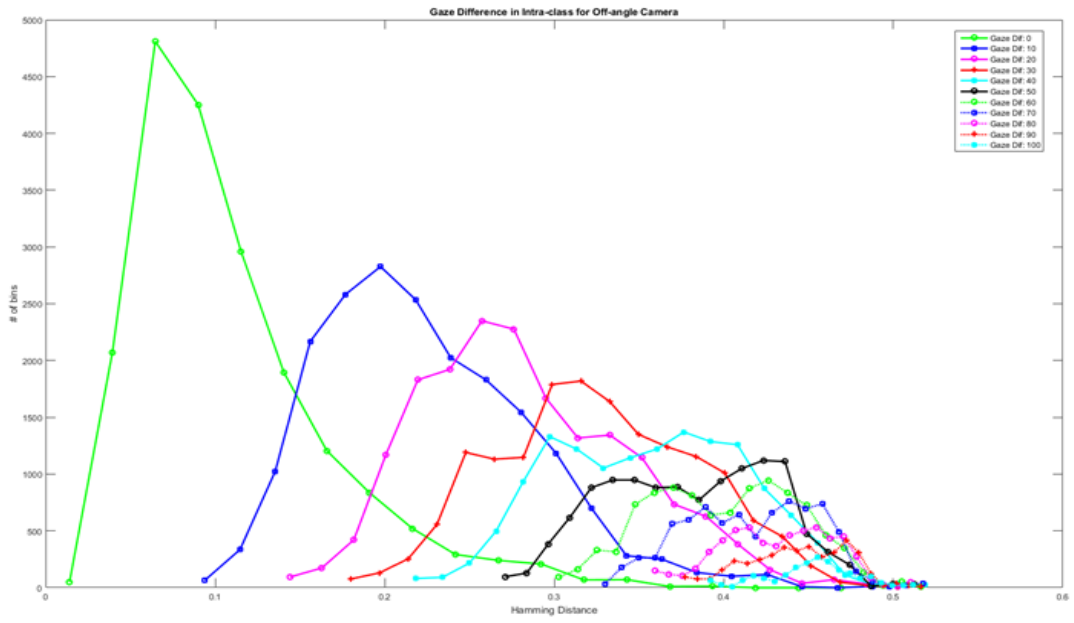

Figure 0.7. The intra-class Hamming distance distribution of irises with different gaze angle differences.

Figure 5.7 shows the Hamming distance distribution of irises with different gaze angle differences. In this figure, we present comparison of iris images with no gaze angle difference for example-50° to -50°, -40° to -40°, -30° to -30°, -20° to -20°, -10° to -10°,

0° to 0°, 10° to 10° 20° to 20°, 30° to 30°, 40° to 40° and 50° to 50° is shown as green solid line with + marker and for no gaze angle difference of iris images Hamming distance changes from 0.02 to 0.30 due to the dilation difference and segmentation variations. We showed that Comparison of iris images with gaze angle difference between images increases, the Hamming distance increases. For example, -50° to -40°, -40° to -30°, -30° to -20°,-20° to -10°,-10° to 0°, 0° to 10°, 10° to 20°, 20° to 30°, 30° to 40° and 40° to 50° has 10° angle difference between images and their Hamming distance changes from 0.09 to 0.35. If the gaze difference between images is more than 30°, Hamming distance score may fall in to false reject region.

We present our experimental results with using iris center for original image. Figure 5.8 shows the Hamming distances distributions for all inter-class and intra-class. Then we observed the error bar of the Hamming distance distribution in Figure 5.9 and we showed that the intra-class Hamming distance distribution of irises with different gaze angle differences in Figure 5.10.

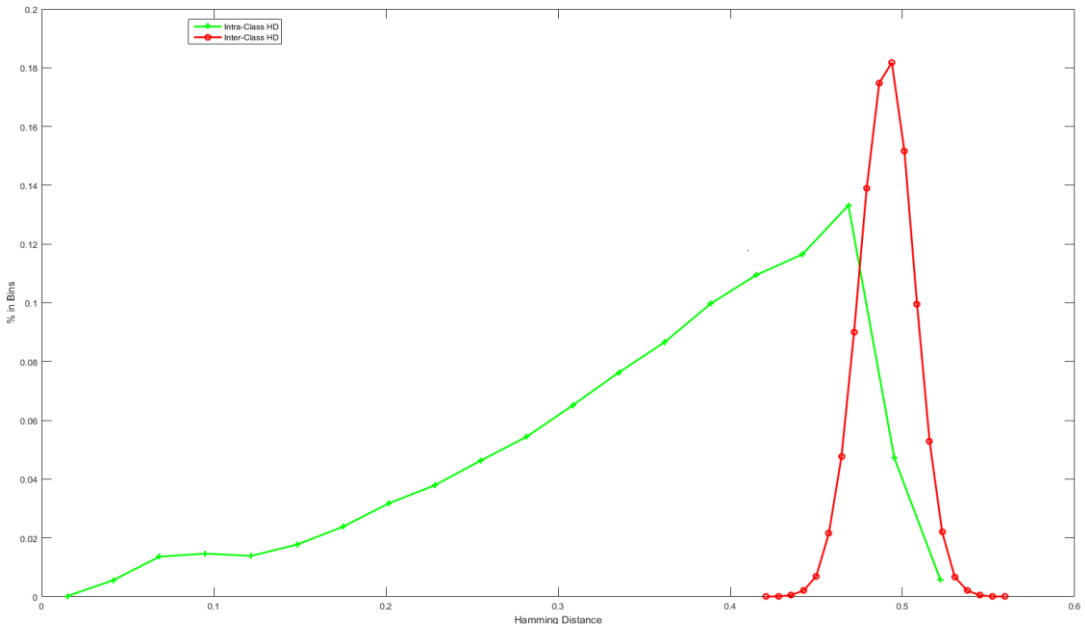

Figure 0.8. The Hamming distances distributions for all inter-class and intra-class iris comparisons in the MUID Off-angle dataset.

Figure 5.8 shows the Hamming distances distributions for all inter-class and intra-class iris comparisons in the MUID Off-angle dataset. We used off-angle image between -50° to +50° with increment 10° for our experiment. The histogram on the left with solid

green line shows the intra-class Hamming distance that represents comparisons between two images of the same subjects. The left histogram with solid green shows Hamming Distance distribution for intra class that represents comparisons between two different subjects. We observe that intra-class Hamming distance varies changed from changes between 0.02-0.54 with a mean value of 0.28. The histogram on the left with solid green line shows the intra-class Hamming distance that represents comparisons between two images of the different subjects. The right histogram with solid red shows Hamming Distance distribution for inter class. Inter class varies changed from 0.44-0.56 with a mean value of 0.50. MUID Off-angle dataset change from -50° to +50° with increment 10° for our experiment, the main reason for the performance degradation in iris recognition system is the comparison of the frontal and off-angle iris images captured from different off-angles.

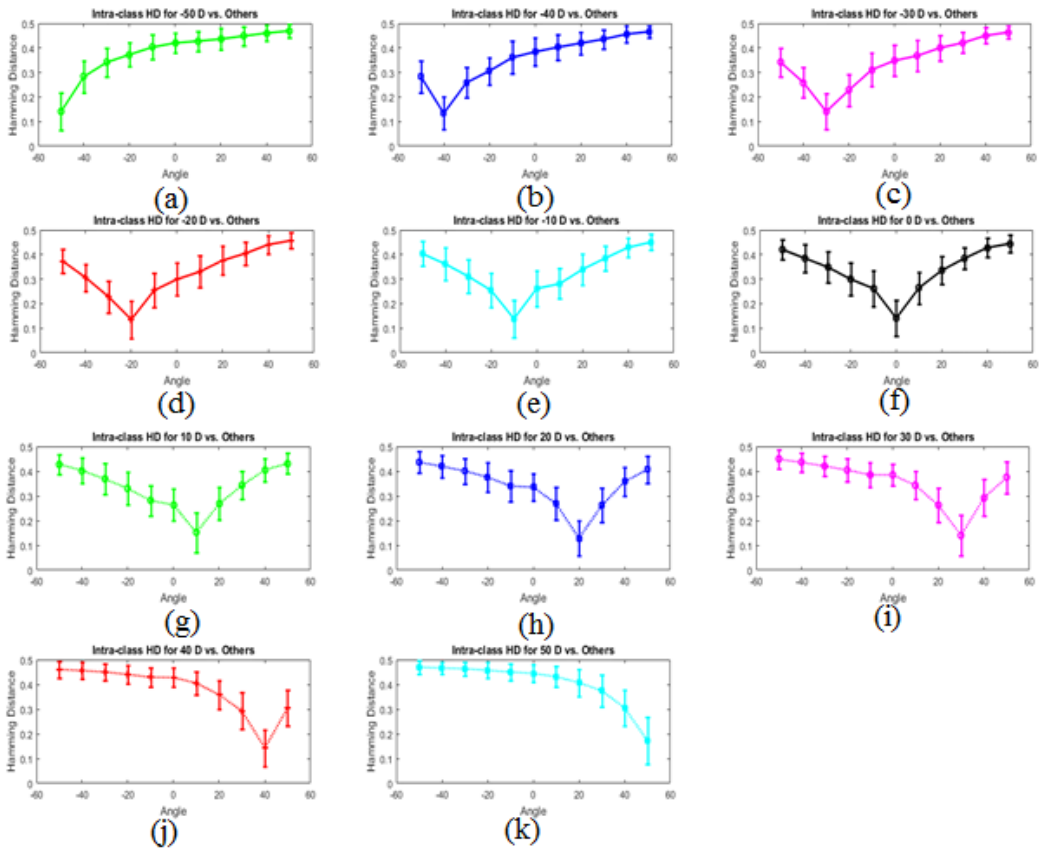

Figure 0.9. The error bar of the Hamming distance distribution of iris comparisons in inter-class comparisons.

Figure 5.9 shows the error bar of the Hamming distance distribution of iris comparisons in inter-class comparisons of the iris images captured from -50° to +50° in angle with other iris images captured from all off-angle degrees. The center of the lines represents the mean values and the bars show the standard deviation. Therefore, this figure contains all possible comparisons in intra-class distribution. For example, Figure 5.9(a) represents the comparison of iris images captured at -50° with other iris images captured from -50° to +50°. We observe that mean of Hamming Distance distribution increases from 0.13-0.48 as the gaze angle increase increases from -50° to +50°. The lowest Hamming distance is observed at iris images captured at -50° in angle because they are captured at the same angle. The highest Hamming distance is seen at iris images captured at 50° in angle because the difference between image acquisition angles of the compared iris images is 100° in angle that is the highest difference in the off-angle iris dataset. Figure 5.9(b) represents the comparison of iris images captured at -40° with other iris images captured from -50° to +50°. We observe that mean of Hamming Distance distribution increases from 0.33-0.48 as the gaze angle increase decreases from -50° to -40°and then increase from -40° to +50°. The lowest Hamming distance is observed at iris images captured at -40° in angle because they are captured at the same angle. The highest Hamming distance is seen at iris images captured at 50° in angle because the difference between image acquisition angles of the compared iris images is 90° in angle that is the highest difference in the off-angle iris dataset. Figure 5.9(c) represents the comparison of iris images captured at -30° with other iris images captured from -50° to +50°. We observe that mean of Hamming Distance distribution increases from 0.33-0.48 as the gaze angle increase decreases from -50° to -30°and then increase from -30° to +50°. The lowest Hamming distance is observed at iris images captured at -30° in angle because they are captured at the same angle. The highest Hamming distance is seen at iris images captured at 50° in angle because the difference between image acquisition angles of the compared iris images is 80° in angle that is the highest difference in the off-angle iris dataset. Figure 5.9(d) represents the comparison of iris images captured at -20° with other iris images captured from -50° to +50°. We observe that mean of Hamming Distance distribution increases from 0.36-0.46 as the gaze angle increase decreases from -50° to -20°and then increase from -20° to +50°. The lowest Hamming distance is observed at iris images captured at -20° in angle because they are captured at the same angle. The highest Hamming distance is seen at iris images

captured at 50° in angle because the difference between image acquisition angles of the compared iris images is 70° in angle that is the highest difference in the off-angle iris dataset. Figure 5.9(e) represents the comparison of iris images captured at -10° with other iris images captured from -50° to +50°. We observe that mean of Hamming Distance distribution increases from 0.40-0.46 as the gaze angle increase decreases from -50° to -10°and then increase from -10° to +50°. The lowest Hamming distance is observed at iris images captured at -10° in angle because they are captured at the same angle. The highest Hamming distance is seen at iris images captured at 50° in angle because the difference between image acquisition angles of the compared iris images is 60° in angle that is the highest difference in the off-angle iris dataset. Figure 5.9(f) represents the comparison of iris images captured at 0° with other iris images captured from -50° to +50°. We observe that mean of Hamming Distance distribution increases from 0.42-0.45 as the gaze angle increase decreases from -50° to 0°and then increase from 0° to +50°. The lowest Hamming distance is observed at iris images captured at 0° in angle because they are captured at the same angle. The highest Hamming distance is seen at iris images captured at 50° in angle and nearly values of -50° same because the difference between image acquisition angles of the compared iris images is 50° in angle that is the highest difference in the both off-angle iris dataset. Figure 5.9(g) represents the comparison of iris images captured at 10° with other iris images captured from -50° to +50°. We observe that mean of Hamming Distance distribution increases from 0.42-0.41 as the gaze angle increase decreases from -50° to 10°and then increase from 10° to +50°. The lowest Hamming distance is observed at iris images captured at 10° in angle because they are captured at the same angle. The highest Hamming distance is seen at iris images captured at -50° in angle because the difference between image acquisition angles of the compared iris images is 60° in angle that is the highest difference in the off-angle iris dataset. Figure 5.9(h) represents the comparison of iris images captured at 20° with other iris images captured from -50° to +50°. We observe that mean of Hamming Distance distribution decreases from 0.45-0.40 as the gaze angle increase decreases from -50° to 20°and then increase from 20° to +50°. The lowest Hamming distance is observed at iris images captured at 20° in angle because they are captured at the same angle. The highest Hamming distance is seen at iris images captured at -50° in angle because the difference between image acquisition angles of the compared iris images is 70° in angle that is the highest difference in the off-angle iris dataset. Figure

5.9(i) represents the comparison of iris images captured at 30° with other iris images captured from -50° to +50°. We observe that mean of Hamming Distance distribution decreases from 0.46-0.38 as the gaze angle increase decreases from -50° to 30°and then increase from 30° to +50°. The lowest Hamming distance is observed at iris images captured at 30° in angle because they are captured at the same angle. The highest Hamming distance is seen at iris images captured at -50° in angle because the difference between image acquisition angles of the compared iris images is 80° in angle that is the highest difference in the off-angle iris dataset. Figure 5.9(j) represents the comparison of iris images captured at 40° with other iris images captured from -50° to +50°. We observe that mean of Hamming Distance distribution decreases from 0.48-0.32 as the gaze angle increase decreases from -50° to 40°and then increase from 40° to +50°. The lowest Hamming distance is observed at iris images captured at 40° in angle because they are captured at the same angle. The highest Hamming distance is seen at iris images captured at -50° in angle because the difference between image acquisition angles of the compared iris images is 90° in angle that is the highest difference in the off-angle iris dataset. Figure 5.9(k) represents the comparison of iris images captured at 50° with other iris images captured from -50° to +50°. We observe that mean of Hamming Distance distribution decreases from 0.48-0.14 as the gaze angle decrease from -50° to +50°. The lowest Hamming distance is observed at iris images captured at 50° in angle because they are captured at the same angle. The highest Hamming distance is seen at iris images captured at -50° in angle because the difference between image acquisition angles of the compared iris images is 100° in angle that is the highest difference in the off-angle iris dataset.

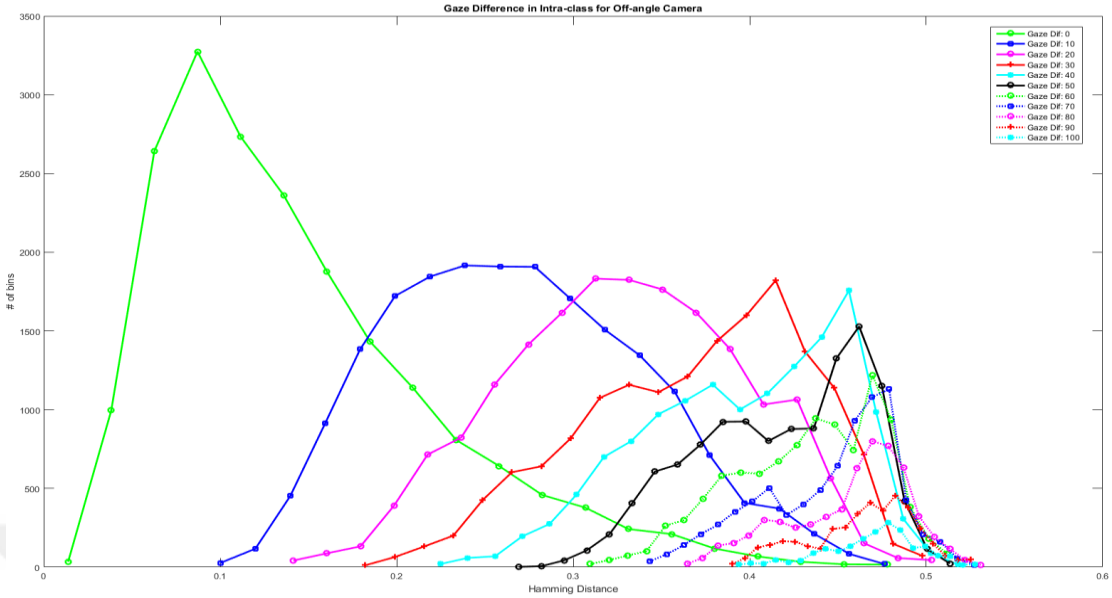

Figure 0.10. The Hamming distance distribution of irises with different gaze angle differences.

Figure 5.10 shows the Hamming distance distribution of irises with different gaze angle differences. In this figure, we present comparison of iris images with no gaze angle difference for example-50° to -50°, -40° to -40°, -30° to -30°, -20° to -20°, -10° to -10°, 0° to 0°, 10° to 10° 20° to 20°, 30° to 30°, 40° to 40° and 50° to 50° is shown as green solid line with + marker and for no gaze angle difference of iris images Hamming distance changes from 0.02 to 0.35 due to the dilation difference and segmentation variations. We showed that Comparison of iris images with gaze angle difference between images increases, the Hamming distance increases. For example, -50° to -40°, -40° to -30°, -30° to -20°,-20° to -10°,-10° to 0°, 0° to 10°, 10° to 20°, 20° to 30°, 30° to 40° and 40° to 50° has 10° angle difference between images and their Hamming distance changes from 0.1 to 0.38. If the gaze difference between images is more than 30°, Hamming distance score may fall in to false reject region.

Based on these results we observed pupil center give us better result than iris center. Because of that we decided using pupil center for our experiments. We showed our experimental result in section 5.2.

5.2. RESULTS OF EFFECT OF ERROR IN OFF-ANGLE SEGMANTATION

In this section, we present effect of off-angle segmentation parameters. We used MUID off-angle dataset (Off-angle iris images between -50° to +50°) for our experimental results. Our experiments based on segmentation parameters which are x, y, $r1$, $r2$ and θ. After we controlled and fixed segmentation errors with using Ground Truth Tool, we added errors each parameters of off-angle iris segmentation for observing effect of parameters on iris segmentation. We grouped this section into three parts as follow:

• Error in Ellipse Center

• Error in Minor and Major Axis

• Error in Orientation

5.2.1. Error in Ellipse Center

We worked on between - 50° to +50° with an increment 10° off-angle iris image. Our dataset have 110 off-angle iris images for each subject and so we worked on 20 subjects (20*110=2200 off-angle iris images) for our experimental result from Meliksah University Dataset. We fixed off-angle iris segmentation parameters by using Ground Truth Tool. We added %1, %2 and %3 error in ellipse center which are x and y. We present Hamming distances distributions for all inter-class and intra-class iris comparisons in the MUID Off-angle dataset showed respectively in Figure 5.11, Figure 5.13 and Figure 5.15.Figure 5.12, Figure 5.14 and Figure 5.16 shows the error bar of the Hamming distance distribution of iris comparisons in inter-class comparisons.

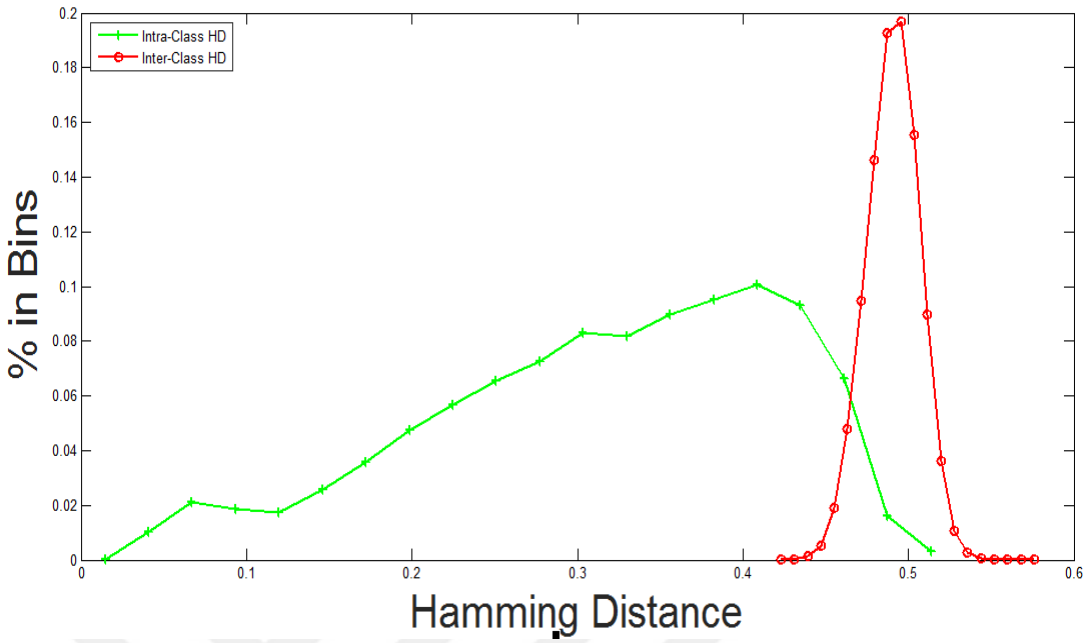

Figure 0.11. The Hamming distances distributions for all inter-class and intra-class iris comparisons in the MUID Off-angle dataset.

Figure 5.11 shows the Hamming distances distributions for all inter-class and intra-class iris comparisons in the MUID Off-angle dataset. Firstly we added %1error in ellipse center. We used off-angle image between -50° to +50° with increment 10° for our experiment. The histogram on the left with solid green line shows the intra-class Hamming distance that represents comparisons between two images of the same subjects. The left histogram with solid green shows Hamming Distance distribution for intra class that represents comparisons between two different subjects. We observe that intra-class Hamming distance varies changed from changes between 0.02-0.52 with a mean value of 0.27. The histogram on the left with solid green line shows the intra-class Hamming distance that represents comparisons between two images of the different subjects. The right histogram with solid red shows Hamming Distance distribution for inter class. Inter class varies changed from 0.43-0.57 with a mean value of 0.50. MUID Off-angle dataset change from -50° to +50° with increment 10° for our experiment, the main reason for the performance degradation in iris recognition system is the comparison of the frontal and off-angle iris images captured from different off-angles.

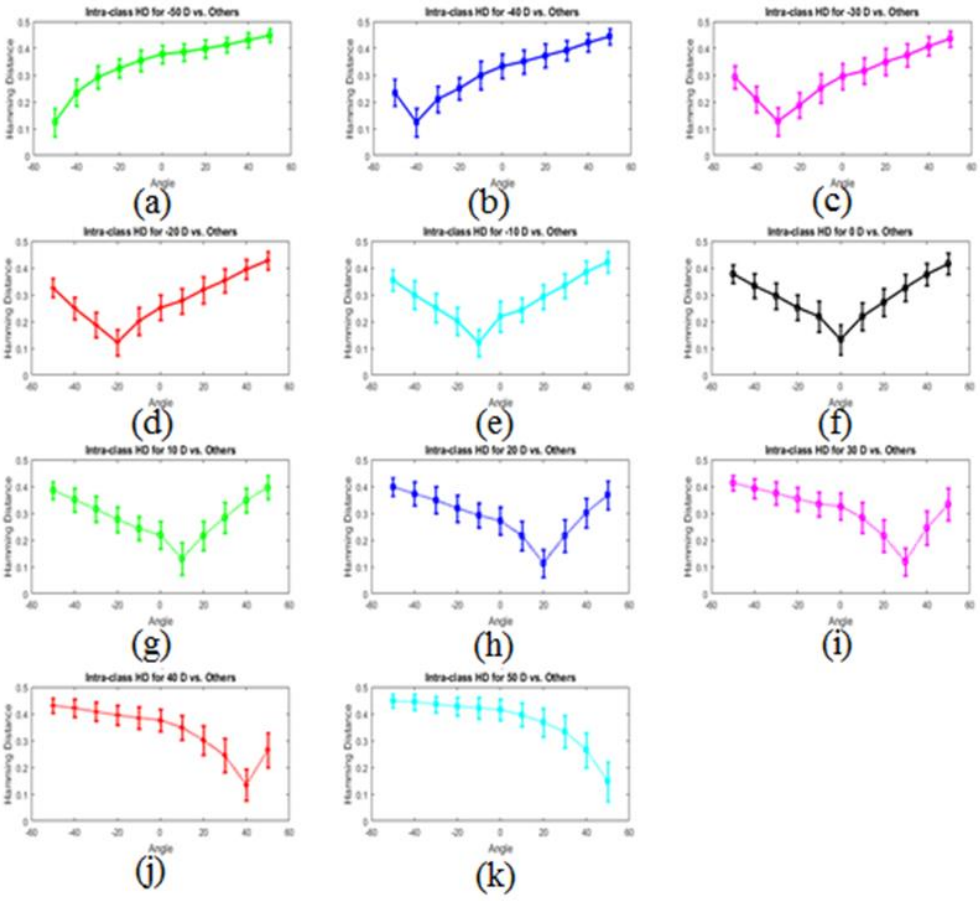

Figure 0.12.The error bar of the Hamming distance distribution of iris comparisons.

Figure 5.12 shows the error bar of the Hamming distance distribution of iris comparisons in inter-class comparisons of the iris images captured from -50° to +50° in angle with other iris images captured from all off-angle degrees. The center of the lines represents the mean values and the bars show the standard deviation. Therefore, this figure contains all possible comparisons in intra-class distribution. Firstly we added %1error in ellipse center. For example, Figure 5.12(a) represents the comparison of iris images captured at -50° with other iris images captured from -50° to +50°. We observe that mean of Hamming Distance distribution increases from 0.15-0.46 as the gaze angle increase increases from -50° to +50°. The lowest Hamming distance is observed at iris images captured at -50° in angle because they are captured at the same angle. The highest Hamming distance is seen at iris images captured at 50° in angle because the difference between image acquisition angles of the compared iris images is 100° in angle that is the highest difference in the off-angle iris dataset. Figure 5.12(b) represents the comparison of iris images captured at -40° with other iris images captured from -50°

to +50°. We observe that mean of Hamming Distance distribution increases from 0.28-0.47 as the gaze angle increase decreases from -50° to -40°and then increase from -40° to +50°. The lowest Hamming distance is observed at iris images captured at -40° in angle because they are captured at the same angle. The highest Hamming distance is seen at iris images captured at 50° in angle because the difference between image acquisition angles of the compared iris images is 90° in angle that is the highest difference in the off-angle iris dataset. Figure 5.12(c) represents the comparison of iris images captured at -30° with other iris images captured from -50° to +50°. We observe that mean of Hamming Distance distribution increases from 0.31-0.45 as the gaze angle increase decreases from -50° to -30°and then increase from -30° to +50°. The lowest Hamming distance is observed at iris images captured at -30° in angle because they are captured at the same angle. The highest Hamming distance is seen at iris images captured at 50° in angle because the difference between image acquisition angles of the compared iris images is 80° in angle that is the highest difference in the off-angle iris dataset. Figure 5.12(d) represents the comparison of iris images captured at -20° with other iris images captured from -50° to +50°. We observe that mean of Hamming Distance distribution increases from 0.35-0.42 as the gaze angle increase decreases from -50° to -20°and then increase from -20° to +50°. The lowest Hamming distance is observed at iris images captured at -20° in angle because they are captured at the same angle. The highest Hamming distance is seen at iris images captured at 50° in angle because the difference between image acquisition angles of the compared iris images is 70° in angle that is the highest difference in the off-angle iris dataset. Figure 5.12(e) represents the comparison of iris images captured at -10° with other iris images captured from -50° to +50°. We observe that mean of Hamming Distance distribution increases from 0.38-0.42 as the gaze angle increase decreases from -50° to -10°and then increase from -10° to +50°. The lowest Hamming distance is observed at iris images captured at -10° in angle because they are captured at the same angle. The highest Hamming distance is seen at iris images captured at 50° in angle because the difference between image acquisition angles of the compared iris images is 60° in angle that is the highest difference in the off-angle iris dataset. Figure 5.12(f) represents the comparison of iris images captured at 0° with other iris images captured from -50° to +50°. We observe that mean of Hamming Distance distribution increases from 0.39-0.41 as the gaze angle increase decreases from -50° to 0°and then increase from 0° to +50°. The lowest

Hamming distance is observed at iris images captured at 0° in angle because they are captured at the same angle. The highest Hamming distance is seen at iris images captured at 50° in angle and nearly values of -50° same because the difference between image acquisition angles of the compared iris images is 50° in angle that is the highest difference in the both off-angle iris dataset. Figure 5.12(g) represents the comparison of iris images captured at 10° with other iris images captured from -50° to +50°. We observe that mean of Hamming Distance distribution increases from 0.40-0.39 as the gaze angle increase decreases from -50° to 10°and then increase from 10° to +50°. The lowest Hamming distance is observed at iris images captured at 10° in angle because they are captured at the same angle. The highest Hamming distance is seen at iris images captured at -50° in angle because the difference between image acquisition angles of the compared iris images is 60° in angle that is the highest difference in the off-angle iris dataset. Figure 5.12(h) represents the comparison of iris images captured at 20° with other iris images captured from -50° to +50°. We observe that mean of Hamming Distance distribution decreases from 0.40-0.38 as the gaze angle increase decreases from -50° to 20°and then increase from 20° to +50°. The lowest Hamming distance is observed at iris images captured at 20° in angle because they are captured at the same angle. The highest Hamming distance is seen at iris images captured at -50° in angle because the difference between image acquisition angles of the compared iris images is 70° in angle that is the highest difference in the off-angle iris dataset. Figure 5.12(i) represents the comparison of iris images captured at 30° with other iris images captured from -50° to +50°. We observe that mean of Hamming Distance distribution decreases from 0.42-0.36 as the gaze angle increase decreases from -50° to 30°and then increase from 30° to +50°. The lowest Hamming distance is observed at iris images captured at 30° in angle because they are captured at the same angle. The highest Hamming distance is seen at iris images captured at -50° in angle because the difference between image acquisition angles of the compared iris images is 80° in angle that is the highest difference in the off-angle iris dataset. Figure 5.12(j) represents the comparison of iris images captured at 40° with other iris images captured from -50° to +50°. We observe that mean of Hamming Distance distribution decreases from 0.45-0.28 as the gaze angle increase decreases from -50° to 40°and then increase from 40° to +50°. The lowest Hamming distance is observed at iris images captured at 40° in angle because they are captured at the same angle. The highest Hamming distance is seen at iris

images captured at -50° in angle because the difference between image acquisition angles of the compared iris images is 90° in angle that is the highest difference in the off-angle iris dataset. Figure 5.12(k) represents the comparison of iris images captured at 50° with other iris images captured from -50° to +50°. We observe that mean of Hamming Distance distribution decreases from 0.46-0.15 as the gaze angle decrease from -50° to +50°. The lowest Hamming distance is observed at iris images captured at 50° in angle because they are captured at the same angle. The highest Hamming distance is seen at iris images captured at -50° in angle because the difference between image acquisition angles of the compared iris images is 100° in angle that is the highest difference in the off-angle iris dataset.

Secondly we add %2 error on ellipse center and we present how change Hamming distances distributions for all inter-class and intra-class iris comparisons and the error bar of the Hamming distance distribution of iris comparisons in inter-class comparisons.

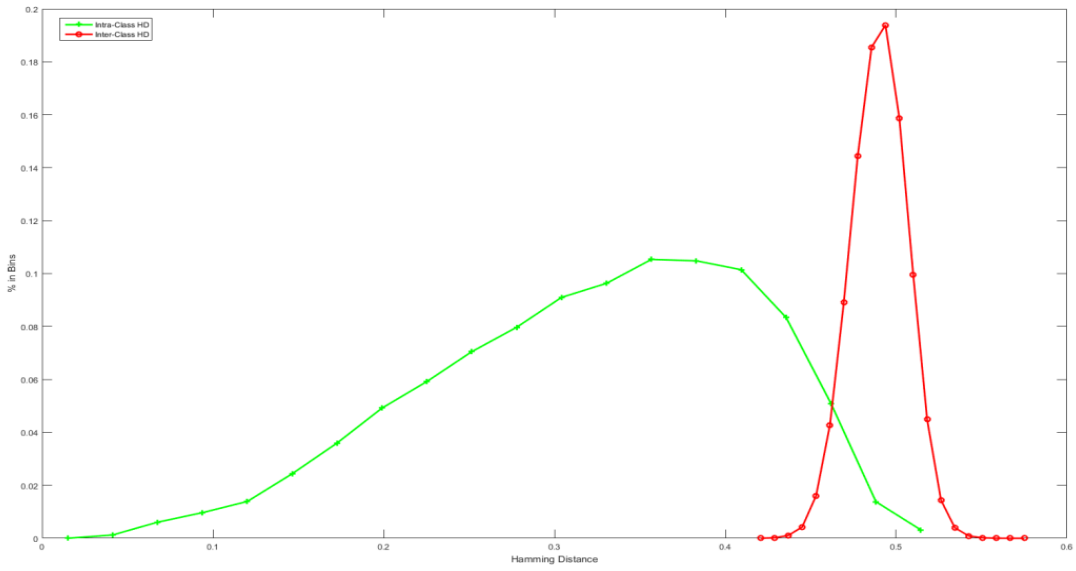

Figure 0.13. The Hamming distances distributions for all inter-class and intra-class iris comparisons in the MUID Off-angle dataset.

Figure 5.13 shows the Hamming distances distributions for all inter-class and intra-class iris comparisons in the MUID Off-angle dataset. We used off-angle image between -50° to +50° with increment 10° for our experiment. The histogram on the left with solid green line shows the intra-class Hamming distance that represents comparisons between two images of the same subjects. The left histogram with solid green shows Hamming

Distance distribution for intra class that represents comparisons between two different subjects. We observe that intra-class Hamming distance varies changed from changes between 0.04-0.52 with a mean value of 0.28. The histogram on the left with solid green line shows the intra-class Hamming distance that represents comparisons between two images of the different subjects. The right histogram with solid red shows Hamming Distance distribution for inter class. Inter class varies changed from 0.44-0.57 with a mean value of 0.55 MUID Off-angle dataset change from -50° to +50° with increment 10° for our experiment, the main reason for the performance degradation in iris recognition system is the comparison of the frontal and off-angle iris images captured from different off-angles.

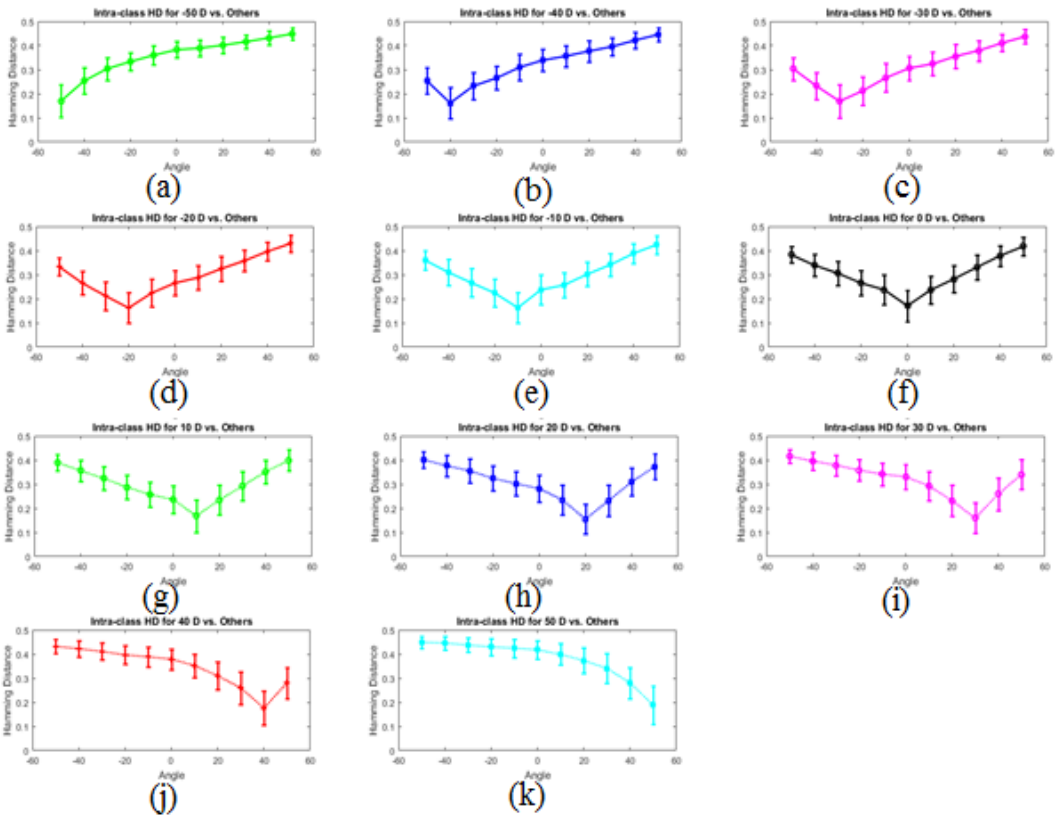

Figure 0.14.The error bar of the Hamming distance distribution of iris comparisons.

Figure 5.14 shows the error bar of the Hamming distance distribution of iris comparisons in inter-class comparisons of the iris images captured from -50° to +50° in angle with other iris images captured from all off-angle degrees. The center of the lines represents the mean values and the bars show the standard deviation. Therefore, this

figure contains all possible comparisons in intra-class distribution. Secondly we added %2 error in ellipse center. For example, Figure 5.14(a) represents the comparison of iris images captured at -50° with other iris images captured from -50° to +50°. We observe that mean of Hamming Distance distribution increases from 0.18-0.46 as the gaze angle increase increases from -50° to +50°. The lowest Hamming distance is observed at iris images captured at -50° in angle because they are captured at the same angle. The highest Hamming distance is seen at iris images captured at 50° in angle because the difference between image acquisition angles of the compared iris images is 100° in angle that is the highest difference in the off-angle iris dataset. Figure 5.14(b) represents the comparison of iris images captured at -40° with other iris images captured from -50° to +50°. We observe that mean of Hamming Distance distribution increases from 0.26-0.46 as the gaze angle increase decreases from -50° to -40°and then increase from -40° to +50°. The lowest Hamming distance is observed at iris images captured at -40° in angle because they are captured at the same angle. The highest Hamming distance is seen at iris images captured at 50° in angle because the difference between image acquisition angles of the compared iris images is 90° in angle that is the highest difference in the off-angle iris dataset. Figure 5.14(c) represents the comparison of iris images captured at -30° with other iris images captured from -50° to +50°. We observe that mean of Hamming Distance distribution increases from 0.32-0.44 as the gaze angle increase decreases from -50° to -30°and then increase from -30° to +50°. The lowest Hamming distance is observed at iris images captured at -30° in angle because they are captured at the same angle. The highest Hamming distance is seen at iris images captured at 50° in angle because the difference between image acquisition angles of the compared iris images is 80° in angle that is the highest difference in the off-angle iris dataset. Figure 5.14(d) represents the comparison of iris images captured at -20° with other iris images captured from -50° to +50°. We observe that mean of Hamming Distance distribution increases from 0.35-0.42 as the gaze angle increase decreases from -50° to -20°and then increase from -20° to +50°. The lowest Hamming distance is observed at iris images captured at -20° in angle because they are captured at the same angle. The highest Hamming distance is seen at iris images captured at 50° in angle because the difference between image acquisition angles of the compared iris images is 70° in angle that is the highest difference in the off-angle iris dataset. Figure 5.14(e) represents the comparison of iris images captured at -10° with other iris images captured

from -50° to +50°. We observe that mean of Hamming Distance distribution increases from 0.38-0.40 as the gaze angle increase decreases from -50° to -10°and then increase from -10° to +50°. The lowest Hamming distance is observed at iris images captured at -10° in angle because they are captured at the same angle. The highest Hamming distance is seen at iris images captured at 50° in angle because the difference between image acquisition angles of the compared iris images is 60° in angle that is the highest difference in the off-angle iris dataset. Figure 5.14(f) represents the comparison of iris images captured at 0° with other iris images captured from -50° to +50°. We observe that mean of Hamming Distance distribution increases from 0.39-0.41 as the gaze angle increase decreases from -50° to 0°and then increase from 0° to +50°. The lowest Hamming distance is observed at iris images captured at 0° in angle because they are captured at the same angle. The highest Hamming distance is seen at iris images captured at 50° in angle and nearly values of -50° same because the difference between image acquisition angles of the compared iris images is 50° in angle that is the highest difference in the both off-angle iris dataset. Figure 5.14(g) represents the comparison of iris images captured at 10° with other iris images captured from -50° to +50°. We observe that mean of Hamming Distance distribution increases from 0.41-0.40 as the gaze angle increase decreases from -50° to 10°and then increase from 10° to +50°. The lowest Hamming distance is observed at iris images captured at 10° in angle because they are captured at the same angle. The highest Hamming distance is seen at iris images captured at -50° in angle because the difference between image acquisition angles of the compared iris images is 60° in angle that is the highest difference in the off-angle iris dataset. Figure 5.14(h) represents the comparison of iris images captured at 20° with other iris images captured from -50° to +50°. We observe that mean of Hamming Distance distribution decreases from 0.40-0.38 as the gaze angle increase decreases from -50° to 20°and then increase from 20° to +50°. The lowest Hamming distance is observed at iris images captured at 20° in angle because they are captured at the same angle. The highest Hamming distance is seen at iris images captured at -50° in angle because the difference between image acquisition angles of the compared iris images is 70° in angle that is the highest difference in the off-angle iris dataset. Figure 5.14(i) represents the comparison of iris images captured at 30° with other iris images captured from -50° to +50°. We observe that mean of Hamming Distance distribution decreases from 0.41-0.36 as the gaze angle increase decreases from -50° to 30°and then

increase from 30° to +50°. The lowest Hamming distance is observed at iris images captured at 30° in angle because they are captured at the same angle. The highest Hamming distance is seen at iris images captured at -50° in angle because the difference between image acquisition angles of the compared iris images is 80° in angle that is the highest difference in the off-angle iris dataset. Figure 5.14(j) represents the comparison of iris images captured at 40° with other iris images captured from -50° to +50°. We observe that mean of Hamming Distance distribution decreases from 0.42-0.26 as the gaze angle increase decreases from -50° to 40°and then increase from 40° to +50°. The lowest Hamming distance is observed at iris images captured at 40° in angle because they are captured at the same angle. The highest Hamming distance is seen at iris images captured at -50° in angle because the difference between image acquisition angles of the compared iris images is 90° in angle that is the highest difference in the off-angle iris dataset. Figure 5.14(k) represents the comparison of iris images captured at 50° with other iris images captured from -50° to +50°. We observe that mean of Hamming Distance distribution decreases from 0.46-0.18 as the gaze angle decrease from -50° to +50°. The lowest Hamming distance is observed at iris images captured at 50° in angle because they are captured at the same angle. The highest Hamming distance is seen at iris images captured at -50° in angle because the difference between image acquisition angles of the compared iris images is 100° in angle that is the highest difference in the off-angle iris dataset.

Finally we add %3 error on ellipse center and we present how change Hamming distances distributions for all inter-class and intra-class iris comparisons and the error bar of the Hamming distance distribution of iris comparisons in inter-class comparisons.

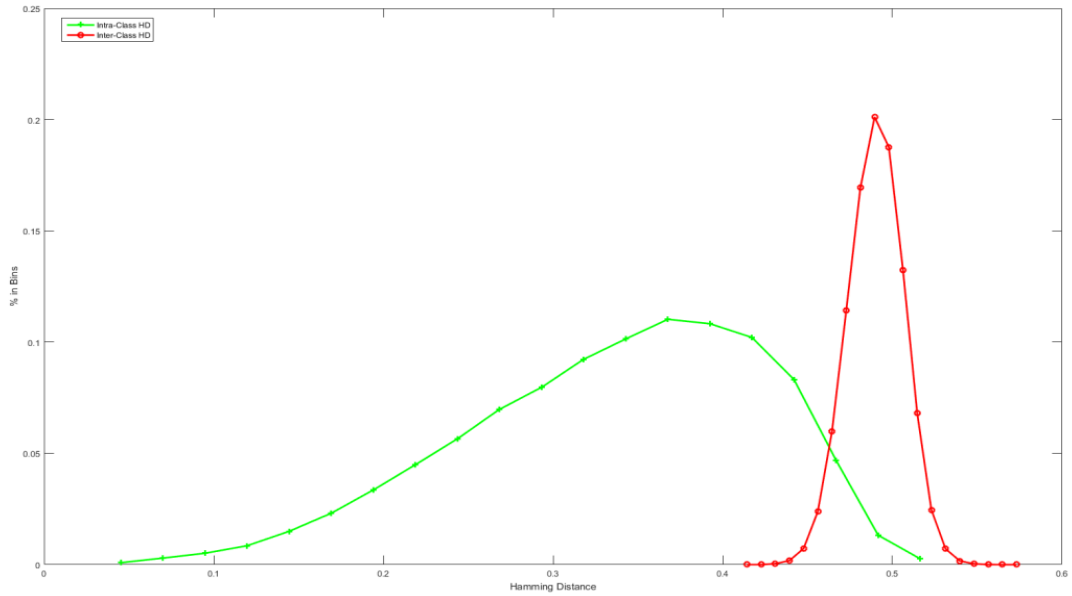

Figure 0.15. The Hamming distances distributions for all inter-class and intra-class iris comparisons in the MUID Off-angle dataset.

Figure 5.15 shows the Hamming distances distributions for all inter-class and intra-class iris comparisons in the MUID Off-angle dataset. We used off-angle image between -50° to +50° with increment 10° for our experiment. The histogram on the left with solid green line shows the intra-class Hamming distance that represents comparisons between two images of the same subjects. The left histogram with solid green shows Hamming Distance distribution for intra class that represents comparisons between two different subjects. We observe that intra-class Hamming distance varies changed from changes between 0.02-0.52 with a mean value of 0.27. The histogram on the left with solid green line shows the intra-class Hamming distance that represents comparisons between two images of the different subjects. The right histogram with solid red shows Hamming Distance distribution for inter class. Inter class varies changed from 0.43-0.57 with a mean value of 0.50. MUID Off-angle dataset change from -50° to +50° with increment 10° for our experiment, the main reason for the performance degradation in iris recognition system is the comparison of the frontal and off-angle iris images captured from different off-angles.

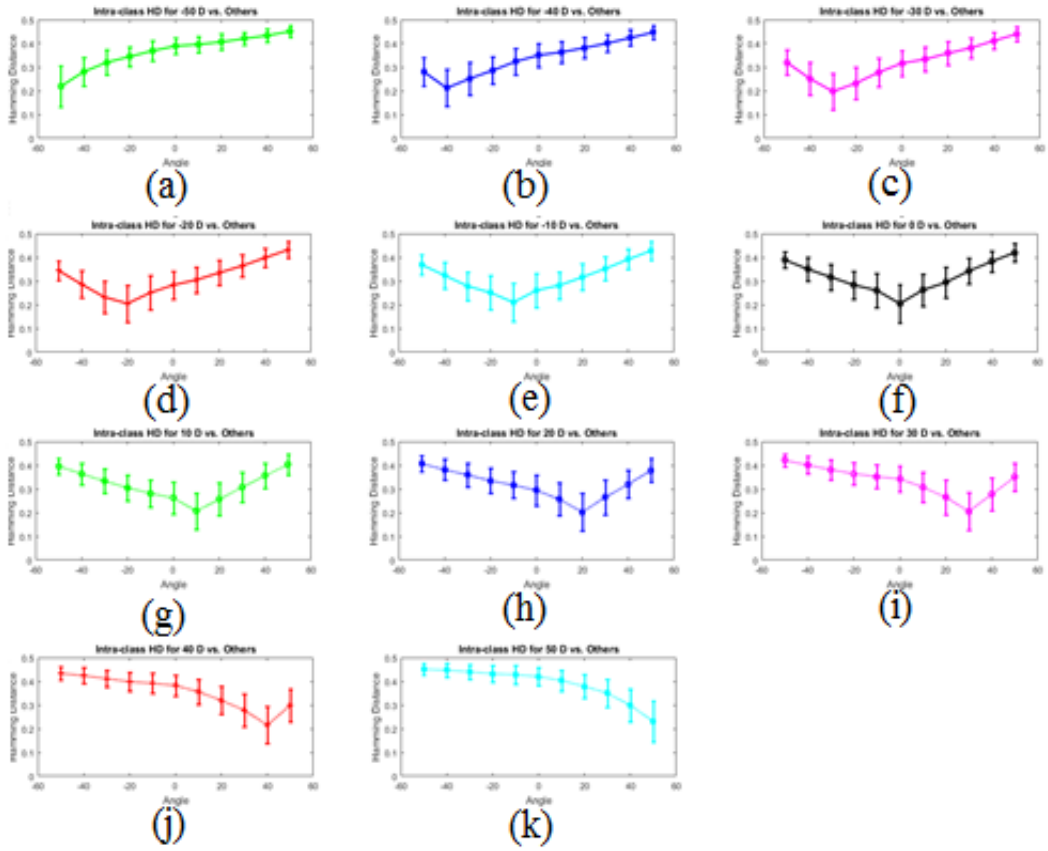

Figure 0.16. The error bar of the Hamming distance distribution of iris comparisons in inter-class comparisons.

Figure 5.16 shows the error bar of the Hamming distance distribution of iris comparisons in inter-class comparisons of the iris images captured from -50° to +50° in angle with other iris images captured from all off-angle degrees. The center of the lines represents the mean values and the bars show the standard deviation. Therefore, this figure contains all possible comparisons in intra-class distribution. For example, Figure 5.16(a) represents the comparison of iris images captured at -50° with other iris images captured from -50° to +50°. We observe that mean of Hamming Distance distribution increases from 0.21-0.46 as the gaze angle increase increases from -50° to +50°. The lowest Hamming distance is observed at iris images captured at -50° in angle because they are captured at the same angle. The highest Hamming distance is seen at iris images captured at 50° in angle because the difference between image acquisition angles of the compared iris images is 100° in angle that is the highest difference in the off-angle iris dataset. Figure 5.16(b) represents the comparison of iris images captured at -40° with other iris images captured from -50° to +50°. We observe that mean of

Hamming Distance distribution increases from 0.28-0.46 as the gaze angle increase decreases from -50° to -40°and then increase from -40° to +50°. The lowest Hamming distance is observed at iris images captured at -40° in angle because they are captured at the same angle. The highest Hamming distance is seen at iris images captured at 50° in angle because the difference between image acquisition angles of the compared iris images is 90° in angle that is the highest difference in the off-angle iris dataset. Figure 5.16(c) represents the comparison of iris images captured at -30° with other iris images captured from -50° to +50°. We observe that mean of Hamming Distance distribution increases from 0.32-0.45 as the gaze angle increase decreases from -50° to -30°and then increase from -30° to +50°. The lowest Hamming distance is observed at iris images captured at -30° in angle because they are captured at the same angle. The highest Hamming distance is seen at iris images captured at 50° in angle because the difference between image acquisition angles of the compared iris images is 80° in angle that is the highest difference in the off-angle iris dataset. Figure 5.16(d) represents the comparison of iris images captured at -20° with other iris images captured from -50° to +50°. We observe that mean of Hamming Distance distribution increases from 0.35-0.42 as the gaze angle increase decreases from -50° to -20°and then increase from -20° to +50°. The lowest Hamming distance is observed at iris images captured at -20° in angle because they are captured at the same angle. The highest Hamming distance is seen at iris images captured at 50° in angle because the difference between image acquisition angles of the compared iris images is 70° in angle that is the highest difference in the off-angle iris dataset. Figure 5.16(e) represents the comparison of iris images captured at -10° with other iris images captured from -50° to +50°. We observe that mean of Hamming Distance distribution increases from 0.38-0.40 as the gaze angle increase decreases from -50° to -10°and then increase from -10° to +50°. The lowest Hamming distance is observed at iris images captured at -10° in angle because they are captured at the same angle. The highest Hamming distance is seen at iris images captured at 50° in angle because the difference between image acquisition angles of the compared iris images is 60° in angle that is the highest difference in the off-angle iris dataset. Figure 5.16(f) represents the comparison of iris images captured at 0° with other iris images captured from -50° to +50°. We observe that mean of Hamming Distance distribution increases from 0.40-0.40 as the gaze angle increase decreases from -50° to 0°and then increase from 0° to +50°. The lowest Hamming distance is observed at iris images

captured at 0° in angle because they are captured at the same angle. The highest Hamming distance is seen at iris images captured at 50° in angle and values of -50° same because the difference between image acquisition angles of the compared iris images is 50° in angle that is the highest difference in the both off-angle iris dataset. Figure 5.16(g) represents the comparison of iris images captured at 10° with other iris images captured from -50° to +50°. We observe that mean of Hamming Distance distribution increases from 0.40-0.39 as the gaze angle increase decreases from -50° to 10°and then increase from 10° to +50°. The lowest Hamming distance is observed at iris images captured at 10° in angle because they are captured at the same angle. The highest Hamming distance is seen at iris images captured at -50° in angle because the difference between image acquisition angles of the compared iris images is 60° in angle that is the highest difference in the off-angle iris dataset. Figure 5.16(h) represents the comparison of iris images captured at 20° with other iris images captured from -50° to +50°. We observe that mean of Hamming Distance distribution decreases from 0.41-0.38 as the gaze angle increase decreases from -50° to 20°and then increase from 20° to +50°. The lowest Hamming distance is observed at iris images captured at 20° in angle because they are captured at the same angle. The highest Hamming distance is seen at iris images captured at -50° in angle because the difference between image acquisition angles of the compared iris images is 70° in angle that is the highest difference in the off-angle iris dataset. Figure 5.16(i) represents the comparison of iris images captured at 30° with other iris images captured from -50° to +50°. We observe that mean of Hamming Distance distribution decreases from 0.42-0.35 as the gaze angle increase decreases from -50° to 30°and then increase from 30° to +50°. The lowest Hamming distance is observed at iris images captured at 30° in angle because they are captured at the same angle. The highest Hamming distance is seen at iris images captured at -50° in angle because the difference between image acquisition angles of the compared iris images is 80° in angle that is the highest difference in the off-angle iris dataset. Figure 5.16(j) represents the comparison of iris images captured at 40° with other iris images captured from -50° to +50°. We observe that mean of Hamming Distance distribution decreases from 0.44-0.30 as the gaze angle increase decreases from -50° to 40°and then increase from 40° to +50°. The lowest Hamming distance is observed at iris images captured at 40° in angle because they are captured at the same angle. The highest Hamming distance is seen at iris images captured at -50° in angle because the difference

between image acquisition angles of the compared iris images is 90° in angle that is the highest difference in the off-angle iris dataset. Figure 5.16(k) represents the comparison of iris images captured at 50° with other iris images captured from -50° to +50°. We observe that mean of Hamming Distance distribution decreases from 0.46-0.21 as the gaze angle decrease from -50° to +50°. The lowest Hamming distance is observed at iris images captured at 50° in angle because they are captured at the same angle. The highest Hamming distance is seen at iris images captured at -50° in angle because the difference between image acquisition angles of the compared iris images is 100° in angle that is the highest difference in the off-angle iris dataset.

5.2.2. Error in Minor and Major Axis

Off-angle iris segmentation is fixed by Ground Truth Tool. We used fixed off-angle iris segmentation parameters for our experimental result. We added %1, %2 and %3 error in minor and major axis which are $r1$ and $r2$ on fixed segmentation parameters. Then we observed how change Hamming Distance. We present Hamming distances distributions for all inter-class and intra-class iris comparisons in the MUID Off-angle dataset showed respectively in Figure 5.17, Figure 5.19 and Figure 5.21. Figure 5.18, Figure 5.20 and Figure 5.22 shows the error bar of the Hamming distance distribution of iris comparisons in inter-class comparisons.

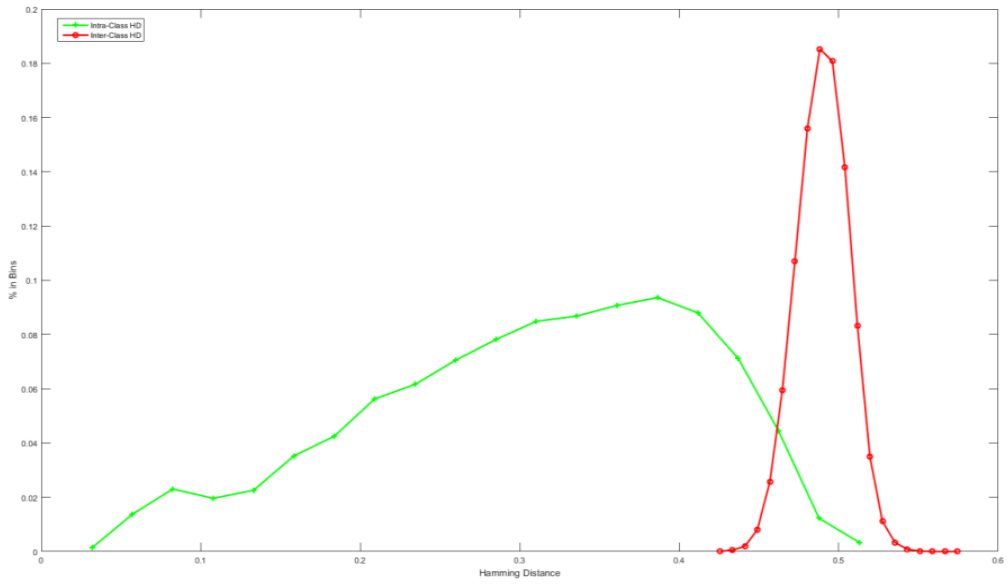

Figure 0.17. Hamming distances distributions for all inter-class and intra-class iris comparisons in the MUID Off-angle dataset.

Figure 5.17 shows the Hamming distances distributions for all inter-class and intra-class iris comparisons in the MUID Off-angle dataset. Firstly we added %1, error in minor and major axis. We used off-angle image between -50° to +50° with increment 10° for our experiment. The histogram on the left with solid green line shows the intra-class Hamming distance that represents comparisons between two images of the same subjects. The left histogram with solid green shows Hamming Distance distribution for intra class that represents comparisons between two different subjects. We observe that intra-class Hamming distance varies changed from changes between 0.03-0.53 with a mean value of 0.28. The histogram on the left with solid green line shows the intra-class Hamming distance that represents comparisons between two images of the different subjects. The right histogram with solid red shows Hamming Distance distribution for inter class. Inter class varies changed from 0.43-0.57 with a mean value of 0.50. MUID Off-angle dataset change from -50° to +50° with increment 10° for our experiment, the main reason for the performance degradation in iris recognition system is the comparison of the frontal and off-angle iris images captured from different off-angles.

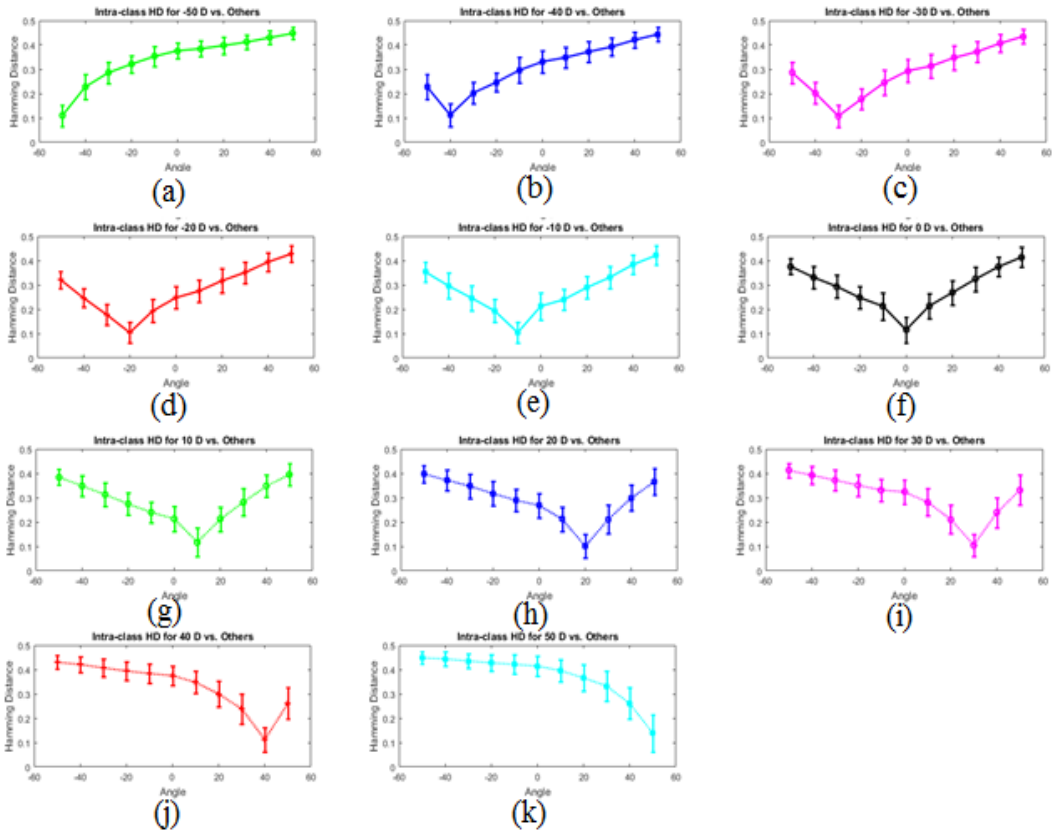

Figure 0.18.The error bar of the Hamming distance distribution of iris comparisons.

Figure 5.18 shows the error bar of the Hamming distance distribution of iris comparisons in inter-class comparisons of the iris images captured from -50° to +50° in angle with other iris images captured from all off-angle degrees. The center of the lines represents the mean values and the bars show the standard deviation. Therefore, this figure contains all possible comparisons in intra-class distribution. For example, Figure 5.18(a) represents the comparison of iris images captured at -50° with other iris images captured from -50° to +50°. We observe that mean of Hamming Distance distribution increases from 0.11-0.46 as the gaze angle increase increases from -50° to +50°. The lowest Hamming distance is observed at iris images captured at -50° in angle because they are captured at the same angle. The highest Hamming distance is seen at iris images captured at 50° in angle because the difference between image acquisition angles of the compared iris images is 100° in angle that is the highest difference in the off-angle iris dataset. Figure 5.18(b) represents the comparison of iris images captured at -40° with other iris images captured from -50° to +50°. We observe that mean of Hamming Distance distribution increases from 0.22-0.46 as the gaze angle increase decreases from -50° to -40°and then increase from -40° to +50°. The lowest Hamming distance is observed at iris images captured at -40° in angle because they are captured at the same angle. The highest Hamming distance is seen at iris images captured at 50° in angle because the difference between image acquisition angles of the compared iris images is 90° in angle that is the highest difference in the off-angle iris dataset. Figure 5.18(c) represents the comparison of iris images captured at -30° with other iris images captured from -50° to +50°. We observe that mean of Hamming Distance distribution increases from 0.29-0.45 as the gaze angle increase decreases from -50° to -30°and then increase from -30° to +50°. The lowest Hamming distance is observed at iris images captured at -30° in angle because they are captured at the same angle. The highest Hamming distance is seen at iris images captured at 50° in angle because the difference between image acquisition angles of the compared iris images is 80° in angle that is the highest difference in the off-angle iris dataset. Figure 5.18(d) represents the comparison of iris images captured at -20° with other iris images captured from -50° to +50°. We observe that mean of Hamming Distance distribution increases from 0.32-0.42 as the gaze angle increase decreases from -50° to -20°and then increase from -20° to +50°. The lowest Hamming distance is observed at iris images captured at -20° in angle

because they are captured at the same angle. The highest Hamming distance is seen at iris images captured at 50° in angle because the difference between image acquisition angles of the compared iris images is 70° in angle that is the highest difference in the off-angle iris dataset. Figure 5.18(e) represents the comparison of iris images captured at -10° with other iris images captured from -50° to +50°. We observe that mean of Hamming Distance distribution increases from 0.35-0.40 as the gaze angle increase decreases from -50° to -10°and then increase from -10° to +50°. The lowest Hamming distance is observed at iris images captured at -10° in angle because they are captured at the same angle. The highest Hamming distance is seen at iris images captured at 50° in angle because the difference between image acquisition angles of the compared iris images is 60° in angle that is the highest difference in the off-angle iris dataset. Figure 5.18(f) represents the comparison of iris images captured at 0° with other iris images captured from -50° to +50°. We observe that mean of Hamming Distance distribution increases from 0.39-0.41 as the gaze angle increase decreases from -50° to 0°and then increase from 0° to +50°. The lowest Hamming distance is observed at iris images captured at 0° in angle because they are captured at the same angle. The highest Hamming distance is seen at iris images captured at 50° in angle and values of -50° nearly same because the difference between image acquisition angles of the compared iris images is 50° in angle that is the highest difference in the both off-angle iris dataset. Figure 5.18(g) represents the comparison of iris images captured at 10° with other iris images captured from -50° to +50°. We observe that mean of Hamming Distance distribution increases from 0.40-0.36 as the gaze angle increase decreases from -50° to 10°and then increase from 10° to +50°. The lowest Hamming distance is observed at iris images captured at 10° in angle because they are captured at the same angle. The highest Hamming distance is seen at iris images captured at -50° in angle because the difference between image acquisition angles of the compared iris images is 60° in angle that is the highest difference in the off-angle iris dataset. Figure 5.18(h) represents the comparison of iris images captured at 20° with other iris images captured from -50° to +50°. We observe that mean of Hamming Distance distribution decreases from 0.40-0.36 as the gaze angle increase decreases from -50° to 20°and then increase from 20° to +50°. The lowest Hamming distance is observed at iris images captured at 20° in angle because they are captured at the same angle. The highest Hamming distance is seen at iris images captured at -50° in angle because the difference between image acquisition

angles of the compared iris images is 70° in angle that is the highest difference in the off-angle iris dataset. Figure 5.18(i) represents the comparison of iris images captured at 30° with other iris images captured from -50° to +50°. We observe that mean of Hamming Distance distribution decreases from 0.41-0.34 as the gaze angle increase decreases from -50° to 30°and then increase from 30° to +50°. The lowest Hamming distance is observed at iris images captured at 30° in angle because they are captured at the same angle. The highest Hamming distance is seen at iris images captured at -50° in angle because the difference between image acquisition angles of the compared iris images is 80° in angle that is the highest difference in the off-angle iris dataset. Figure 5.18(j) represents the comparison of iris images captured at 40° with other iris images captured from -50° to +50°. We observe that mean of Hamming Distance distribution decreases from 0.42-0.25 as the gaze angle increase decreases from -50° to 40°and then increase from 40° to +50°. The lowest Hamming distance is observed at iris images captured at 40° in angle because they are captured at the same angle. The highest Hamming distance is seen at iris images captured at -50° in angle because the difference between image acquisition angles of the compared iris images is 90° in angle that is the highest difference in the off-angle iris dataset. Figure 5.18(k) represents the comparison of iris images captured at 50° with other iris images captured from -50° to +50°. We observe that mean of Hamming Distance distribution decreases from 0.45-0.11 as the gaze angle decrease from -50° to +50°. The lowest Hamming distance is observed at iris images captured at 50° in angle because they are captured at the same angle. The highest Hamming distance is seen at iris images captured at -50° in angle because the difference between image acquisition angles of the compared iris images is 100° in angle that is the highest difference in the off-angle iris dataset.

Secondly we add %2 error on minor and major axis and we present how change Hamming distances distributions for all inter-class and intra-class iris comparisons and the error bar of the Hamming distance distribution of iris comparisons in inter-class comparisons.

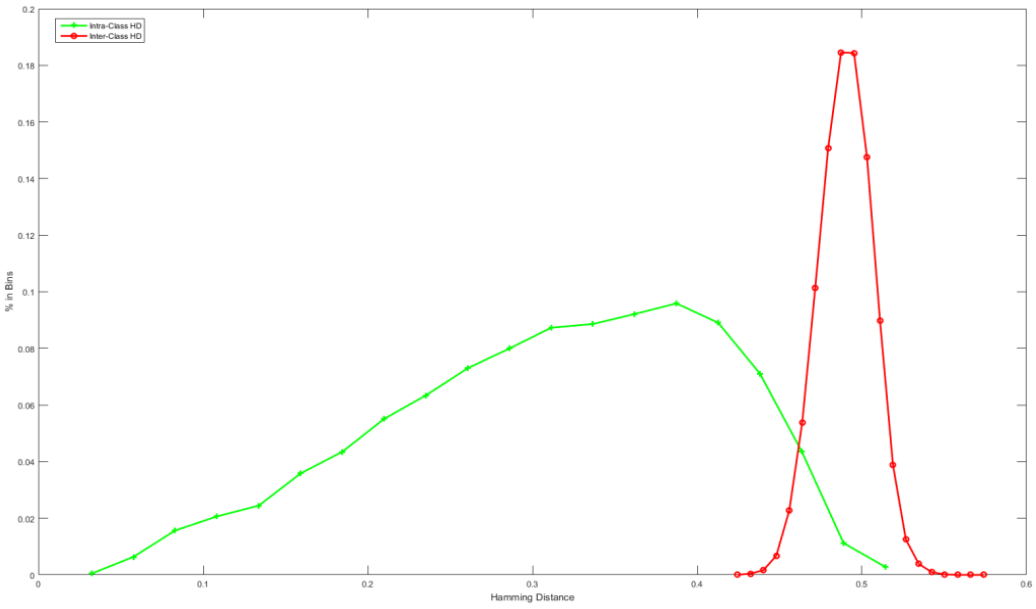

Figure 0.19. The Hamming distances distributions for all inter-class and intra-class iris comparisons in the MUID Off-angle dataset.

Figure 5.19 shows the Hamming distances distributions for all inter-class and intra-class iris comparisons in the MUID Off-angle dataset. We used off-angle image between -50° to +50° with increment 10° for our experiment. The histogram on the left with solid green line shows the intra-class Hamming distance that represents comparisons between two images of the same subjects. The left histogram with solid green shows Hamming Distance distribution for intra class that represents comparisons between two different subjects. We observe that intra-class Hamming distance varies changed from changes between 0.02-0.51 with a mean value of 0.26. The histogram on the left with solid green line shows the intra-class Hamming distance that represents comparisons between two images of the different subjects. The right histogram with solid red shows Hamming Distance distribution for inter class. Inter class varies changed from 0.42-0.56 with a mean value of 0.54 MUID Off-angle dataset change from -50° to +50° with increment 10° for our experiment, the main reason for the performance degradation in iris recognition system is the comparison of the frontal and off-angle iris images captured from different off-angles.

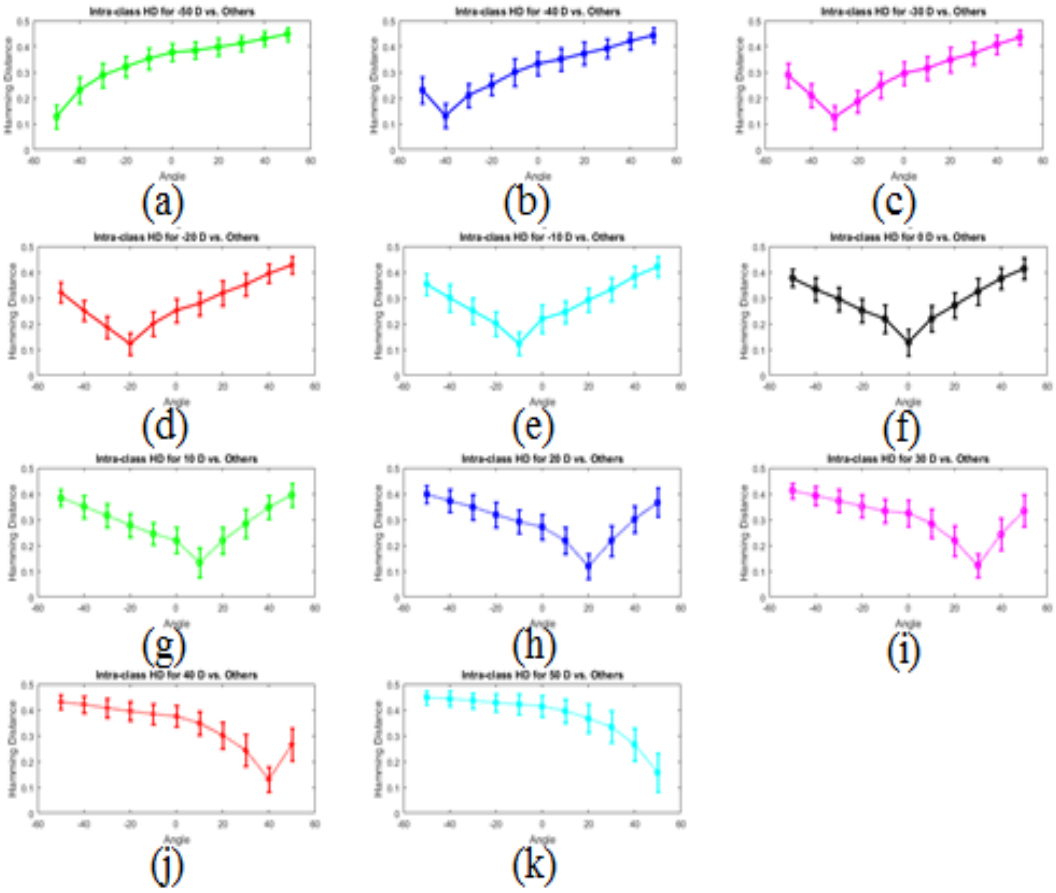

Figure 0.20.The error bar of the Hamming distance distribution of iris comparisons.

Figure 5.20 shows the error bar of the Hamming distance distribution of iris comparisons in inter-class comparisons of the iris images captured from -50° to +50° in angle with other iris images captured from all off-angle degrees. The center of the lines represents the mean values and the bars show the standard deviation. Therefore, this figure contains all possible comparisons in intra-class distribution. For example, Figure 5. 20(a) represents the comparison of iris images captured at -50° with other iris images captured from -50° to +50°. We observe that mean of Hamming Distance distribution increases from 0.14-0.46 as the gaze angle increase increases from -50° to +50°. The lowest Hamming distance is observed at iris images captured at -50° in angle because they are captured at the same angle. The highest Hamming distance is seen at iris images captured at 50° in angle because the difference between image acquisition angles of the compared iris images is 100° in angle that is the highest difference in the off-angle iris dataset. Figure 5.20(b) represents the comparison of iris images captured at -40° with other iris images captured from -50° to +50°. We observe that mean of

Hamming Distance distribution increases from 0.24-0.46 as the gaze angle increase decreases from -50° to -40°and then increase from -40° to +50°. The lowest Hamming distance is observed at iris images captured at -40° in angle because they are captured at the same angle. The highest Hamming distance is seen at iris images captured at 50° in angle because the difference between image acquisition angles of the compared iris images is 90° in angle that is the highest difference in the off-angle iris dataset. Figure 5.20(c) represents the comparison of iris images captured at -30° with other iris images captured from -50° to +50°. We observe that mean of Hamming Distance distribution increases from 0.29-0.45 as the gaze angle increase decreases from -50° to -30°and then increase from -30° to +50°. The lowest Hamming distance is observed at iris images captured at -30° in angle because they are captured at the same angle. The highest Hamming distance is seen at iris images captured at 50° in angle because the difference between image acquisition angles of the compared iris images is 80° in angle that is the highest difference in the off-angle iris dataset. Figure 5.20(d) represents the comparison of iris images captured at -20° with other iris images captured from -50° to +50°. We observe that mean of Hamming Distance distribution increases from 0.31-0.42 as the gaze angle increase decreases from -50° to -20°and then increase from -20° to +50°. The lowest Hamming distance is observed at iris images captured at -20° in angle because they are captured at the same angle. The highest Hamming distance is seen at iris images captured at 50° in angle because the difference between image acquisition angles of the compared iris images is 70° in angle that is the highest difference in the off-angle iris dataset. Figure 5.20(e) represents the comparison of iris images captured at -10° with other iris images captured from -50° to +50°. We observe that mean of Hamming Distance distribution increases from 0.35-0.41 as the gaze angle increase decreases from -50° to -10°and then increase from -10° to +50°. The lowest Hamming distance is observed at iris images captured at -10° in angle because they are captured at the same angle. The highest Hamming distance is seen at iris images captured at 50° in angle because the difference between image acquisition angles of the compared iris images is 60° in angle that is the highest difference in the off-angle iris dataset. Figure 5.20(f) represents the comparison of iris images captured at 0° with other iris images captured from -50° to +50°. We observe that mean of Hamming Distance distribution increases from 0.38-0.40 as the gaze angle increase decreases from -50° to 0°and then increase from 0° to +50°. The lowest Hamming distance is observed at iris images

captured at 0° in angle because they are captured at the same angle. The highest Hamming distance is seen at iris images captured at 50° in angle and values of -50° nearly same because the difference between image acquisition angles of the compared iris images is 50° in angle that is the highest difference in the both off-angle iris dataset. Figure 5.20(g) represents the comparison of iris images captured at 10° with other iris images captured from -50° to +50°. We observe that mean of Hamming Distance distribution increases from 0.40-0.39 as the gaze angle increase decreases from -50° to 10°and then increase from 10° to +50°. The lowest Hamming distance is observed at iris images captured at 10° in angle because they are captured at the same angle. The highest Hamming distance is seen at iris images captured at -50° in angle because the difference between image acquisition angles of the compared iris images is 60° in angle that is the highest difference in the off-angle iris dataset. Figure 5.20(h) represents the comparison of iris images captured at 20° with other iris images captured from -50° to +50°. We observe that mean of Hamming Distance distribution decreases from 0.40-0.35 as the gaze angle increase decreases from -50° to 20°and then increase from 20° to +50°. The lowest Hamming distance is observed at iris images captured at 20° in angle because they are captured at the same angle. The highest Hamming distance is seen at iris images captured at -50° in angle because the difference between image acquisition angles of the compared iris images is 70° in angle that is the highest difference in the off-angle iris dataset. Figure 5.20(i) represents the comparison of iris images captured at 30° with other iris images captured from -50° to +50°. We observe that mean of Hamming Distance distribution decreases from 0.41-0.32 as the gaze angle increase decreases from -50° to 30°and then increase from 30° to +50°. The lowest Hamming distance is observed at iris images captured at 30° in angle because they are captured at the same angle. The highest Hamming distance is seen at iris images captured at -50° in angle because the difference between image acquisition angles of the compared iris images is 80° in angle that is the highest difference in the off-angle iris dataset. Figure 5.20(j) represents the comparison of iris images captured at 40° with other iris images captured from -50° to +50°. We observe that mean of Hamming Distance distribution decreases from 0.42-0.28 as the gaze angle increase decreases from -50° to 40°and then increase from 40° to +50°. The lowest Hamming distance is observed at iris images captured at 40° in angle because they are captured at the same angle. The highest Hamming distance is seen at iris images captured at -50° in angle because the difference

between image acquisition angles of the compared iris images is 90° in angle that is the highest difference in the off-angle iris dataset. Figure 5.20(k) represents the comparison of iris images captured at 50° with other iris images captured from -50° to +50°. We observe that mean of Hamming Distance distribution decreases from 0.45-0.14 as the gaze angle decrease from -50° to +50°. The lowest Hamming distance is observed at iris images captured at 50° in angle because they are captured at the same angle. The highest Hamming distance is seen at iris images captured at -50° in angle because the difference between image acquisition angles of the compared iris images is 100° in angle that is the highest difference in the off-angle iris dataset.

Finally we add %3 error on minor and major axis and we present how change Hamming distances distributions for all inter-class and intra-class iris comparisons and the error bar of the Hamming distance distribution of iris comparisons in inter-class comparisons.

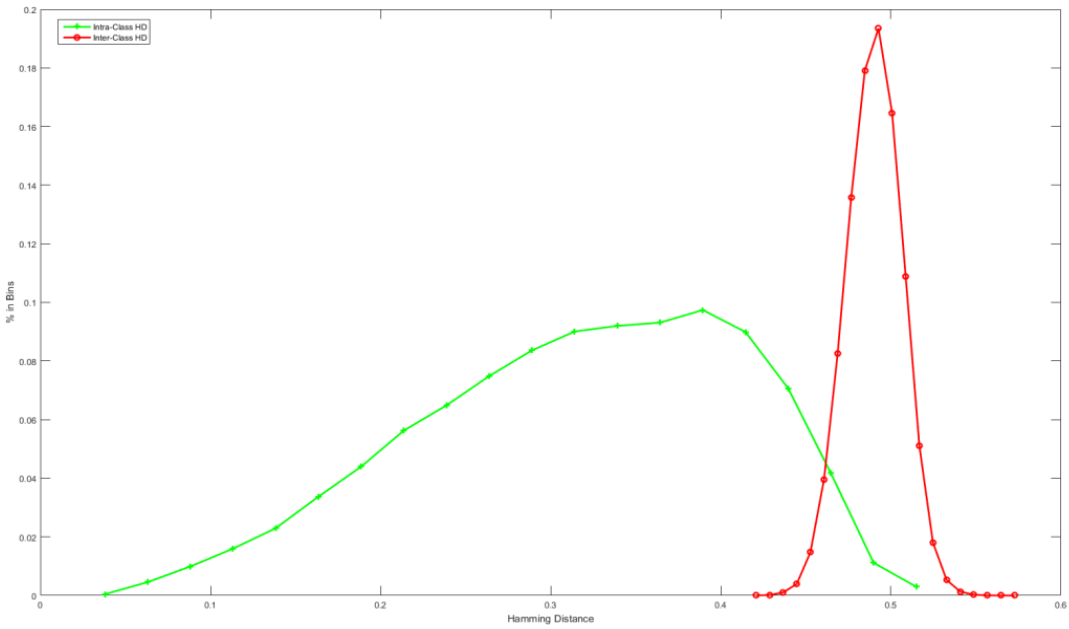

Figure 0.21. Hamming distances distributions for all inter-class and intra-class iris comparisons in the MUID Off-angle dataset.

Figure 5.21 shows the Hamming distances distributions for all inter-class and intra-class iris comparisons in the MUID Off-angle dataset. We used off-angle image between -50° to +50° with increment 10° for our experiment. The histogram on the left with solid green line shows the intra-class Hamming distance that represents comparisons between two images of the same subjects. The left histogram with solid green shows Hamming

Distance distribution for intra class that represents comparisons between two different subjects. We observe that intra-class Hamming distance varies changed from changes between 0.04-0.52 with a mean value of 0.28. The histogram on the left with solid green line shows the intra-class Hamming distance that represents comparisons between two images of the different subjects. The right histogram with solid red shows Hamming Distance distribution for inter class. Inter class varies changed from 0.42-0.56 with a mean value of 0.54 MUID Off-angle dataset change from -50° to +50° with increment 10° for our experiment, the main reason for the performance degradation in iris recognition system is the comparison of the frontal and off-angle iris images captured from different off-angles.

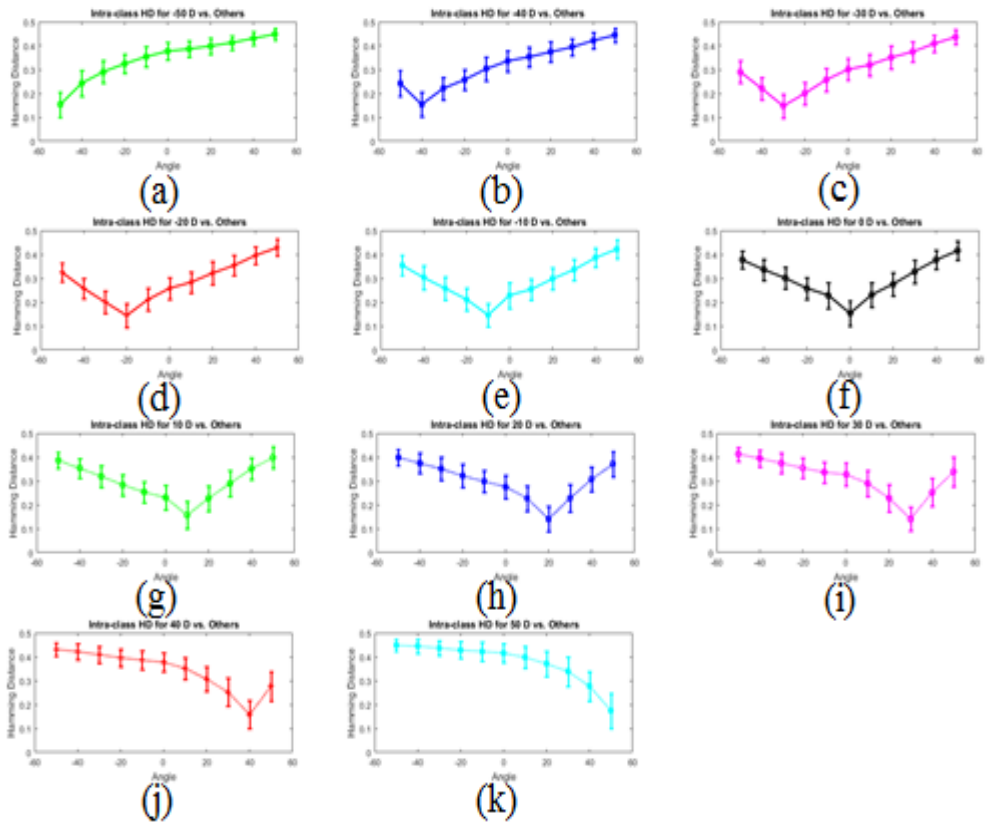

Figure 0.22. The error bar of the Hamming distance distribution of iris comparisons.

Figure 5.22 shows the error bar of the Hamming distance distribution of iris comparisons in inter-class comparisons of the iris images captured from -50° to +50° in angle with other iris images captured from all off-angle degrees. The center of the lines represents the mean values and the bars show the standard deviation. Therefore, this

figure contains all possible comparisons in intra-class distribution. For example, Figure 5.22(a) represents the comparison of iris images captured at -50° with other iris images captured from -50° to +50°. We observe that mean of Hamming Distance distribution increases from 0.15-0.46 as the gaze angle increase increases from -50° to +50°. The lowest Hamming distance is observed at iris images captured at -50° in angle because they are captured at the same angle. The highest Hamming distance is seen at iris images captured at 50° in angle because the difference between image acquisition angles of the compared iris images is 100° in angle that is the highest difference in the off-angle iris dataset. Figure 5.22(b) represents the comparison of iris images captured at -40° with other iris images captured from -50° to +50°. We observe that mean of Hamming Distance distribution increases from 0.25-0.46 as the gaze angle increase decreases from -50° to -40°and then increase from -40° to +50°. The lowest Hamming distance is observed at iris images captured at -40° in angle because they are captured at the same angle. The highest Hamming distance is seen at iris images captured at 50° in angle because the difference between image acquisition angles of the compared iris images is 90° in angle that is the highest difference in the off-angle iris dataset. Figure 5.22(c) represents the comparison of iris images captured at -30° with other iris images captured from -50° to +50°. We observe that mean of Hamming Distance distribution increases from 0.30-0.45 as the gaze angle increase decreases from -50° to -30°and then increase from -30° to +50°. The lowest Hamming distance is observed at iris images captured at -30° in angle because they are captured at the same angle. The highest Hamming distance is seen at iris images captured at 50° in angle because the difference between image acquisition angles of the compared iris images is 80° in angle that is the highest difference in the off-angle iris dataset. Figure 5.22(d) represents the comparison of iris images captured at -20° with other iris images captured from -50° to +50°. We observe that mean of Hamming Distance distribution increases from 0.32-0.44 as the gaze angle increase decreases from -50° to -20°and then increase from -20° to +50°. The lowest Hamming distance is observed at iris images captured at -20° in angle because they are captured at the same angle. The highest Hamming distance is seen at iris images captured at 50° in angle because the difference between image acquisition angles of the compared iris images is 70° in angle that is the highest difference in the off-angle iris dataset. Figure 5.22(e) represents the comparison of iris images captured at -10° with other iris images captured from -50° to +50°. We observe that mean of

Hamming Distance distribution increases from 0.35-0.42 as the gaze angle increase decreases from -50° to -10°and then increase from -10° to +50°. The lowest Hamming distance is observed at iris images captured at -10° in angle because they are captured at the same angle. The highest Hamming distance is seen at iris images captured at 50° in angle because the difference between image acquisition angles of the compared iris images is 60° in angle that is the highest difference in the off-angle iris dataset. Figure 5.22(f) represents the comparison of iris images captured at 0° with other iris images captured from -50° to +50°. We observe that mean of Hamming Distance distribution increases from 0.38-0.41 as the gaze angle increase decreases from -50° to 0°and then increase from 0° to +50°. The lowest Hamming distance is observed at iris images captured at 0° in angle because they are captured at the same angle. The highest Hamming distance is seen at iris images captured at 50° in angle and values of -50° nearly same because the difference between image acquisition angles of the compared iris images is 50° in angle that is the highest difference in the both off-angle iris dataset. Figure 5.22(g) represents the comparison of iris images captured at 10° with other iris images captured from -50° to +50°. We observe that mean of Hamming Distance distribution increases from 0.40-0.39 as the gaze angle increase decreases from -50° to 10°and then increase from 10° to +50°. The lowest Hamming distance is observed at iris images captured at 10° in angle because they are captured at the same angle. The highest Hamming distance is seen at iris images captured at -50° in angle because the difference between image acquisition angles of the compared iris images is 60° in angle that is the highest difference in the off-angle iris dataset. Figure 5.22(h) represents the comparison of iris images captured at 20° with other iris images captured from -50° to +50°. We observe that mean of Hamming Distance distribution decreases from 0.40-0.36 as the gaze angle increase decreases from -50° to 20°and then increase from 20° to +50°. The lowest Hamming distance is observed at iris images captured at 20° in angle because they are captured at the same angle. The highest Hamming distance is seen at iris images captured at -50° in angle because the difference between image acquisition angles of the compared iris images is 70° in angle that is the highest difference in the off-angle iris dataset. Figure 5.22(i) represents the comparison of iris images captured at 30° with other iris images captured from -50° to +50°. We observe that mean of Hamming Distance distribution decreases from 0.41-0.35 as the gaze angle increase decreases from -50° to 30°and then increase from 30° to +50°. The lowest Hamming

distance is observed at iris images captured at 30° in angle because they are captured at the same angle. The highest Hamming distance is seen at iris images captured at -50° in angle because the difference between image acquisition angles of the compared iris images is 80° in angle that is the highest difference in the off-angle iris dataset. Figure 5.22(j) represents the comparison of iris images captured at 40° with other iris images captured from -50° to +50°. We observe that mean of Hamming Distance distribution decreases from 0.45-0.25 as the gaze angle increase decreases from -50° to 40°and then increase from 40° to +50°. The lowest Hamming distance is observed at iris images captured at 40° in angle because they are captured at the same angle. The highest Hamming distance is seen at iris images captured at -50° in angle because the difference between image acquisition angles of the compared iris images is 90° in angle that is the highest difference in the off-angle iris dataset. Figure 5.22(k) represents the comparison of iris images captured at 50° with other iris images captured from -50° to +50°. We observe that mean of Hamming Distance distribution decreases from 0.45-0.15 as the gaze angle decrease from -50° to +50°. The lowest Hamming distance is observed at iris images captured at 50° in angle because they are captured at the same angle. The highest Hamming distance is seen at iris images captured at -50° in angle because the difference between image acquisition angles of the compared iris images is 100° in angle that is the highest difference in the off-angle iris dataset.

5.2.3. Error in Orientation

Off-angle iris segmentation find by using ellipse parameters. We added 1° and 2° error in orientation. We present Hamming distances distributions for all inter-class and intra-class iris comparisons in the MUID Off-angle dataset showed respectively in Figure 5.23 and Figure 5.25. Figure 5.24 and Figure 5.26 shows the error bar of the Hamming distance distribution of iris comparisons in inter-class comparisons.

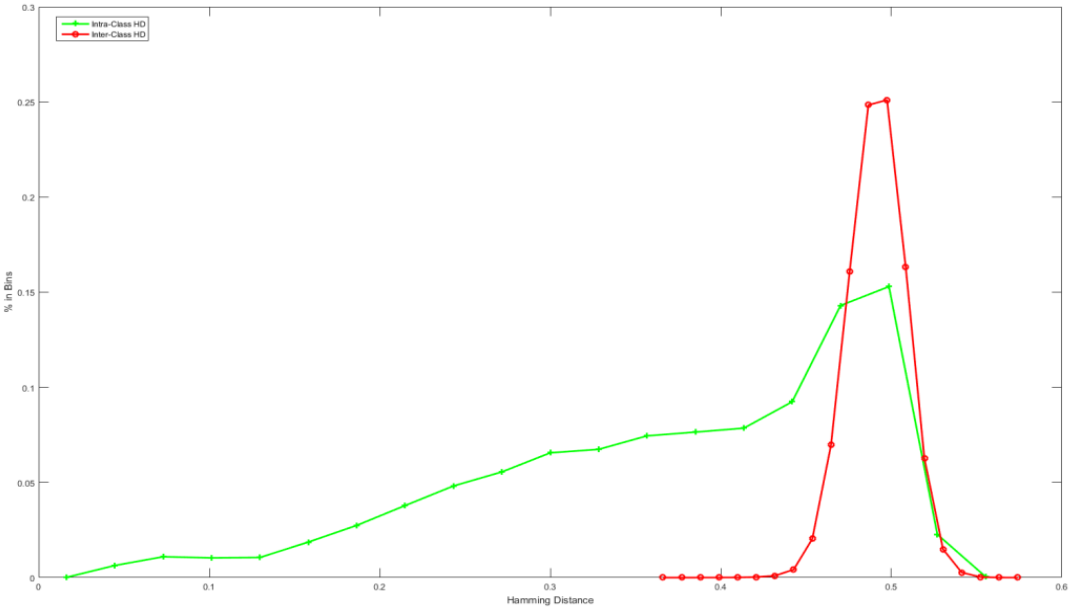

Figure 0.23. Hamming distances distributions for all inter-class and intra-class iris comparisons in the MUID Off-angle dataset.

Figure 5.23 shows the Hamming distances distributions for all inter-class and intra-class iris comparisons in the MUID Off-angle dataset. We used off-angle image between -50° to +50° with increment 10° for our experiment. The histogram on the left with solid green line shows the intra-class Hamming distance that represents comparisons between two images of the same subjects. The left histogram with solid green shows Hamming Distance distribution for intra class that represents comparisons between two different subjects. We observe that intra-class Hamming distance varies changed from changes between 0.01-0.55 with a mean value of 0.28. The histogram on the left with solid green line shows the intra-class Hamming distance that represents comparisons between two images of the different subjects. The right histogram with solid red shows Hamming Distance distribution for inter class. Inter class varies changed from 0.36-0.57 with a mean value of 0.47 MUID Off-angle dataset change from -50° to +50° with increment 10° for our experiment, the main reason for the performance degradation in iris recognition system is the comparison of the frontal and off-angle iris images captured from different off-angles.

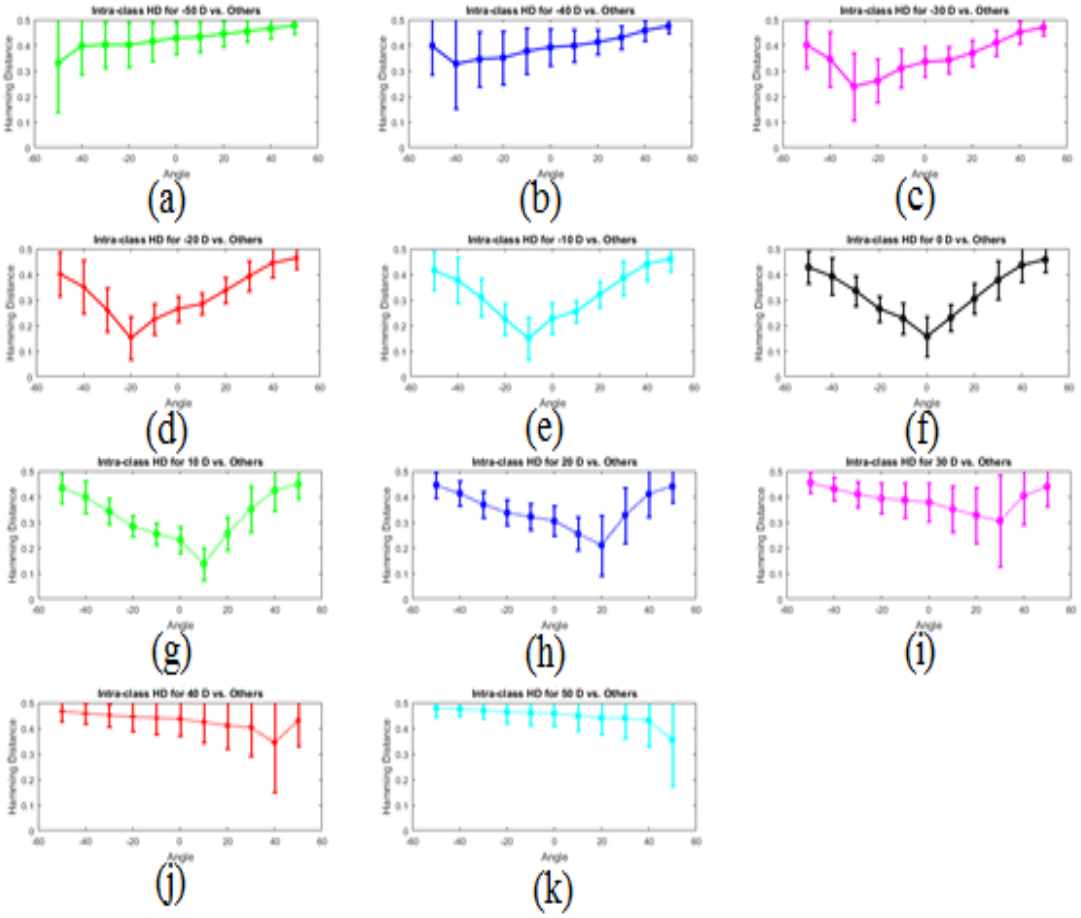

Figure 0.24.The error bar of the Hamming distance distribution of iris comparisons.

Figure 5.24 shows the error bar of the Hamming distance distribution of iris comparisons in inter-class comparisons of the iris images captured from -50° to +50° in angle with other iris images captured from all off-angle degrees. The center of the lines represents the mean values and the bars show the standard deviation. Therefore, this figure contains all possible comparisons in intra-class distribution. For example, Figure 5.24(a) represents the comparison of iris images captured at -50° with other iris images captured from -50° to +50°. We observe that mean of Hamming Distance distribution increases from 0.32-0.49 as the gaze angle increase increases from -50° to +50°. The lowest Hamming distance is observed at iris images captured at -50° in angle because they are captured at the same angle. The highest Hamming distance is seen at iris images captured at 50° in angle because the difference between image acquisition angles of the compared iris images is 100° in angle that is the highest difference in the

off-angle iris dataset. Figure 5.24(b) represents the comparison of iris images captured at -40° with other iris images captured from -50° to +50°. We observe that mean of Hamming Distance distribution increases from 0.38-0.49 as the gaze angle increase decreases from -50° to -40°and then increase from -40° to +50°. The lowest Hamming distance is observed at iris images captured at -40° in angle because they are captured at the same angle. The highest Hamming distance is seen at iris images captured at 50° in angle because the difference between image acquisition angles of the compared iris images is 90° in angle that is the highest difference in the off-angle iris dataset. Figure 5.24(c) represents the comparison of iris images captured at -30° with other iris images captured from -50° to +50°. We observe that mean of Hamming Distance distribution increases from 0.40-0.48 as the gaze angle increase decreases from -50° to -30°and then increase from -30° to +50°. The lowest Hamming distance is observed at iris images captured at -30° in angle because they are captured at the same angle. The highest Hamming distance is seen at iris images captured at 50° in angle because the difference between image acquisition angles of the compared iris images is 80° in angle that is the highest difference in the off-angle iris dataset. Figure 5.24(d) represents the comparison of iris images captured at -20° with other iris images captured from -50° to +50°. We observe that mean of Hamming Distance distribution increases from 0.40-0.45 as the gaze angle increase decreases from -50° to -20°and then increase from -20° to +50°. The lowest Hamming distance is observed at iris images captured at -20° in angle because they are captured at the same angle. The highest Hamming distance is seen at iris images captured at 50° in angle because the difference between image acquisition angles of the compared iris images is 70° in angle that is the highest difference in the off-angle iris dataset. Figure 5.24(e) represents the comparison of iris images captured at -10° with other iris images captured from -50° to +50°. We observe that mean of Hamming Distance distribution increases from 0.42-0.46 as the gaze angle increase decreases from -50° to -10°and then increase from -10° to +50°. The lowest Hamming distance is observed at iris images captured at -10° in angle because they are captured at the same angle. The highest Hamming distance is seen at iris images captured at 50° in angle because the difference between image acquisition angles of the compared iris images is 60° in angle that is the highest difference in the off-angle iris dataset. Figure 5.24(f) represents the comparison of iris images captured at 0° with other iris images captured from -50° to +50°. We observe that mean of Hamming Distance distribution

increases from 0.45-0.45 as the gaze angle increase decreases from -50° to 0°and then increase from 0° to +50°. The lowest Hamming distance is observed at iris images captured at 0° in angle because they are captured at the same angle. The highest Hamming distance is seen at iris images captured at 50° in angle and values of -50° nearly same because the difference between image acquisition angles of the compared iris images is 50° in angle that is the highest difference in the both off-angle iris dataset. Figure 5.24(g) represents the comparison of iris images captured at 10° with other iris images captured from -50° to +50°. We observe that mean of Hamming Distance distribution increases from 0.43-0.42 as the gaze angle increase decreases from -50° to 10°and then increase from 10° to +50°. The lowest Hamming distance is observed at iris images captured at 10° in angle because they are captured at the same angle. The highest Hamming distance is seen at iris images captured at -50° in angle because the difference between image acquisition angles of the compared iris images is 60° in angle that is the highest difference in the off-angle iris dataset. Figure 5.24(h) represents the comparison of iris images captured at 20° with other iris images captured from -50° to +50°. We observe that mean of Hamming Distance distribution decreases from 0.45-0.44 as the gaze angle increase decreases from -50° to 20°and then increase from 20° to +50°. The lowest Hamming distance is observed at iris images captured at 20° in angle because they are captured at the same angle. The highest Hamming distance is seen at iris images captured at -50° in angle because the difference between image acquisition angles of the compared iris images is 70° in angle that is the highest difference in the off-angle iris dataset. Figure 5.24(i) represents the comparison of iris images captured at 30° with other iris images captured from -50° to +50°. We observe that mean of Hamming Distance distribution decreases from 0.46-0.42 as the gaze angle increase decreases from -50° to 30°and then increase from 30° to +50°. The lowest Hamming distance is observed at iris images captured at 30° in angle because they are captured at the same angle. The highest Hamming distance is seen at iris images captured at -50° in angle because the difference between image acquisition angles of the compared iris images is 80° in angle that is the highest difference in the off-angle iris dataset. Figure 5.24(j) represents the comparison of iris images captured at 40° with other iris images captured from -50° to +50°. We observe that mean of Hamming Distance distribution decreases from 0.46-0.40 as the gaze angle increase decreases from -50° to 40°and then increase from 40° to +50°. The lowest Hamming distance is observed at iris images

captured at 40° in angle because they are captured at the same angle. The highest Hamming distance is seen at iris images captured at -50° in angle because the difference between image acquisition angles of the compared iris images is 90° in angle that is the highest difference in the off-angle iris dataset. Figure 5.24(k) represents the comparison of iris images captured at 50° with other iris images captured from -50° to +50°. We observe that mean of Hamming Distance distribution decreases from 0.48-0.38 as the gaze angle decrease from -50° to +50°. The lowest Hamming distance is observed at iris images captured at 50° in angle because they are captured at the same angle. The highest Hamming distance is seen at iris images captured at -50° in angle because the difference between image acquisition angles of the compared iris images is 100° in angle that is the highest difference in the off-angle iris dataset.

Secondly we add 2°error on orientation and we present how change Hamming distances distributions for all inter-class and intra-class iris comparisons and the error bar of the Hamming distance distribution of iris comparisons in inter-class comparisons.

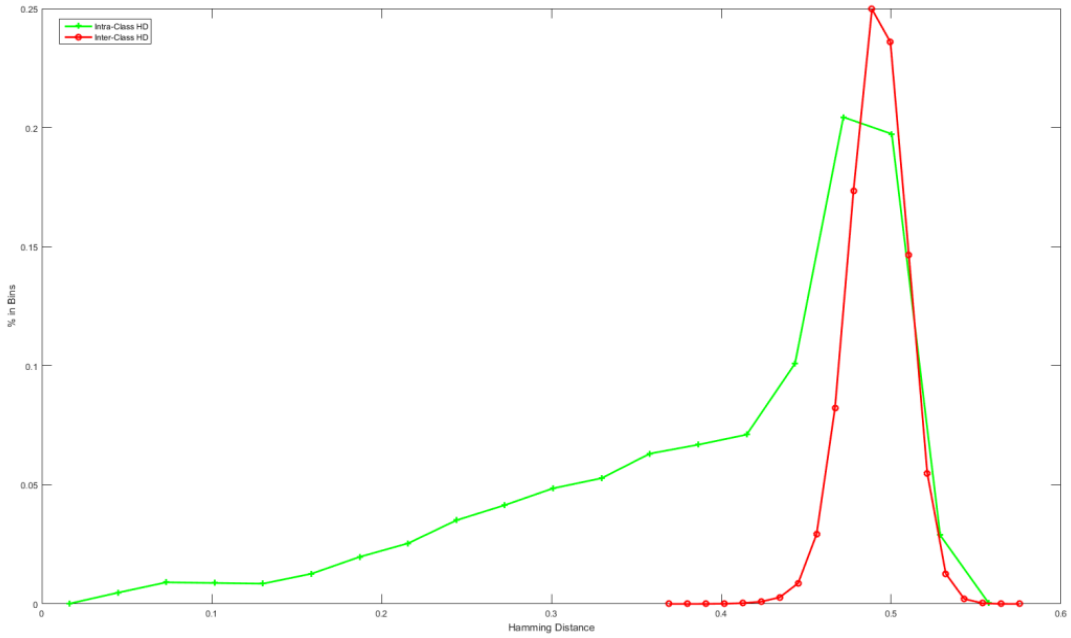

Figure 0.25. Hamming distances distributions for all inter-class and intra-class iris comparisons in the MUID Off-angle dataset.

Figure 5.25 shows the Hamming distances distributions for all inter-class and intra-class iris comparisons in the MUID Off-angle dataset. We used off-angle image between -50° to +50° with increment 10° for our experiment. The histogram on the left with solid

green line shows the intra-class Hamming distance that represents comparisons between two images of the same subjects. The left histogram with solid green shows Hamming Distance distribution for intra class that represents comparisons between two different subjects. We observe that intra-class Hamming distance varies changed from changes between 0.01-0.56 with a mean value of 0.28. The histogram on the left with solid green line shows the intra-class Hamming distance that represents comparisons between two images of the different subjects. The right histogram with solid red shows Hamming Distance distribution for inter class. Inter class varies changed from 0.37-0.57 with a mean value of 0.47 MUID Off-angle dataset change from -50° to +50° with increment 10° for our experiment, the main reason for the performance degradation in iris recognition system is the comparison of the frontal and off-angle iris images captured from different off-angles.

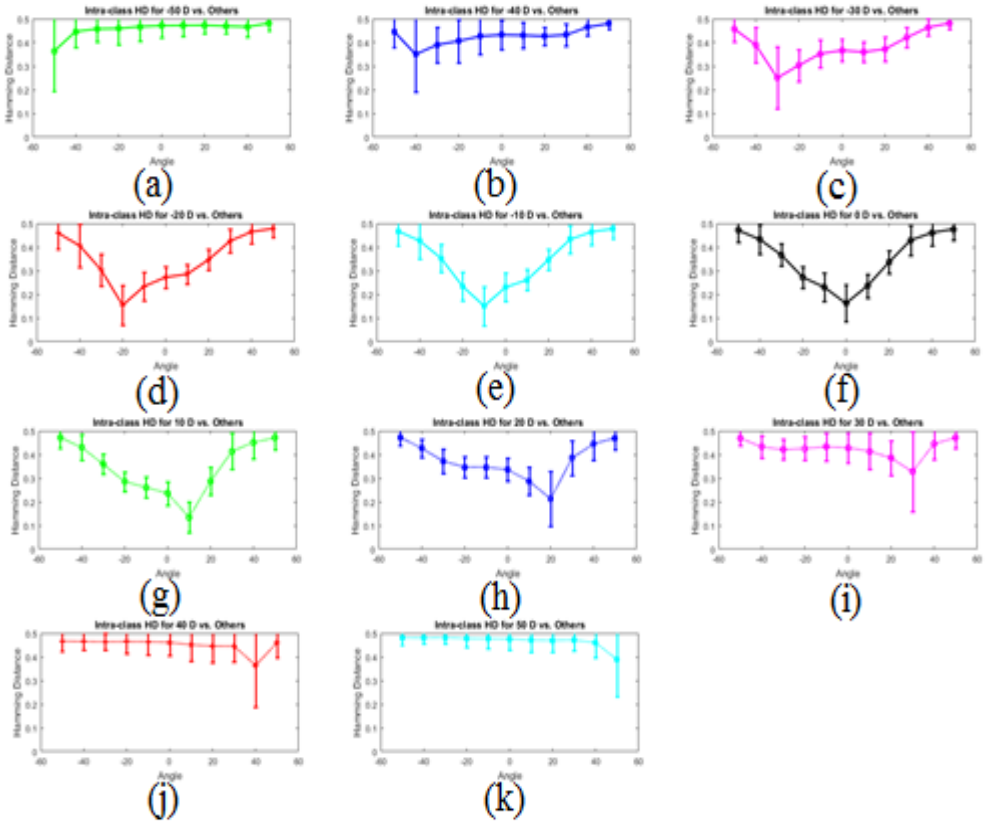

Figure 0.26.The error bar of the Hamming distance distribution of iris comparisons.

Figure 5.26 shows the error bar of the Hamming distance distribution of iris comparisons in inter-class comparisons of the iris images captured from -50° to +50° in angle with other iris images captured from all off-angle degrees. The center of the lines

represents the mean values and the bars show the standard deviation. Therefore, this figure contains all possible comparisons in intra-class distribution. For example, Figure 5.26(a) represents the comparison of iris images captured at -50° with other iris images captured from -50° to +50°. We observe that mean of Hamming Distance distribution increases from 0.35-0.49 as the gaze angle increase increases from -50° to +50°. The lowest Hamming distance is observed at iris images captured at -50° in angle because they are captured at the same angle. The highest Hamming distance is seen at iris images captured at 50° in angle because the difference between image acquisition angles of the compared iris images is 100° in angle that is the highest difference in the off-angle iris dataset. Figure 5.26(b) represents the comparison of iris images captured at -40° with other iris images captured from -50° to +50°. We observe that mean of Hamming Distance distribution increases from 0.45-0.49 as the gaze angle increase decreases from -50° to -40°and then increase from -40° to +50°. The lowest Hamming distance is observed at iris images captured at -40° in angle because they are captured at the same angle. The highest Hamming distance is seen at iris images captured at 50° in angle because the difference between image acquisition angles of the compared iris images is 90° in angle that is the highest difference in the off-angle iris dataset. Figure 5.26(c) represents the comparison of iris images captured at -30° with other iris images captured from -50° to +50°. We observe that mean of Hamming Distance distribution increases from 0.46-0.49 as the gaze angle increase decreases from -50° to -30°and then increase from -30° to +50°. The lowest Hamming distance is observed at iris images captured at -30° in angle because they are captured at the same angle. The highest Hamming distance is seen at iris images captured at 50° in angle because the difference between image acquisition angles of the compared iris images is 80° in angle that is the highest difference in the off-angle iris dataset. Figure 5.26(d) represents the comparison of iris images captured at -20° with other iris images captured from -50° to +50°. We observe that mean of Hamming Distance distribution increases from 0.46-0.49 as the gaze angle increase decreases from -50° to -20°and then increase from -20° to +50°. The lowest Hamming distance is observed at iris images captured at -20° in angle because they are captured at the same angle. The highest Hamming distance is seen at iris images captured at 50° in angle because the difference between image acquisition angles of the compared iris images is 70° in angle that is the highest difference in the off-angle iris dataset. Figure 5.26(e) represents the comparison of iris images captured

at -10° with other iris images captured from -50° to +50°. We observe that mean of Hamming Distance distribution increases from 0.48-0.49 as the gaze angle increase decreases from -50° to -10°and then increase from -10° to +50°. The lowest Hamming distance is observed at iris images captured at -10° in angle because they are captured at the same angle. The highest Hamming distance is seen at iris images captured at 50° in angle because the difference between image acquisition angles of the compared iris images is 60° in angle that is the highest difference in the off-angle iris dataset. Figure 5.26(f) represents the comparison of iris images captured at 0° with other iris images captured from -50° to +50°. We observe that mean of Hamming Distance distribution increases from 0.49-0.49 as the gaze angle increase decreases from -50° to 0°and then increase from 0° to +50°. The lowest Hamming distance is observed at iris images captured at 0° in angle because they are captured at the same angle. The highest Hamming distance is seen at iris images captured at 50° in angle and values of -50° nearly same because the difference between image acquisition angles of the compared iris images is 50° in angle that is the highest difference in the both off-angle iris dataset. Figure 5.26(g) represents the comparison of iris images captured at 10° with other iris images captured from -50° to +50°. We observe that mean of Hamming Distance distribution increases from 0.49-0.48 as the gaze angle increase decreases from -50° to 10°and then increase from 10° to +50°. The lowest Hamming distance is observed at iris images captured at 10° in angle because they are captured at the same angle. The highest Hamming distance is seen at iris images captured at -50° in angle because the difference between image acquisition angles of the compared iris images is 60° in angle that is the highest difference in the off-angle iris dataset. Figure 5.26(h) represents the comparison of iris images captured at 20° with other iris images captured from -50° to +50°. We observe that mean of Hamming Distance distribution decreases from 0.49-0.48 as the gaze angle increase decreases from -50° to 20°and then increase from 20° to +50°. The lowest Hamming distance is observed at iris images captured at 20° in angle because they are captured at the same angle. The highest Hamming distance is seen at iris images captured at -50° in angle because the difference between image acquisition angles of the compared iris images is 70° in angle that is the highest difference in the off-angle iris dataset. Figure 5.26(i) represents the comparison of iris images captured at 30° with other iris images captured from -50° to +50°. We observe that mean of Hamming Distance distribution decreases from 0.48-0.47 as the gaze angle increase

decreases from -50° to 30°and then increase from 30° to +50°. The lowest Hamming distance is observed at iris images captured at 30° in angle because they are captured at the same angle. The highest Hamming distance is seen at iris images captured at -50° in angle because the difference between image acquisition angles of the compared iris images is 80° in angle that is the highest difference in the off-angle iris dataset. Figure 5.26(j) represents the comparison of iris images captured at 40° with other iris images captured from -50° to +50°. We observe that mean of Hamming Distance distribution decreases from 0.48-0.46 as the gaze angle increase decreases from -50° to 40°and then increase from 40° to +50°. The lowest Hamming distance is observed at iris images captured at 40° in angle because they are captured at the same angle. The highest Hamming distance is seen at iris images captured at -50° in angle because the difference between image acquisition angles of the compared iris images is 90° in angle that is the highest difference in the off-angle iris dataset. Figure 5.26(k) represents the comparison of iris images captured at 50° with other iris images captured from -50° to +50°. We observe that mean of Hamming Distance distribution decreases from 0.49-0.39 as the gaze angle decrease from -50° to +50°. The lowest Hamming distance is observed at iris images captured at 50° in angle because they are captured at the same angle. The highest Hamming distance is seen at iris images captured at -50° in angle because the difference between image acquisition angles of the compared iris images is 100° in angle that is the highest difference in the off-angle iris dataset.

5.3. RESULTS OF BIT SHIFT METHOD

In this part we present how to decrease error on orientation along with error. Firstly we used bit shift method for decrease error on orientation with 1° errors. We observed bit shift method decrease error on orientation. We present Hamming distances distributions for all inter-class and intra-class iris comparisons in the MUID off-angle dataset showed in Figure 5.27. Figure 5.28 shows the error bar of the Hamming distance distribution of iris comparisons in inter-class comparisons.

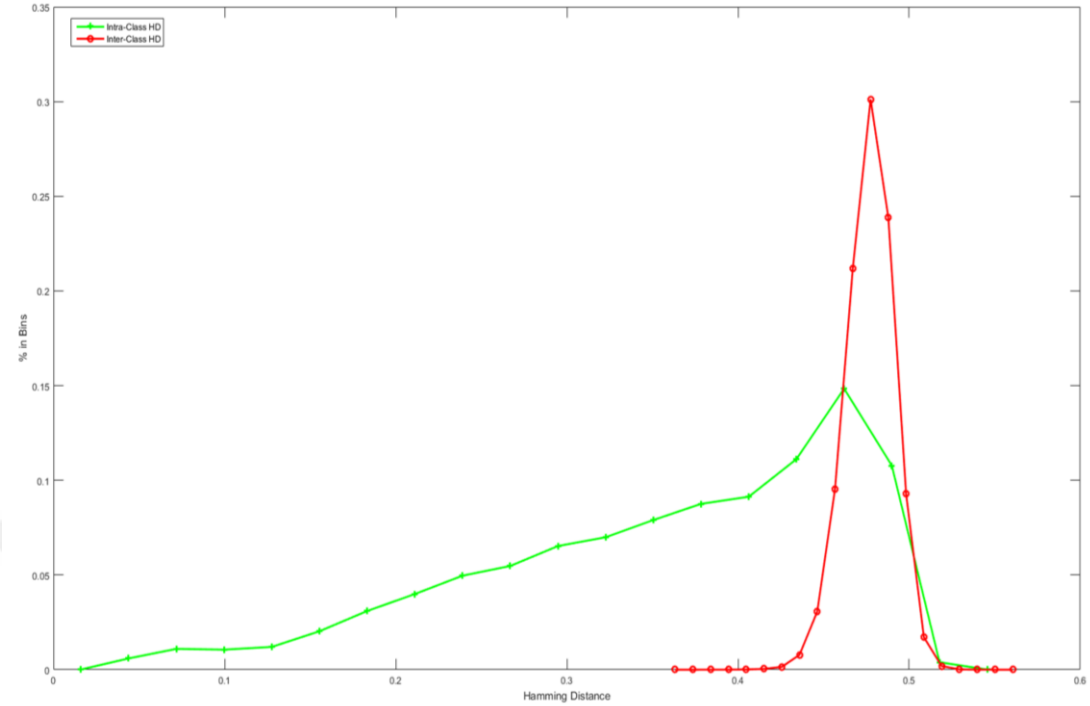

Figure 0.27. The Hamming distances distributions for all inter-class and intra-class iris comparisons in the MUID off-angle dataset.

Figure 5.27 shows the Hamming distances distributions for all inter-class and intra-class iris comparisons in the MUID off-angle dataset. We used off-angle image between -50° to +50° with increment 10° for our experiment. The histogram on the left with solid green line shows the intra-class Hamming distance that represents comparisons between two images of the same subjects. The left histogram with solid green shows Hamming Distance distribution for intra class that represents comparisons between two different subjects. We observe that intra-class Hamming distance varies changed from changes between 0.01-0.54 with a mean value of 0.275. The histogram on the left with solid green line shows the intra-class Hamming distance that represents comparisons between two images of the different subjects. The right histogram with solid red shows Hamming Distance distribution for inter class. Inter class varies changed from 0.34-0.56 with a mean value of 0.45 MUID Off-angle dataset change from -50° to +50° with increment 10° for our experiment, the main reason for the performance degradation in iris recognition system is the comparison of the frontal and off-angle iris images captured from different off-angles.

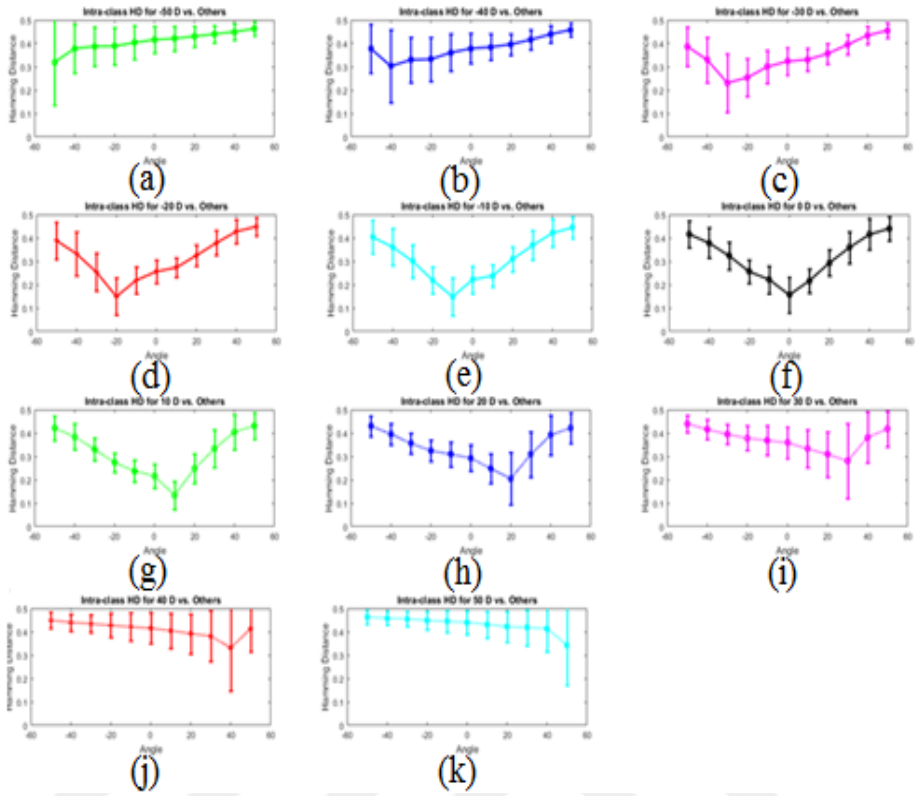

Figure 0.28. The error bar of the Hamming distance distribution of iris comparisons in inter-class comparisons.

Figure 5.28 shows the error bar of the Hamming distance distribution of iris comparisons in inter-class comparisons of the iris images captured from -50° to +50° in angle with other iris images captured from all off-angle degrees. The center of the lines represents the mean values and the bars show the standard deviation. Therefore, this figure contains all possible comparisons in intra-class distribution. For example, Figure 5.28(a) represents the comparison of iris images captured at -50° with other iris images captured from -50° to +50°. We observe that mean of Hamming Distance distribution increases from 0.31-0.48 as the gaze angle increase increases from -50° to +50°. The lowest Hamming distance is observed at iris images captured at -50° in angle because they are captured at the same angle. The highest Hamming distance is seen at iris images captured at 50° in angle because the difference between image acquisition angles of the compared iris images is 100° in angle that is the highest difference in the off-angle iris dataset. Figure 5.28(b) represents the comparison of iris images captured at -40° with other iris images captured from -50° to +50°. We observe that mean of Hamming Distance distribution increases from 0.37-0.48 as the gaze angle increase decreases from -50° to -40°and then increase from -40° to +50°. The lowest Hamming

distance is observed at iris images captured at -40° in angle because they are captured at the same angle. The highest Hamming distance is seen at iris images captured at 50° in angle because the difference between image acquisition angles of the compared iris images is 90° in angle that is the highest difference in the off-angle iris dataset. Figure 5.28(c) represents the comparison of iris images captured at -30° with other iris images captured from -50° to +50°. We observe that mean of Hamming Distance distribution increases from 0.38-0.47 as the gaze angle increase decreases from -50° to -30°and then increase from -30° to +50°. The lowest Hamming distance is observed at iris images captured at -30° in angle because they are captured at the same angle. The highest Hamming distance is seen at iris images captured at 50° in angle because the difference between image acquisition angles of the compared iris images is 80° in angle that is the highest difference in the off-angle iris dataset. Figure 5.28(d) represents the comparison of iris images captured at -20° with other iris images captured from -50° to +50°. We observe that mean of Hamming Distance distribution increases from 0.39-0.45 as the gaze angle increase decreases from -50° to -20°and then increase from -20° to +50°. The lowest Hamming distance is observed at iris images captured at -20° in angle because they are captured at the same angle. The highest Hamming distance is seen at iris images captured at 50° in angle because the difference between image acquisition angles of the compared iris images is 70° in angle that is the highest difference in the off-angle iris dataset. Figure 5.28(e) represents the comparison of iris images captured at -10° with other iris images captured from -50° to +50°. We observe that mean of Hamming Distance distribution increases from 0.40-0.46 as the gaze angle increase decreases from -50° to -10°and then increase from -10° to +50°. The lowest Hamming distance is observed at iris images captured at -10° in angle because they are captured at the same angle. The highest Hamming distance is seen at iris images captured at 50° in angle because the difference between image acquisition angles of the compared iris images is 60° in angle that is the highest difference in the off-angle iris dataset. Figure 5.28(f) represents the comparison of iris images captured at 0° with other iris images captured from -50° to +50°. We observe that mean of Hamming Distance distribution increases from 0.42-0.42 as the gaze angle increase decreases from -50° to 0°and then increase from 0° to +50°. The lowest Hamming distance is observed at iris images captured at 0° in angle because they are captured at the same angle. The highest Hamming distance is seen at iris images captured at 50° in angle and values of -50°

nearly same because the difference between image acquisition angles of the compared iris images is 50° in angle that is the highest difference in the both off-angle iris dataset. Figure 5.28(g) represents the comparison of iris images captured at 10° with other iris images captured from -50° to +50°. We observe that mean of Hamming Distance distribution increases from 0.42-0.41 as the gaze angle increase decreases from -50° to 10°and then increase from 10° to +50°. The lowest Hamming distance is observed at iris images captured at 10° in angle because they are captured at the same angle. The highest Hamming distance is seen at iris images captured at -50° in angle because the difference between image acquisition angles of the compared iris images is 60° in angle that is the highest difference in the off-angle iris dataset. Figure 5.28(h) represents the comparison of iris images captured at 20° with other iris images captured from -50° to +50°. We observe that mean of Hamming Distance distribution decreases from 0.43-0.42 as the gaze angle increase decreases from -50° to 20°and then increase from 20° to +50°. The lowest Hamming distance is observed at iris images captured at 20° in angle because they are captured at the same angle. The highest Hamming distance is seen at iris images captured at -50° in angle because the difference between image acquisition angles of the compared iris images is 70° in angle that is the highest difference in the off-angle iris dataset. Figure 5.28(i) represents the comparison of iris images captured at 30° with other iris images captured from -50° to +50°. We observe that mean of Hamming Distance distribution decreases from 0.44-0.42 as the gaze angle increase decreases from -50° to 30°and then increase from 30° to +50°. The lowest Hamming distance is observed at iris images captured at 30° in angle because they are captured at the same angle. The highest Hamming distance is seen at iris images captured at -50° in angle because the difference between image acquisition angles of the compared iris images is 80° in angle that is the highest difference in the off-angle iris dataset. Figure 5.28(j) represents the comparison of iris images captured at 40° with other iris images captured from -50° to +50°. We observe that mean of Hamming Distance distribution decreases from 0.45-0.38 as the gaze angle increase decreases from -50° to 40°and then increase from 40° to +50°. The lowest Hamming distance is observed at iris images captured at 40° in angle because they are captured at the same angle. The highest Hamming distance is seen at iris images captured at -50° in angle because the difference between image acquisition angles of the compared iris images is 90° in angle that is the highest difference in the off-angle iris dataset. Figure 5.28(k) represents the comparison

of iris images captured at 50° with other iris images captured from -50° to +50°. We observe that mean of Hamming Distance distribution decreases from 0.48-0.34 as the gaze angle decrease from -50° to +50°. The lowest Hamming distance is observed at iris images captured at 50° in angle because they are captured at the same angle. The highest Hamming distance is seen at iris images captured at -50° in angle because the difference between image acquisition angles of the compared iris images is 100° in angle that is the highest difference in the off-angle iris dataset.

Secondly we used bit shift method for decrease error on orientation with 2° errors. We observed bit shift method decrease error on orientation. We present Hamming distances distributions for all inter-class and intra-class iris comparisons in the MUID off-angle dataset showed in Figure 5.29. Figure 5.30 shows the error bar of the Hamming distance distribution of iris comparisons in inter-class comparisons.

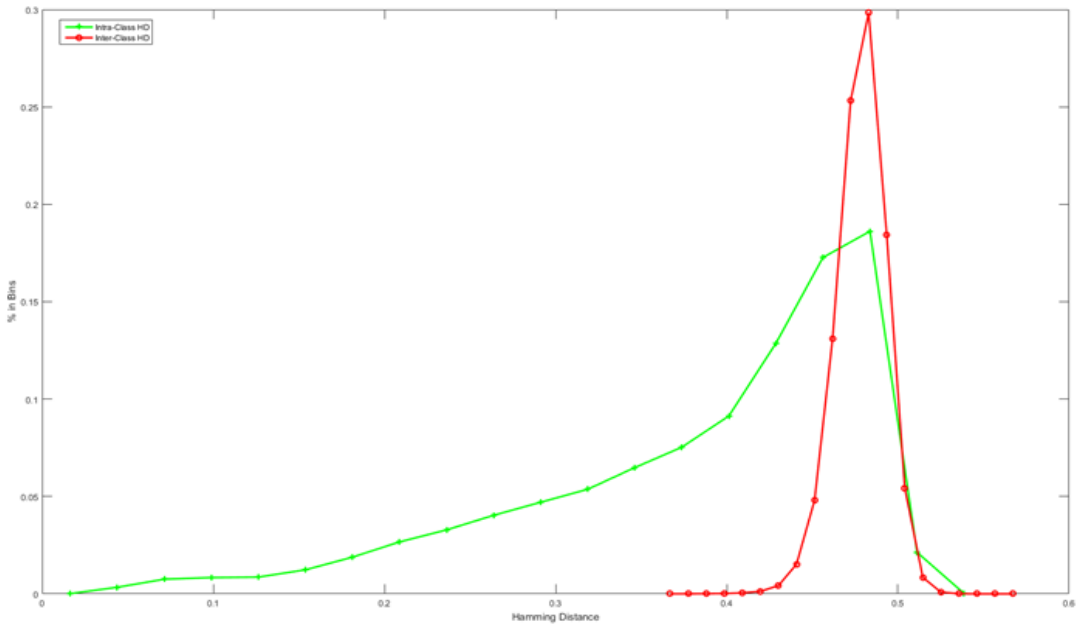

Figure 0.29. The Hamming distances distributions for all inter-class and intra-class iris comparisons in the MUID Off-angle dataset.

Figure 5.29 shows the Hamming distances distributions for all inter-class and intra-class iris comparisons in the MUID Off-angle dataset. We used off-angle image between -50° to +50° with increment 10° for our experiment. The histogram on the left with solid green line shows the intra-class Hamming distance that represents comparisons between two images of the same subjects. The left histogram with solid green shows Hamming

Distance distribution for intra class that represents comparisons between two different subjects. We observe that intra-class Hamming distance varies changed from changes between 0.01-0.53 with a mean value of 0.27. The histogram on the left with solid green line shows the intra-class Hamming distance that represents comparisons between two images of the different subjects. The right histogram with solid red shows Hamming Distance distribution for inter class. Inter class varies changed from 0.36-0.56 with a mean value of 0.46 MUID Off-angle dataset change from -50° to +50° with increment 10° for our experiment, the main reason for the performance degradation in iris recognition system is the comparison of the frontal and off-angle iris images captured from different off-angles.

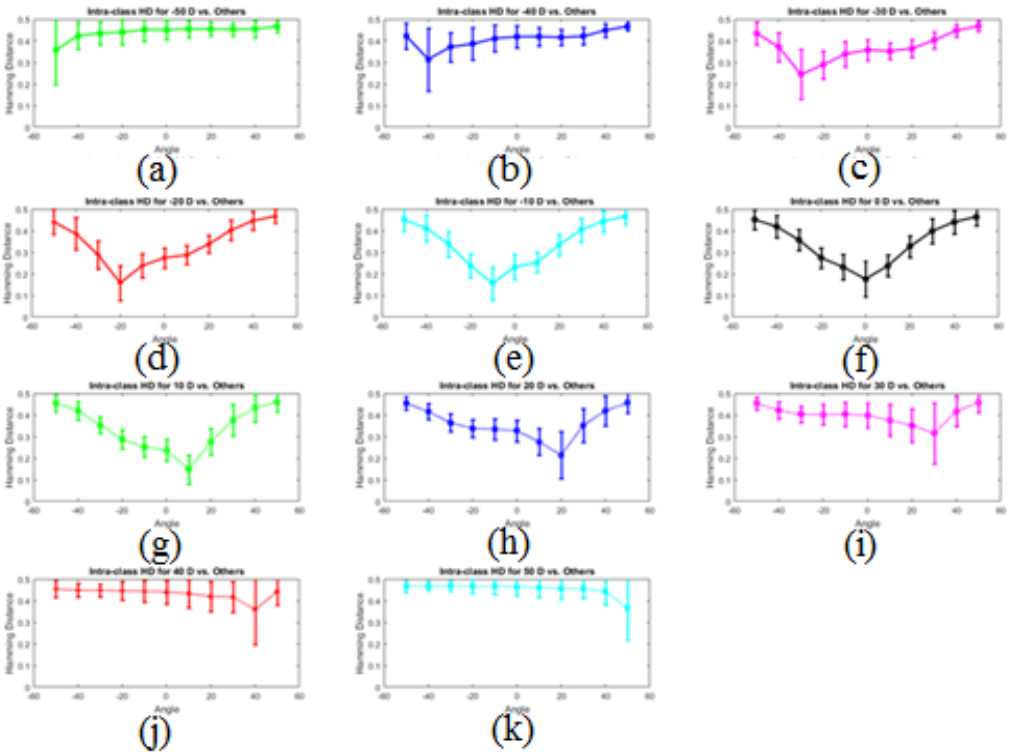

Figure 0.30.The error bar of the Hamming distance distribution of iris comparisons.

Figure 5.30 shows the error bar of the Hamming distance distribution of iris comparisons in inter-class comparisons of the iris images captured from -50° to +50° in angle with other iris images captured from all off-angle degrees. The center of the lines represents the mean values and the bars show the standard deviation. Therefore, this figure contains all possible comparisons in intra-class distribution. For example, Figure 5.30(a) represents the comparison of iris images captured at -50° with other iris images

captured from -50° to +50°. We observe that mean of Hamming Distance distribution increases from 0.34-0.48 as the gaze angle increase increases from -50° to +50°. The lowest Hamming distance is observed at iris images captured at -50° in angle because they are captured at the same angle. The highest Hamming distance is seen at iris images captured at 50° in angle because the difference between image acquisition angles of the compared iris images is 100° in angle that is the highest difference in the off-angle iris dataset. Figure 5.30(b) represents the comparison of iris images captured at -40° with other iris images captured from -50° to +50°. We observe that mean of Hamming Distance distribution increases from 0.44-0.48 as the gaze angle increase decreases from -50° to -40°and then increase from -40° to +50°. The lowest Hamming distance is observed at iris images captured at -40° in angle because they are captured at the same angle. The highest Hamming distance is seen at iris images captured at 50° in angle because the difference between image acquisition angles of the compared iris images is 90° in angle that is the highest difference in the off-angle iris dataset. Figure 5.30(c) represents the comparison of iris images captured at -30° with other iris images captured from -50° to +50°. We observe that mean of Hamming Distance distribution increases from 0.45-0.48 as the gaze angle increase decreases from -50° to -30°and then increase from -30° to +50°. The lowest Hamming distance is observed at iris images captured at -30° in angle because they are captured at the same angle. The highest Hamming distance is seen at iris images captured at 50° in angle because the difference between image acquisition angles of the compared iris images is 80° in angle that is the highest difference in the off-angle iris dataset. Figure 5.30(d) represents the comparison of iris images captured at -20° with other iris images captured from -50° to +50°. We observe that mean of Hamming Distance distribution increases from 0.44-0.48 as the gaze angle increase decreases from -50° to -20°and then increase from -20° to +50°. The lowest Hamming distance is observed at iris images captured at -20° in angle because they are captured at the same angle. The highest Hamming distance is seen at iris images captured at 50° in angle because the difference between image acquisition angles of the compared iris images is 70° in angle that is the highest difference in the off-angle iris dataset. Figure 5.30(e) represents the comparison of iris images captured at -10° with other iris images captured from -50° to +50°. We observe that mean of Hamming Distance distribution increases from 0.47-0.48 as the gaze angle increase decreases from -50° to -10°and then increase from -10° to +50°. The lowest Hamming

distance is observed at iris images captured at -10° in angle because they are captured at the same angle. The highest Hamming distance is seen at iris images captured at 50° in angle because the difference between image acquisition angles of the compared iris images is 60° in angle that is the highest difference in the off-angle iris dataset. Figure 5.30(f) represents the comparison of iris images captured at 0° with other iris images captured from -50° to +50°. We observe that mean of Hamming Distance distribution increases from 0.48-0.47 as the gaze angle increase decreases from -50° to 0°and then increase from 0° to +50°. The lowest Hamming distance is observed at iris images captured at 0° in angle because they are captured at the same angle. The highest Hamming distance is seen at iris images captured at 50° in angle and values of -50° nearly same because the difference between image acquisition angles of the compared iris images is 50° in angle that is the highest difference in the both off-angle iris dataset. Figure 5.30(g) represents the comparison of iris images captured at 10° with other iris images captured from -50° to +50°. We observe that mean of Hamming Distance distribution increases from 0.48-0.47 as the gaze angle increase decreases from -50° to 10°and then increase from 10° to +50°. The lowest Hamming distance is observed at iris images captured at 10° in angle because they are captured at the same angle. The highest Hamming distance is seen at iris images captured at -50° in angle because the difference between image acquisition angles of the compared iris images is 60° in angle that is the highest difference in the off-angle iris dataset. Figure 5.30(h) represents the comparison of iris images captured at 20° with other iris images captured from -50° to +50°. We observe that mean of Hamming Distance distribution decreases from 0.47-0.46 as the gaze angle increase decreases from -50° to 20°and then increase from 20° to +50°. The lowest Hamming distance is observed at iris images captured at 20° in angle because they are captured at the same angle. The highest Hamming distance is seen at iris images captured at -50° in angle because the difference between image acquisition angles of the compared iris images is 70° in angle that is the highest difference in the off-angle iris dataset. Figure 5.30(i) represents the comparison of iris images captured at 30° with other iris images captured from -50° to +50°. We observe that mean of Hamming Distance distribution decreases from 0.47-0.46 as the gaze angle increase decreases from -50° to 30°and then increase from 30° to +50°. The lowest Hamming distance is observed at iris images captured at 30° in angle because they are captured at the same angle. The highest Hamming distance is seen at iris images captured at -50° in

angle because the difference between image acquisition angles of the compared iris images is 80° in angle that is the highest difference in the off-angle iris dataset. Figure 5.30(j) represents the comparison of iris images captured at 40° with other iris images captured from -50° to +50°. We observe that mean of Hamming Distance distribution decreases from 0.46-0.45 as the gaze angle increase decreases from -50° to 40°and then increase from 40° to +50°. The lowest Hamming distance is observed at iris images captured at 40° in angle because they are captured at the same angle. The highest Hamming distance is seen at iris images captured at -50° in angle because the difference between image acquisition angles of the compared iris images is 90° in angle that is the highest difference in the off-angle iris dataset. Figure 5.30(k) represents the comparison of iris images captured at 50° with other iris images captured from -50° to +50°. We observe that mean of Hamming Distance distribution decreases from 0.48-0.38 as the gaze angle decrease from -50° to +50°. The lowest Hamming distance is observed at iris images captured at 50° in angle because they are captured at the same angle. The highest Hamming distance is seen at iris images captured at -50° in angle because the difference between image acquisition angles of the compared iris images is 100° in angle that is the highest difference in the off-angle iris dataset.

CHAPTER 6

CONCLUSIONS

In this thesis, we present a segmentation algorithm for off-angle iris images by using automatic segmentation algorithm [2] and Ground Truth Tool. We worked on between -50° to +50° with an increment 10° off-angle iris image. Our dataset have 110 off-angle iris images for each subject and so we worked on 20 subjects (20*110=2200 off-angle iris images) for our experimental result from Melikşah University Dataset. In our approach, we first segmented all off angle iris images by using automatic segmentation algorithm. Then we fixed segmentation errors born of automatic segmentation algorithm by using Ground Truth Tool.

After that we present our experimental results for without errors for without errors for using pupil center and iris center. We observe pupil center Hamming distance result better than iris center Hamming distance result. So we choose pupil center for doing better normalization on off-angle iris images. Secondly we add errors on off-angle segmentation parameters. These are $x, y, r1, r2$ and θ. We add %1, %2 and %3 errors in ellipse center which are x and y and minor and major axis which are $r1$ and $r2$ then we added 1° and 2 ° error on orientation which means θ. Thirdly we observe off-angle segmentation parameters along with error on Hamming distance result. Hamming distance results show us orientation along with error more increase Hamming distance than other parameters along with errors. Finally we use bit shift method for decrease Hamming distance result on orientation. Based on these results from our experiments, bit shift method shows effective result for Hamming distance on parameter of off-angle segmentation.

REFERENCES

1. Daugman, J. (2004). How iris recognition works. **IEEE Transactions on circuits and systems for video technology, 14**(1), 21-30.

2. Karakaya, M., Barstow, D., Santos-Villalobos, H., & Boehnen, C. (2013, March). An iris segmentation algorithm based on edge orientation for off-angle iris recognition. In IS&T/SPIE Electronic Imaging (pp. 866108-866108). International Society for Optics and Photonics.

3. Proença, H., & Alexandre, L. A. (2006). Iris segmentation methodology for non-cooperative recognition. **IEE Proceedings-Vision, Image and Signal Processing, 153**(2), 199-205.

4. Gafurov, D., Helkala, K., & Søndrol, T. (2006). Biometric gait authentication using accelerometer sensor. **Journal of computers**, **1**(7), 51-59.

5. Bowyer, K. W., Hollingsworth, K., & Flynn, P. J. (2008). Image understanding for iris biometrics: A survey. **Computer vision and image understanding**, **110**(2), 281-307.

6. Matey, J. R., Naroditsky, O., Hanna, K., Kolczynski, R., LoIacono, D. J., Mangru, S., ... & Zhao, W. Y. (2006). Iris on the move: Acquisition of images for iris recognition in less constrained environments. **Proceedings of the IEEE**, **94**(11), 1936-1947.

7. Proenca, H., & Alexandre, L. A. (2007). Toward noncooperative iris recognition: a classification approach using multiple signatures. **IEEE Transactions on Pattern Analysis and Machine Intelligence**, **29**(4), 607-612.

8. Yoon, S., Jung, H. G., Suhr, J. K., & Kim, J. (2007, June). Non-intrusive iris image capturing system using light stripe projection and pan-tilt-zoom camera. *In 2007 IEEE Conference on Computer Vision and Pattern Recognition* (pp. 1-7). IEEE.

9. Schuckers, S. A., Schmid, N. A., Abhyankar, A., Dorairaj, V., Boyce, C. K., & Hornak, L. A. (2007). On techniques for angle compensation in nonideal iris recognition. **IEEE Transactions on Systems, Man, and Cybernetics, Part B (Cybernetics)**, **37**(5), 1176-1190.

10. Frigerio, E., Marcon, M., Sarti, A., & Tubaro, S. (2012, September). Correction method for nonideal iris recognition. *In 2012 19th IEEE International Conference on Image Processing* (pp. 1149-1152). IEEE.

11. Proença, H. (2006). Towards non-cooperative biometric iris recognition. **University of Beira Interior. Department of Computer Science**.

12. Wildes, R. P., Asmuth, J. C., Green, G. L., Hsu, S. C., Kolczynski, R. J., Matey, J. R., & McBride, S. E. (1994, December). A system for automated iris recognition. *In Applications of Computer Vision, 1994., Proceedings of the Second IEEE Workshop on* (pp. 121-128). IEEE.

13. Wildes, R. P. (1997). Iris recognition: an emerging biometric technology. **Proceedings of the IEEE**, **85**(9), 1348-1363.

14. Aligholizadeh, M. J., Javadi, S., Sabbaghi-Nadooshan, R., & Kangarloo, K. (2011, October). Eyelid and eyelash segmentation based on wavelet transform for iris recognition. *In Image and Signal Processing (CISP), 2011 4th International Congress on* (Vol. 3, pp. 1231-1235). IEEE.

15. Oyster, C. W. (1999). The Human eye: Structure and function. Sinauer Assoc. Inc, Publishers. Sunderland.

16. Cerme M.K.. Effects of 3D Iris Texture on Off-angle Iris Recognition. *in Proceedings of IEEE 23rd Conference of Signal Processing and Communication Applications* (SIU 2015). May 2015. Malatya, TURKEY.

17. Karakaya, M., Barstow, D., Santos-Villalobos, H., & Thompson, J. (2013, June). Limbus impact on off-angle iris degradation. *In 2013 International Conference on Biometrics (ICB)* (pp. 1-6). IEEE.

18. Cassin, B., Solomon, S., & Rubin, M. L. (1984). Dictionary of eye terminology. Triad Pub. Co..

19. Shah, S., & Ross, A. (2009). Iris segmentation using geodesic active contours. **IEEE Transactions on Information Forensics and Security**, **4**(4), 824-836.

20. Thompson, J. W., & Flynn, P. J. (2010, September). A segmentation perturbation method for improved iris recognition. In Fourth IEEE International Conference on Biometrics: Theory Applications and Systems (BTAS 10).

21. Si, Y., Mei, J., & Gao, H. (2012). Novel approaches to improve robustness, accuracy and rapidity of iris recognition systems. **IEEE transactions on industrial informatics**, **8**(1), 110-117.

22. Kalka, N. D., Zuo, J., Schmid, N. A., & Cukic, B. (2006, April). Image quality assessment for iris biometric. *In Defense and Security Symposium (pp. 62020D-62020D)*. International Society for Optics and Photonics.

23. He, Z., Tan, T., Sun, Z., & Qiu, X. (2009). Toward accurate and fast iris segmentation for iris biometrics. **IEEE transactions on pattern analysis and machine intelligence**, **31**(9), 1670-1684.

24. Ma, L., Tan, T., Wang, Y., & Zhang, D. (2003). Personal identification based on iris texture analysis. **IEEE Transactions on Pattern Analysis and Machine Intelligence**, **25**(12), 1519-1533.

25. Zuo, J., & Schmid, N. A. (2010). On a methodology for robust segmentation of nonideal iris images. **IEEE Transactions on Systems, Man, and Cybernetics, Part B (Cybernetics)**, **40**(3), 703-718.

26. Huang, J., Wang, Y., Tan, T., & Cui, J. (2004, August). A new iris segmentation method for recognition. *In Pattern Recognition, 2004. ICPR 2004. Proceedings of the 17th International Conference on* (Vol. 3, pp. 554-557). IEEE.

27. Santos-Villalobos, H. J., Barstow, D. R., Karakaya, M., Boehnen, C. B., & Chaum, E. (2012, September). ORNL biometric eye model for iris recognition. *In Biometrics: Theory, Applications and Systems (BTAS), 2012 IEEE Fifth International Conference on* (pp. 176-182). IEEE.

28. Mohammadi Arvacheh, E. (2006). A study of segmentation and normalization for iris recognition systems.

CURRICILUM VITAE

PERSONAL DATA

Name and Surname:	:	Sema Keleş ÇETİN
Nationality	:	T.C.
Birth Dateand Place	:	September 26, 1987, Mardin
Marital Status	:	Married
Tel:	:	+90 534 412 41 21
Email	:	skelescetin@gmail.com
Address	:	Yıldırım Beyazıt Mah., Uzay Cad., Kınaş Belinay Sitesi, A Blok, Kat: 2, No: 5 Melikgazi/KAYSERİ

EDUCATION

Degree	Institute	Date of Graduation
Bachelor's	Başkent University	2013
High School	Milli Piyango Anadolu Lisesi	2005

PROFESSIONAL EXPERIENCE

Year	Institute/Company	Mission
2008-2013	Başkent University	Electric and Electronic Engineering

Foreign Languages

English and Turkish